Work Package 1 Final Report: Sea Lice Dispersal Modelling in Shuna Sound

January 2023

Scottish Government
Riaghaltas na h-Alba

Work Package 1 Final Report:

Sea Lice Dispersal Modelling in Shuna Sound

Authors: Philip Gillibrand, Meadhbh Moriarty, Stevie Brain.

Internal reviewers: Tom Adams, Alejandro Gallego

Report to satisfy requirements for WP1 Milestone 4

Contents

1. Executive Summary

The report describes simulations of sea lice dispersal in the area around Shuna Sound (See section 1.3 for details), carried out using various combinations of hydrodynamic models (HDM) and particle tracking models (PTM), principally:

i) Wider Loch Linnhe System (WLLS) HDM + FISCM PTM (Marine Scotland)

ii) WestCOMS HDM + BioTracker PTM (SAMS)

iii) WLLSshuna HDM + UnPTRACK PTM (Mowi Scotland Ltd)

The model configurations were used to investigate the potential variability in dispersal patterns of sea lice in Shuna Sound, with a focus on the field sampling season of 2021 (see Work Package (WP) 3 Reinardy et al., 2023). The dispersal models used weekly adult female lice counts and fish numbers from eight farms in the Sound to provide the source of lice larvae. The resulting modelled distributions of infective lice larvae in the water column were compared to monthly planktonic sea lice sampling at six locations (Reinardy et al., 2023).

Comparisons between the predicted lice densities from all model combinations and the observed planktonic lice densities were all quantitatively poor. The data were heavily zero-inflated, as discussed by Reinardy et al. (2023). In contrast, whilst predicted densities at the sample locations were zero (or very low) more than 50% of the time, the modelled lice densities were also often non-zero. The cause of the poor agreement between model results and planktonic lice data is thought to be high spatial and temporal variability in larval lice distributions, making accurate prediction extremely challenging. High spatial and temporal variability in sea lice larvae distributions is not unexpected, given that the larvae are thought to proactively stay at the sea surface (at least during daylight

hours) and are therefore subject to complex ocean dynamics arising from the combination of tidal, wind-driven and freshwater-driven dynamics, likely accumulating at fronts and being advected around the coastal zone by winds and tides. Similar findings and conclusions regarding the high spatiotemporal variability of sea lice distributions were reported by Skarðhamar et al. (2019).

Plankton sampling using traditional methods does not, therefore, currently appear to provide robust datasets for model calibration and validation. The apparent very high temporal and spatial variability of sea lice distributions demands (an unachievable level of) pinpoint accuracy from models in order to deliver positive relationships between the observed and modelled sea lice larval density. Field sampling of planktonic sea lice requires innovations in methodology (Bui et al., 2021), and dramatically upscaled sampling/analytical capacity, before adequate *in situ* data for model calibration can become available.

Outcomes from sea lice dispersal models depend fundamentally on the underlying hydrodynamic model. Sea lice larvae are transported around the coastal zone for approximately 15 days. Over these time scales, lagrangian modelling can integrate small differences in modelled velocity into large differences in individual larval transport pathways and potentially radically different predicted infective sea lice distributions. The use of different hydrodynamic models, even with identical sea lice dispersal models, resulted in different predicted distributions of lice.

Combining the results from a number of model runs into an ensemble-mean smoothed out some of the idiosyncrasies of particular model runs and illustrated regions of the domain where the results were more consistent, at both high and low densities. The ensemble methodology, explored more fully in WP4 (Moriarty et al. 2022), allowed some interpretation of the uncertainty of model predictions to be made.

Based on the results here, the ensemble approach seems particularly pertinent for the hydrodynamic model outputs, which led to substantial differences between predicted sea lice distributions. The challenges involved in incorporating ensemble methods into a management and regulatory regime are recognised. Nevertheless, where multiple predictions of sea lice distributions using different hydrodynamic models are made, some effort to assess the relative robustness of the results will be necessary.

1.1 Description of work package & its importance

There has recently been an increasing emphasis on the use of modelling approaches to investigate the potential impacts of aquaculture activities on the near shore environment (Scottish Environmental Protection Agency 2019). Modelling is a necessary tool due to challenges in directly monitoring particular impacts, but also in assessing potential responses of the system to changes in environmental conditions.

A particular environmental challenge presented by aquaculture is that of sea lice (Costelloe et al. 2009). These small parasitic organisms can infest both farmed and wild populations of salmon, potentially moving large distances during a pelagic larval phase of around 14 days (Adams et al. 2012). Sea lice can cause a wide range of impacts on host fish, particularly if they reach high densities. As such, their management and control is a key topic for aquaculture regulation. Lice are found on wild salmonid populations, but due to the numbers of fish stocked in farms, farm-sourced lice almost certainly greatly outnumber wild-sourced lice in the water column.

Tracking lice infestations in the wild is challenging due to the large numbers of larvae that are produced, the long distances they travel, and the low (and patchy) densities at which they are found in the water column. Identifying sources of larval lice is also difficult due to the high levels of

mixing between larvae releases from natal populations. As a result, biophysical models are a fundamental tool in understanding their spread, and the resulting impacts on farmed and wild fish.

1.2 Description of overall work package goals

A range of hydrodynamic models have been developed in recent years, with a notable improvement in the ability to predict water movements in complex coastal environments becoming possible through the increased use of unstructured meshes by finite volume and finite element models. Flow fields from these models can be used to drive particle tracking models to predict the dispersal of sea lice larvae from farm sites. Specific examples of such models which have been developed for the Scottish west coast environment are WestCOMS (Aleynik et al. 2016) and the Scottish Shelf Model (SSM) (Wolf et al. 2016), both of which are based on the Finite Volume Coastal Ocean Model (FVCOM, Chen et al. 2003). Other general-purpose hydrodynamic models, such as the River and Coastal Ocean Model (RiCOM), which uses mixed finite volume and finite element methods (Walters, 2005a), and the Danish Hydraulic Institute model MIKE (https://www.mikepoweredbydhi.com/), have also been applied to Scottish coastal waters. However, there remains a need to understand the robustness of model outputs, both in terms of how results derived using one model compare with another, but also in quantifying the variability predicted as a result of changes in meteorological and other forcing. For example, most hydrodynamic model applications are driven by time-specific meteorological forcing, whereas the primary products of the SSM are “climatological”, being forced by a 25-year average meteorology; in this work package, both year-specific and climatological SSM outputs were used in order to assess the effects of the time specific versus climatological meteorological forcing. Understanding the implications of using these different forcing methods for sea lice dispersal predictions is of great

interest to regulators and industry alike. In order to assist in validating the outputs of the models developed, the SPILLS project carried out a long season of field sampling for sea lice larval stages in Shuna Sound area (Figure 1.1) on the west coast of Scotland, in April-October 2021 (see Work Package 3). This is used to help determine the utility of the different models developed in predicting sea lice infestation pressure and the potential threat to wild fish in the area.

1.3 Overview of Study Area – Shuna Sound

The domain for this study was Shuna Sound, which is located on the southern portion of the west coast of Scotland (Figure 1.1). This is a complex area of fjordic sea lochs, islands and constrictions with strong tidal movements, including the well-known Gulf of Corryvreckan on the western edge. The area plays host to 8 fish farm sites, which are managed by two operators, Mowi Scotland Limited and Kames Fish Farming Limited. The locations and consented biomass at each site are listed in Table 1.1.

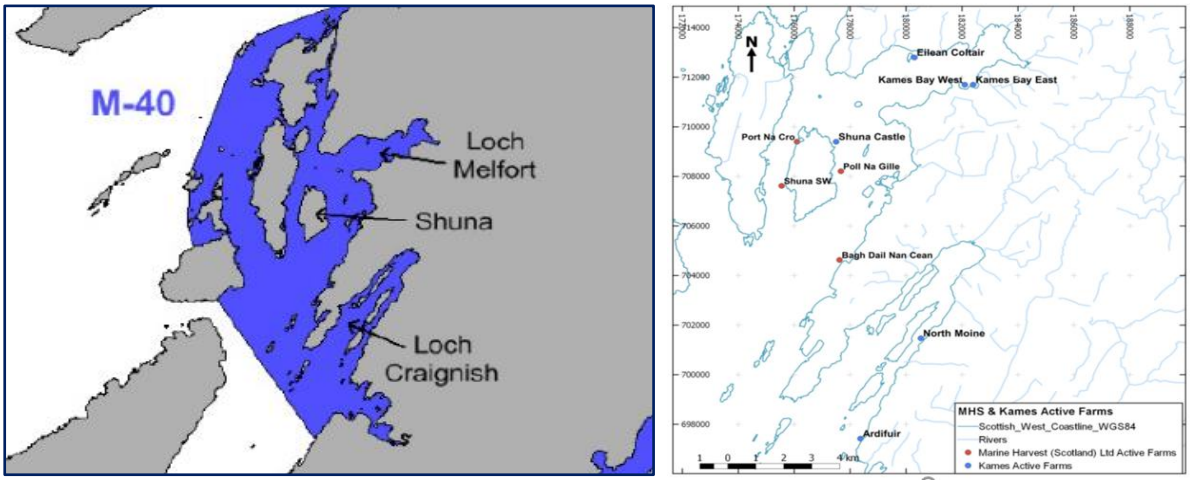

Figure 1.1: Study area at Shuna Sound, on the west coast of Scotland (left), with the locations of the local salmon farms shown on the right. The farm at Eilean Coltair was not operational during the study period.

Table 1.1. Site coordinates and consented biomass for the eight active fish farms in Shuna Sound system used in the modelling study.

Site	Easting	Northing	Consented Biomass (Tonnes)
Kames Bay East	182380	711720	250
Kames Bay West	182100	711700	205
Shuna Castle	177500	709600	894.9
Shuna SW	175600	707500	2500
Port Na Cro	176000	709700	1000
Port Na Gille	177600	708100	2262
BDNC	177400	704600	3000
North Moine	180500	701500	1238

2. Hydrodynamic Modelling in Shuna Sound

2.1 Description of Hydrodynamic Models

2.1.1 WLLSshuna

WLLSshuna is an implementation of RiCOM (River and Coastal Ocean Model), a general-purpose hydrodynamics and transport model, which solves the standard Reynolds-averaged Navier-Stokes equation (RANS) and the incompressibility condition, applying the hydrostatic and Boussinesq approximations. RiCOM has been tested on a variety of benchmarks against both analytical and experimental data sets (e.g., Walters & Casulli 1998; Walters 2005a, b). The model has been previously used to investigate the inundation risk from tsunamis and storm surge on the New Zealand coastline (Walters 2005a; Gillibrand et al. 2011; Lane et al. 2011), to study tidal currents in high energy tidal environments (Walters et al. 2010) and, more recently, to study tidal energy resource (Plew & Stevens 2013; Walters et al. 2013; Walters 2016) and the effects of energy extraction on the ambient environment in Scotland (McIlvenny et al. 2016; Gillibrand et al. 2016b).

The model solves the three-dimensional (3D) shallow water equations, derived from the Reynolds-averaged Navier-Stokes equations

using the hydrostatic assumption and the Boussinesq approximation. The continuity equation for incompressible flows is used to solve for the vertical velocity, and the free surface equation is formed by vertically integrating the continuity equation and applying the kinematic free surface and bottom boundary conditions. The equations are discretized on an unstructured grid of triangular elements using mixed finite element and finite volume methods. This approach permits greater resolution of complex coastlines. The model is forced by a tidal open boundary condition, wind forcing applied as a surface stress and freshwater inputs at point sources along the coast.

The momentum and free surface equations are solved using semi-implicit techniques to optimize solution time and avoid the CFL stability constraint (Walters 2016). The material derivative is discretized using semi-Lagrangian methods to remove stability constraints on advection (Walters et al. 2008). The Coriolis term is solved using a 3rd order Adams-Bashforth method (Walters et al. 2009). Full details of the model discretization and solution methods can be found in Walters et al. (2013) and Walters (2016). The solution methods provide a fast, accurate and robust code that runs efficiently on multi-core desktop workstations with shared memory using OpenMP.

For this work package, RiCOM (WLLSshuna) was applied in 3D mode using a modified adaptation of the WLLS mesh (see §2.1.3) with 10 layers in the vertical. The node spacing varies from about 25m within Loch Linnhe to approximately 6 km along the open boundary. The model was forced along its open boundary by eight tidal constituents (O_1, K_1, Q_1, P_1, M_2, S_2, N_2, K_2), amplitudes and phase of which were obtained from the full Scottish Shelf Model (SSM). Spatially- and temporally-varying wind speed and direction data were taken from the ERA5 global reanalysis dataset (https://www.ecmwf.int/en/forecasts/datasets/reanalysis-datasets/era5)

for the 2021 simulation period, with the data converted to surface stress using a standard algorithm. River flows were taken from the Grid2Grid climatological forcing data used by the SSM (Table 2.1).

2.1.2 WeStCOMS 2020/2021

WeStCOMS (West Coast of Scotland Coastal Ocean Modelling System) is an implementation of FVCOM (Finite Volume Community Ocean Model; Chen et al. 2003) coupled with a meteorological WRF (Weather Research Forecasting) model. The model has been developed through multiple iterations in domain extent and operational capability (Aleynik et al. 2016), and has been used to simulate fate of sea lice in several projects (Adams et al. 2016, 2021; Aleynik et al. 2022). The domain used in the present version of the model covers the Scottish west coast from the northern Irish Sea in the south to Cape Wrath in the north, north and west to encompass the Western Isles (Davidson et al. 2021, Corrochano-Fraile et al. 2022). The grid is unstructured with non-overlapping triangular elements, allowing for higher resolution of complex areas such as the coastline of Loch Linnhe. Horizontally, the grid comprises 99999 nodes describing 177236 elements. Vertically, the model has 10 layers, in the terrain-following sigma-coordinate system with concentration of levels in the upper most and lower most parts of water column. The model is forced by a tidal open boundary condition, with time series of sea surface elevations predicted at the open boundary nodes using the 11 dominant tidal constituents, freshwater inputs from the 228 largest rivers, computed from 3-hourly rainfall data, and surface heat, wind and precipitation forcing from the Scottish-WRF model.

2.1.3 Wider Loch Linnhe System Model (WLLS)

The Wider Loch Linnhe System (WLLS) model is also an implementation of FVCOM, and has a domain covering many of the Inner Hebrides from the southern tip of the Mull of Kintyre to the Isle of Skye in the north. The western boundary extends to approximately 7.5° W from

Northern Ireland to the southern Outer Hebrides. The model grid is unstructured with the highest horizontal resolution in Loch Linnhe, Loch Leven and Loch Sunart, where the node spacing goes down to 15 m. The typical node spacing of these sea lochs is around 50 – 100 m, with Lower Loch Linnhe having a typical node spacing of 100 – 150 m. Beyond Loch Linnhe, its side lochs, and Loch Sunart, the unstructured grid resolution reduces further, with the node spacing at the western boundary being around 5 km. The water column is resolved using a hybrid sigma layer scheme with 10 standard terrain following sigma layers, each representing 10% of the water column, in water depths shallower than 13 m. In areas deeper than 13 m, the water column is resolved with 2 fixed layers at the surface, each 1 m thick, 2 fixed layers at the bottom, each 2.5 m thick, and 6 sigma layers of equal spacing for the mid depths. This enables the freshwater output from Upper Loch Linnhe to be well resolved.

Two outputs from the model are used here, the one-year Climatology representing typical present-day conditions (1990-2014), and the 2021 hindcast, see Table 2.1 for details.

Table 2.1: Summary of model setup differences between hydrodynamic versions

HD Model	Time Period	Boundary Forcing	Atmospheric Forcing	Fresh Water Forcing	Output Variables*
WLLSshuna	2021 hindcast	The wider SSM version 2.01	ECMWF ERA5	Grid2Grid climatology (1962-2011)	U, V, W, η, S
WeStCOMS	2021 hindcast	North-East Atlantic ROMS operational model, provided by the Marine Institute, Ireland (Dabrowski et al., 2016).	WeStCOMS-WRF 2 km resolution, run at SAMS, (Aleynik 2016; Davidson 2021)	Derived precipitation from WeStCOMS-WRF over 228 river catchment areas	U, V, W, η, T, S
WLLS 2021	2021 hindcast	AMM15 (Graham et al., 2018)	WRF 1/18° resolution supplied by CEH (Vieno et al. 2016, Vieno et al. 2014)	Grid2Grid river discharge climatology (1962-2011), River temperature climatology applied based on data from the Scotland River Temperature Monitoring Network (Jackson et al. 2016).	U, V, W, η, T, S
WLLS Climatology	1 year climatology (representing 1990 – 2014)	The wider SSM version 2.01	Climatology derived from ECMWF ERA-Interim (1990-2014)	Grid2Grid climatology (1962-2011)	U, V, W, η, T, S

* U, V – East and North components of velocity
W – Vertical velocity
η – Sea surface height (elevation above MLOS)
T – Water temperature
S – Water salinity

2.2 Physical field data

Relatively few observations of current speed and direction suitable for calibrating the hydrodynamic models were available from Shuna Sound in 2021, since emphasis in the project (and limited financial resources) was placed on field sampling for larval sea lice. A deployment of a bed-mounted 300 kHz Teledyne RD Instruments Sentinel V100 Acoustic Doppler Current Profiler (ADCP) was made at the Poll na Gille (PNG) fish farm site (Figure 1.1) from 19th May – 11th August 2021, and these data have been used to evaluate the performance of the various hydrodynamic models. The deployment location was 56° 12.844'N 005° 34.924'W. The mooring was twice disturbed from unknown causes during the deployment period, meaning that only data from 10th June – 11th August were used for evaluation of the hydrodynamic model performance. The instrument was deployed in 32m of water, and configured with a vertical cell size of 1m. Data were recorded every 20 minutes following a 10-minute burst of sampling.

2.3 Comparison of hydrodynamic models to physical field data

Since sea lice larvae spend much of their time near the water surface, only the observed and predicted velocity data for the near-surface are shown here. The full comparison between model and data is presented in Appendix 1. The near-surface data was taken from the closest valid ADCP cell below the sea-surface, at a depth of -4.3 m. Modelled velocity results were interpolated in the vertical to provide results at the same depth as the observed data.

The model – data comparison is illustrated in two ways. Firstly, a scatter plot showing the observed and predicted near-surface components of velocity are presented. The comparison could have been presented as time series plots, but the WLLS climatology, which is based on tides from 1993, has a different velocity phase from the observations and the other

models, which distorts the comparison. Scatter plots do not reveal the phase. Secondly, the comparisons are presented as cumulative vector plots, which highlight the residual (non-tidal) currents at the measurement site. The residual flows are important for transport of sea lice over the period of their lifetime (~2 weeks).

The results of the scatter plot comparison demonstrate that all models do a reasonable job of reproducing tidal currents at the PNG site (Figure 2.1). All four models have near-surface current speeds very similar in magnitude to the observed data. The peak current speeds from WeStCOMS are slightly enhanced relative to the observed peaks on both flood and ebb tides. Further, the orientations of all four sets of modelled currents are slightly offset relative to the observed data; this may be due to some inaccuracy in the model bathymetries, which inevitably are smoother than the real bathymetry, or due to the ADCP not being deployed in exactly the recorded location. Nevertheless, the performance of the models at reproducing the tidal currents is satisfactory.

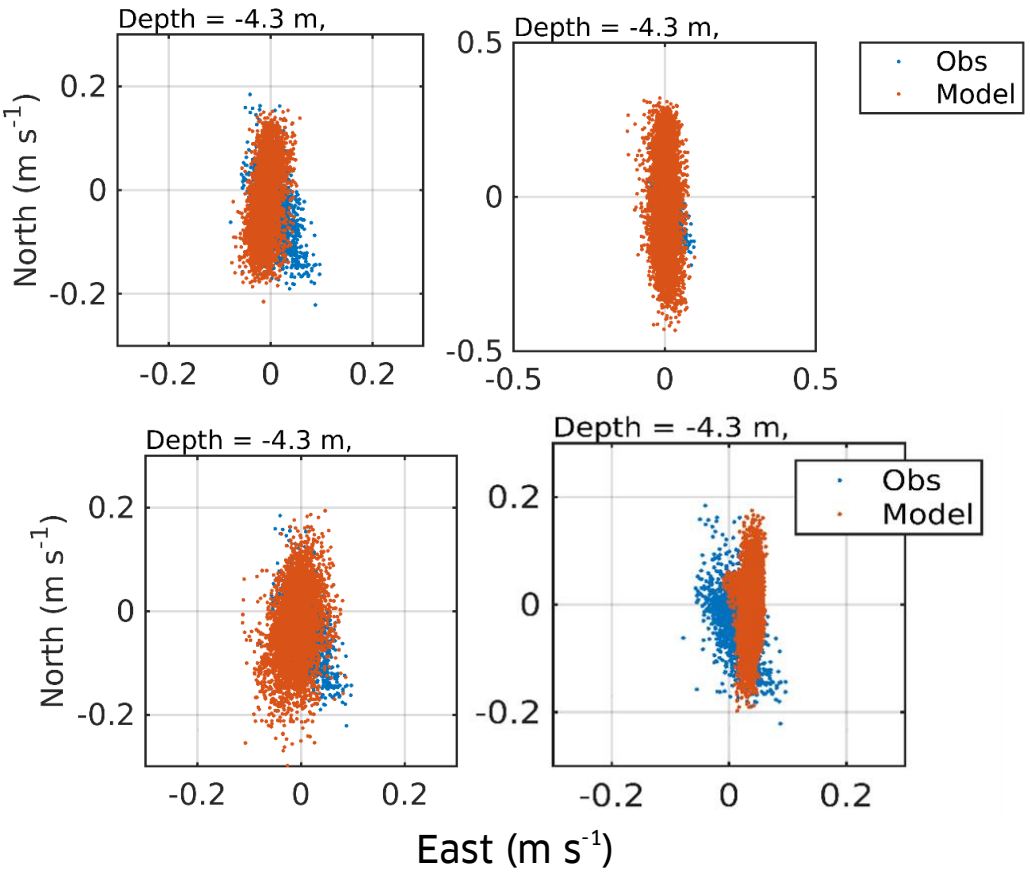

Figure 2.1. Scatter plots of observed and modelled East and North components of velocity in the near-surface layer from four hydrodynamic models: WLLSshuna (top left); WeStCOMS(top right); WLLS 2021 (bottom left); WLLS Climatology (bottom right).

Cumulative vector plots integrate the measured velocity over time, converting the velocity into distance. These plots principally illustrate the residual flow. For the results shown here, the observed and modelled near-surface currents over the time period of the observations were integrated to determine near-surface displacements over the deployment period.

The predicted residual currents from the WLLSshuna and WeStCOMS models reproduce the magnitude of the observed cumulative displacements well, with WeStCOMS in particular simulating the residual flows very accurately (Figure 2.2). The direction of the modelled displacements is westward of the observed data. The two WLLS models over-predict the residual current strength by a factor of about 3, with the direction of the climatological simulation also being somewhat wayward. This is perhaps

not surprising given the steady south-westerly winds that are used to force the climatological simulation. The two WLLS simulations appear to have the potential (based on this single-point comparison) to transport sea lice larvae out of Shuna Sound more quickly than is realistic. The WLLSshuna and WeStCOMS models should produce more realistic flushing of larvae from the system.

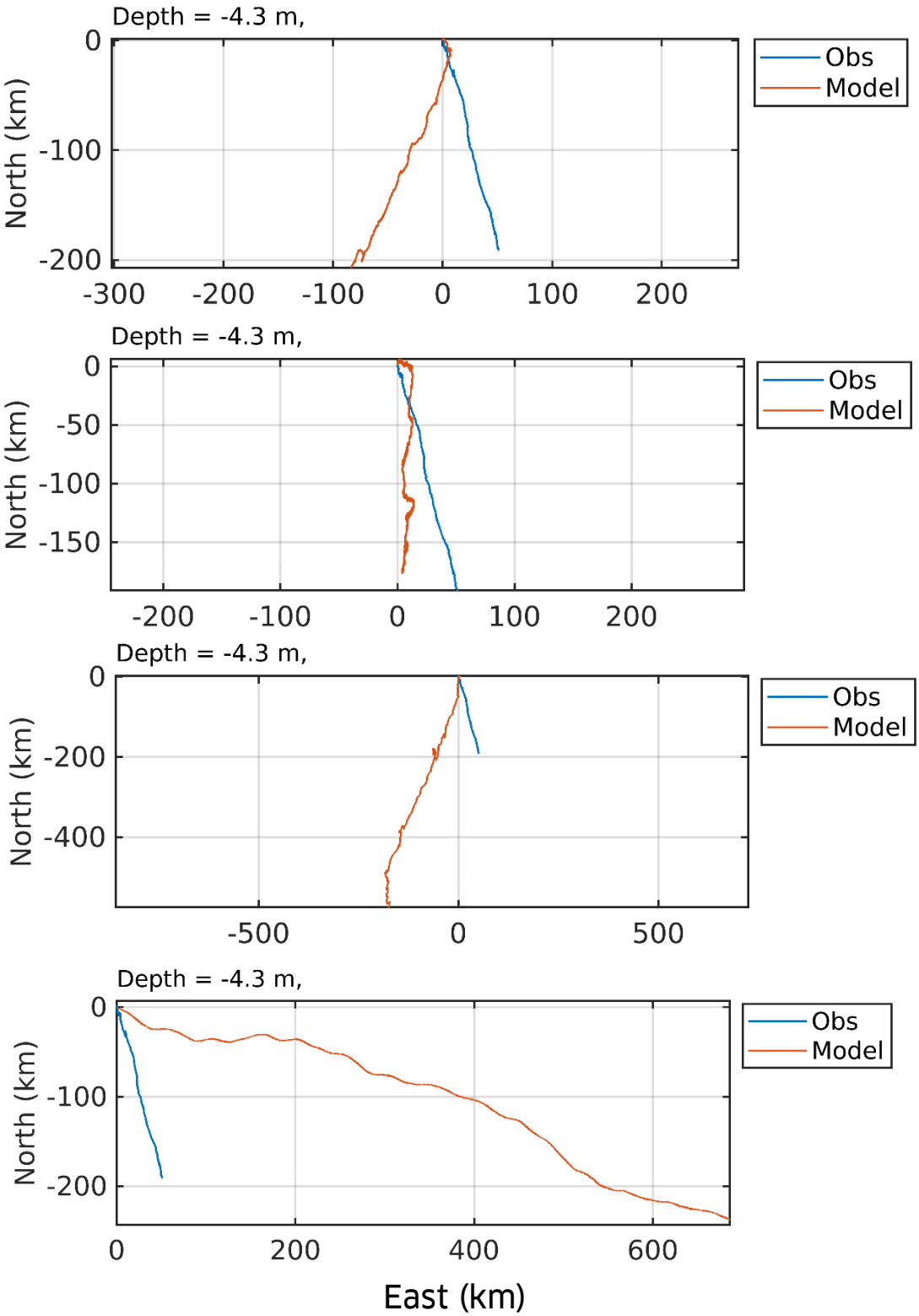

Figure 2.2. Cumulative vector plots of observed and modelled velocity in the near-surface layer from four hydrodynamic models: WLLSshuna (top); WeStCOMS (upper middle); WLLS 2021 (lower middle); WLLS Climatology (bottom). The observations are from the topmost valid ADCP cell; the modelled velocities have been interpolated in the vertical to the same depth.

3. Biophysical Modelling in Shuna Sound

3.1 Description of Particle Tracking Applications

3.1.1 BioTracker

SAMS' BioTracker code (Adams et al. 2012, 2014, 2016) was written to be driven using the outputs of the 'WeStCOMS' hydrodynamic model (Aleynik et al. 2016; Davidson et al., 2021). Both this model and the Scottish Shelf Model (SSM) (Wolf et al. 2016) are based on the Finite Volume Coastal Ocean Model (FVCOM) system (Chen et al. 2003), and as such the outputs are in a fairly similar form. However, some variables differ between the two models, see "Preliminary report on Loch Linnhe dispersal model simulations setup using Biotracker and SSM" for details of methodology used to couple this particle tracking model with the SSM.

Particles are moved horizontally subject to the water currents predicted by the hydrodynamic model, in addition to random turbulent diffusion. Larval particles inhabit the upper layer of the water column, and were not allowed to move vertically between layers (Cantrell et al. 2019). Stage durations are dependent on water temperature (which typically vary between 8 – 14 °C in this locality), with particles moving from the non-infective nauplii stage to the infective copepodid stage after accumulating 40 degree-days (1 day at 10 degrees C equates to 10 degree-days). Particles are removed from the simulation after 150-degree days (Johnsen et al. 2016, Samsing et al. 2019). Particles are viewed as "super-particles". This means lice particles are able to infect multiple sites; i.e., they do not end their movement when an infection/arrival event occurs. Particles also have a density (reduced over time by mortality) which governs the predicted overall spatial. Weighting of (number of lice represented by) each

larval particle was assumed to decay over time at a rate of 0.01 hr^{-1} (Amundrud & Murray 2009, Adams et al. 2016). The particle tracking code is available in an online repository (Adams 2019b).

3.1.2 FISCM

The tracking simulations undertaken by Marine Scotland Science were performed using FISCM (FVCOM i-state configuration model), an offline Lagrangian / individual based model for FVCOM (Ji et al. 2011; Liu et al. 2015). Particles positions are updated by FISCM using a 4th-order Runge-Kutta scheme to solve the Lagrangian equation of motion, here the time step was updated every 10 minutes. Boundary conditions ensure that particles stay within the model domain: when reaching the land at a new time step the particle position is reset to the previous time step and reflecting conditions are used for the seabed and the free surface. Finally, MSS adapted FISCM to allow particles to reproduce a diel vertical migration using the following coefficient set by the user. FISCM does not currently have a function for changing behaviour from non-infective to the infective stage, so this is done in a post processing stage, based on age in hours or degree days based on equations in Stien et al. (2005).

3.1.3 UnPTRACK

UnPTRACK (Unstructured mesh Particle TRACKing model) is a multi-purpose Lagrangian particle-tracking model designed to simulate the transport pathways of pelagic biota, chemical contaminants or particulate wastes using flow fields generated by unstructured mesh hydrodynamic (HD) models. UnPTRACK was developed from an earlier particle-tracking model that used hydrodynamic flow fields from regular grid models; the earlier version has been used to simulate the transport and dispersion of solute veterinary medicines (Willis et al., 2005) and dispersal of pelagic

organisms, including sea lice larvae (Gillibrand and Willis, 2007) and harmful algal blooms (Gillibrand et al., 2016a).

The model runs offline; velocity data to drive the model can be obtained from current meter observations or from hydrodynamic model simulations. Advection can be treated using either a fourth-order Runge-Kutta algorithm or a simple Euler approach. A random walk model is used to simulate horizontal and vertical eddy diffusion (Hunter et al., 1993; Visser, 1997). Various aspects of biological development (e.g., temperature-dependent stage development, mortality) and behaviour (e.g., vertical migration, low salinity avoidance) can be simulated. For chemical contaminants, a decay half-life can be simulated. The basic advection, diffusion and biological algorithms in the model have been described by Gillibrand and Willis (2007) and Gillibrand et al. (2016a).

For the simulations in this work package, UnPTRACK was run with the flow fields produced by all four hydrodynamic models. Particle behaviour included upward swimming during daylight hours (6am – 6pm) and avoidance of low salinity water by downward swimming when the salinity at the particle location was less than 20 psu. Upward swimming speeds were 1.25 cm s^{-1} for nauplii and 2.14 cm s^{-1} for copepodids (Brooker et al., 2018). In practice, these swimming speeds are used only in the initial period of first light, when the larvae return to the surface. Once at the surface, much lower swimming speeds would be sufficient to overcome vertical diffusion and keep the larvae at the surface i.e. the larvae do not swim at the prescribed speeds continuously for 12 hours. With a vertical diffusion coefficient of 0.001 m s^{-1} used by the models (Table 3.1), a swimming speed of 0.3 cm s^{-1} would be sufficient to keep the larva at the sea surface throughout most of the open sea, except at isolated locations where downwelling may occur. During hours of darkness (6pm – 6am), lice

particles were either passive, subject only to physical processes of advection and diffusion, or had a small sinking velocity of 0.1 cm s^{-1}.

3.2 Model Configuration

3.2.1 Common configuration parameters across all models

Some basic parameter settings were used by all the biological lice dispersal models and are listed in Table 3.1 with values shown.

Table 3.1: Summary of common setup parameters between the dispersal (particle tracking) models

Parameter	Value
Horizontal diffusion coefficient (m^2 s^{-1})	0.1
Mortality constant (h^{-1})	0.01

3.2.2 Differences in model configuration parameters

In a number of respects, the three dispersal models used were different (Table 3.2). Particles in the simulations using Biotracker were kept at a fixed depth at the surface (0 m), whereas the particles in the UnPTRACK and FISCM simulations allowed particles to move vertically in response to physical and biological triggers. These included vertical velocity, vertical diffusion, swimming behaviour and low salinity water avoidance (UnPTRACK only). Vertical velocities were taken directly from the hydrodynamic model output. Vertical diffusion was treated as a random walk algorithm, analogous to horizontal diffusion, with the vertical diffusivity of 0.001 m^2 s^{-1} in UnPTRACK, while in FISCM vertical diffusion varied with depth (Table 3.2). Swimming behaviour in UnPTRACK involved upward swimming during daylight hours (6am – 6pm) at swimming speeds appropriate for nauplii and copepodids (Table 3.2; Brooker et al. 2018).

While swimming, nauplii and copepodid particles also respond to low salinity water by swimming downwards (at the same speed as the upward swimming rate) until the salinity is greater than the threshold value (in these simulations, 20 PSU). At night, particles in UnPTRACK were passive, responding only to physical forcing (vertical advection and diffusion). Swimming behaviour in FISCM was a single upward swimming value, as it does not yet distinguish between nauplii and copepodids and distinguishing between the stages is carried out in a post processing step (Table 3.2).

Development rates were typically temperature dependent, with the nauplii stage moulting to the copepodid stage after 40 degree-days (Johnsen et al., 2016; Sandvik et al., 2020) and the total larval lifespan lasting either 150 (Johnsen et al. 2016, Samsing et al. 2019) or 170 (Sandvik et al., 2020) degree-days. However, water temperature was not simulated by the WLLSshuna model and a fixed development rate was used in these simulations (Table 3.2).

Not listed in Table 3.2 are the model time steps. Biotracker used a time step of 120s, FISCM 30 s, and UnPTRACK used 600 s with sub-time-stepping (down to 9.375 s) enabled when required to ensure particles were not lost.

Table 3.2: Summary of setup differences between biological (particle tracking) models

PT Model	HD Model	Vertical Diffusion (m^2 s^{-1})	Stage-development (nauplii, copepodid)	Vertical Velocity & upward swimming	Low Salinity Avoidance	Particle Source Rate (Np/src/hr)
Biotracker	WeStCOMS	N/A	Temperature-dependent (40 degree-days, 150 degree-days)	No (Fixed depth = 1m)	No	10
FISCM	WLLS 2021	Variable	Fixed (86 hours, 15 days)	Yes: Downward: 0 cm s^{-1}; Upward: 1.8 cm s^{-1}; 6am - 6pm	No	10
FISCM	WLLS Climatology	Variable	Fixed (86 hours, 15 days)	Yes: Downward: 0 cm s^{-1}; Upward: 1.8 cm s^{-1}; 6am - 6pm	No	10
UnPTRACK	WLLSshuna	0.001	Fixed (96 hours, 15 days)	Yes Nauplii: 1.25 cm s^{-1}; Copepodids: 2.14 cm s^{-1} 6am – 6pm	Yes (20 PSU)	50
UnPTRACK	WeStCOMS	0.001	Temperature-dependent (40 degree-days, 170 degree-days)	Yes Nauplii: 1.25 cm s^{-1}; Copepodids: 2.14 cm s^{-1} 6am – 6pm	Yes (20 PSU)	50
UnPTRACK	WLLS 2021	0.001	Temperature-dependent (40 degree-days, 170 degree-days)	Yes Nauplii: 1.25 cm s^{-1}; Copepodids: 2.14 cm s^{-1} 6am – 6pm	Yes (20 PSU)	50
UnPTRACK	WLLS Climatology	0.001	Temperature-dependent (40 degree-days, 170 degree-days)	Yes Nauplii: 1.25 cm s^{-1}; Copepodids: 2.14 cm s^{-1} 6am – 6pm	Yes (20 PSU)	50

3.3 Model Simulations

The model simulations covered the entire field sampling season of 2021, running from 1st April – 31st October 2021. Particle locations were output hourly. Analysis focussed on the period after 15th April, when a full generation of larval lice had been released and dispersed, providing an initial distribution of copepodids.

3.4 Calculation of lice densities

Modelled distributions of particles were converted to densities of larval sea lice in two ways. Firstly, numbers of particles (each representing a known number of sea lice larvae, decreasing with time) within a radial distance of each sampling location were counted and converted to lice density. The area of water within which particles were counted was simply calculated as the area of the circle of radius r ($A = \pi r^2$). Six values of r (75 m, 100 m, 150 m, 200 m, 250 m, 500 m) were used to explore the variability in this calculation method. Where the model allowed particles to move vertically, a 2 m depth window (sample depth +/- 1 m) was used to calculate densities at the sample depths (1 m, 6 m, 12 m). Modelled densities at the time of the sampled data were extracted for the comparison.

Secondly, predicted infective lice densities were calculated and presented as spatial maps across Shuna Sound region. Although the hydrodynamic and particle tracking models operated on unstructured meshes with variable cell sizes (Figure 3.1), the particle counts were performed on a rectangular grid with square cells. The advantage of using a regular grid to calculate densities is that the resolution and accuracy of the calculated densities is known and is the same across the domain; this is not the case when a variable mesh size is used. The boundaries used for the

counting grid were 161000 E – 187000 E and 690000 N to 729000 N (OSGB1936 coordinate reference system). The square counting cells were 100m x 100m in size when plotting instantaneous distributions ("snapshots") and 250 m x 250 m for the model inter-comparisons.

3.4.1 Number of Particles

The number of particles used in any particle tracking simulation needs careful consideration, and is dependent on the planned outputs. Particle simulations with planned output concentrations averaged over many time steps may need fewer particles than simulations where instantaneous distributions are required. There are no hard-and-fast rules, although Brickman et al. (2009) did note that "there is no excuse for using too few particles" and recommended that tests be done to check whether or not sufficient particles are being used. Calculating particle concentrations on a regular grid of square (or rectangular) cells mean concentration accuracy and resolution are constant across the grid domain, whereas those metrics are variable if an unstructured mesh is used to calculate concentrations.

One approach to setting particle numbers is to specify that a particle tracking model should be able to simulate a uniform horizontal distribution of the modelled variable, analogous to the requirement to be able to simulate a well-mixed vertical distribution (North et al., 2006). In the horizontal, that means that there should be enough particles in the simulation such that *each grid cell in the counting grid can be populated by at least one active particle*. A rule-of-thumb, therefore, might be that the number of active particles at every time step needs to be at least the number of wet grid cells in the counting grid. If temporal-mean values were being output, then the numbers of particles could arguably be reduced, depending on the averaging period. Ultimately, care needs to be taken so

that distributions of the modelled variable are fully represented and concentrations calculated at a numerical resolution that is adequate for the purposes of the modelling exercise. The resolution is determined by the density calculated when a grid cell on the counting grid is occupied by a single particle, which is, therefore, the lowest concentration that can be calculated. Since the number of lice represented by each particle reduces over time due to mortality, the resolution of the model increases with time (i.e. lower densities can be calculated).

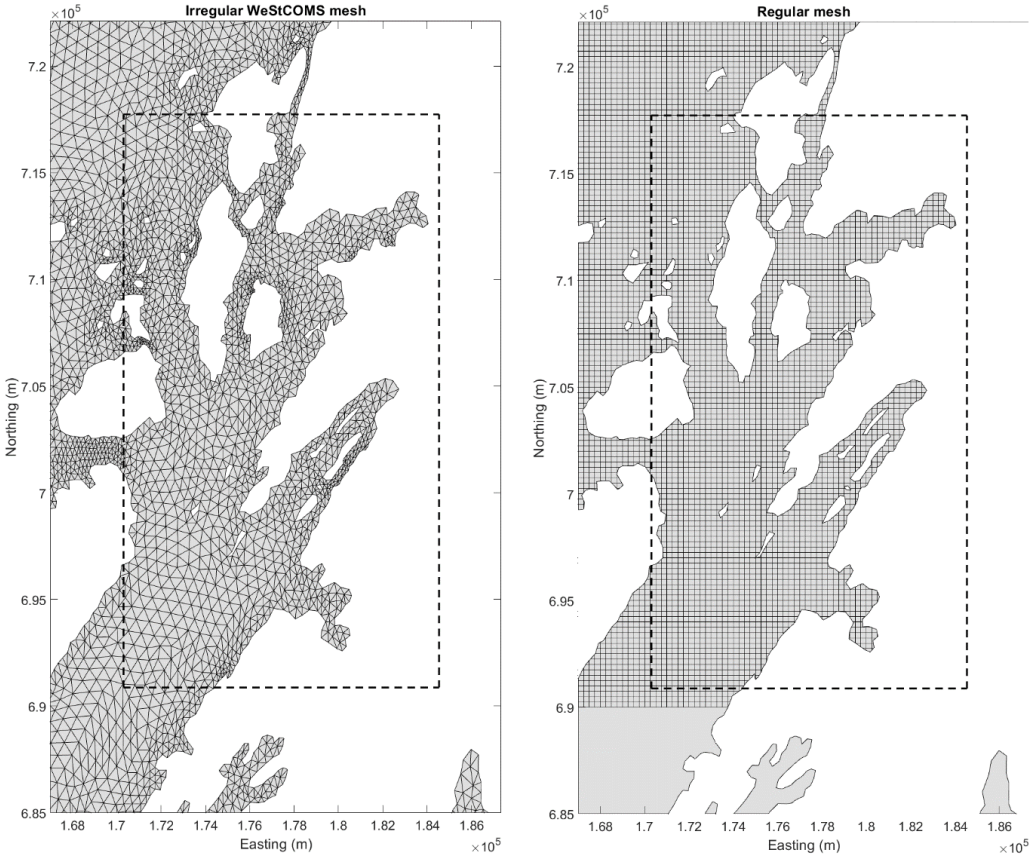

Figure 3.1. The unstructured mesh from the WestCOMS hydrodynamic model (left) and (right) the regular square mesh used for computation of lice density and prevalence.

Two approaches to particle releases are commonly used: 1) a fixed particle release rate per source per hour, whereby each particle represents a different number of lice depending on the source of lice at the time of

particle release; 2) using particles that represent a fixed number of lice (Np), whereby the number of particles released from each source each hour varies as the source of lice varies. An advantage with the latter approach is that the resolution of the calculated densities is known and is fixed. A disadvantage is that, in order to represent small sources of lice, a relatively low value of Np may be required, which means that large numbers of numerical particles may be required to represent large sources of lice, increasing the computational demand. However, the second approach means that the largest sources of lice are represented by the most particles, where the first approach may overplay the importance of smaller sources.

Both the approaches described above provide only a nominal, theoretical estimate of the resolution of the calculated lice densities. In practice, the number of particles used may be limited by the available computational power, but the sufficiency of the number of particles used in the simulation can, and should, be tested by checking that that the results of interest, whether time series of density or distributions of sea lice, do not change if the number of particles is further increased (Brickman et al., 2009; van Sebille et al., 2018).

In the present study, simulations used a fixed release rate of 10, 50 or 100 particles per source per hour. Tests assessing the effect of particle numbers on calculated lice densities were made for particle sources rates varying from 2 particles per source per hour to 100 particles per source per hour. Time series of lice densities at the six sampling locations (see §3.5) were cross-correlated against the time series using Np = 100 particles per source per hour (which was assumed to be most accurate). The resulting correlation coefficients, r, are shown in Table 3.3. The results demonstrate the stronger correlation with the Np = 100 simulation when larger numbers of particles are used, but also suggest that performance is dependent on location. The open water site in the Southern Approaches had lower values

of r than the sites within Shuna Sound , which were more enclosed. However, values of r also deteriorated with declining particle numbers for Loch Melfort. Ultimately, as many particles as the available computational power reasonably allows should be used for particle tracking simulations, and the implications for calculated outputs should be borne in mind.

Table 3.3. Correlation coefficients, r, between time series of modelled particle density at the six sampling locations (see §3.5) using different particle source rates. The time series for each source rate was correlated against the time series with N = 100 particles per source per hour.

	Particle Source Rate (N per source per hour)					
Site	100	50	20	10	5	2
Asknish Bay	1.000	0.994	0.986	0.978	0.951	0.890
Arsa Island	1.000	0.996	0.988	0.977	0.967	0.876
Loch Melfort	1.000	0.965	0.910	0.844	0.721	0.609
Musgan	1.000	0.996	0.992	0.985	0.969	0.904
NE Shuna	1.000	0.981	0.961	0.924	0.910	0.704
Southern Approaches	1.000	0.868	0.804	0.739	0.578	0.429

3.5 Aquaculture study area

Particles were released from the sites of eight active farms in Shuna Sound during summer 2021 (Figure 3.2), including the Mowi sites of Port na Cro (PNC), Poll na Gille (PNG) and Bagh Dail Nan Cean (BDNC) and the Kames sites of Kames Bay (East), Kames Bay (West), Shuna Castle, Shuna SW and North Moine. The locations and consented biomass of the sites are given in Table 1.1.

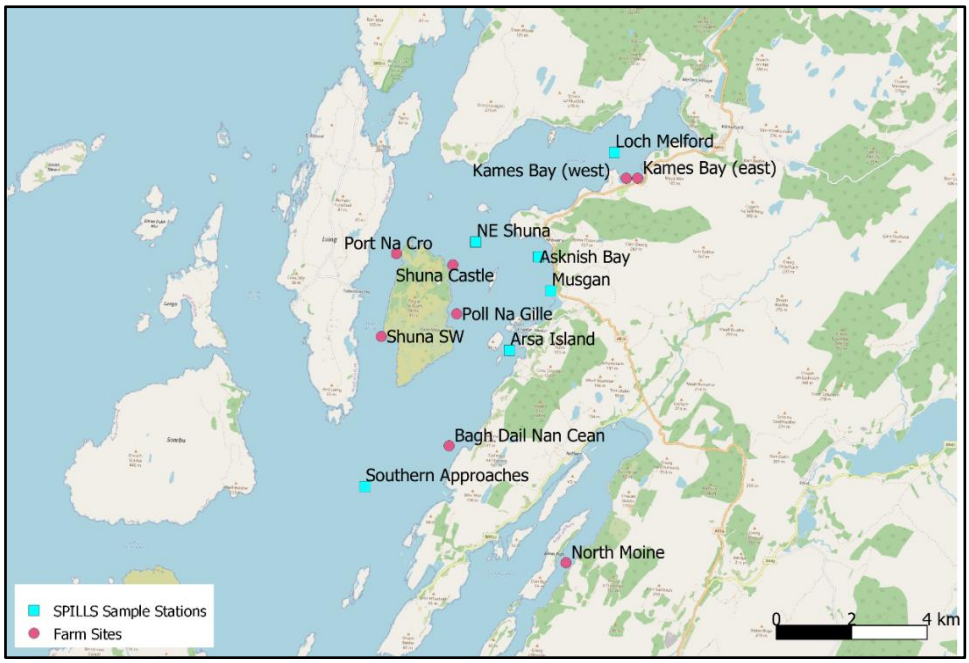

Figure 3.2. Map of Shuna Sound showing locations of particle release points (aquaculture sites, ●) and plankton tow sampling locations (■).

3.5.1 Estimating Lice Loads on Farms for Model Validation

Weekly counts of adult female lice and numbers of fish on each site were provided by farm operators on a weekly basis. From these values, and assuming that each adult female louse releases 30 larval lice per day (Stien et al. 2005, Murray et al., 2022), the numbers of lice larvae released each day from each site were estimated (Figure 3.3).

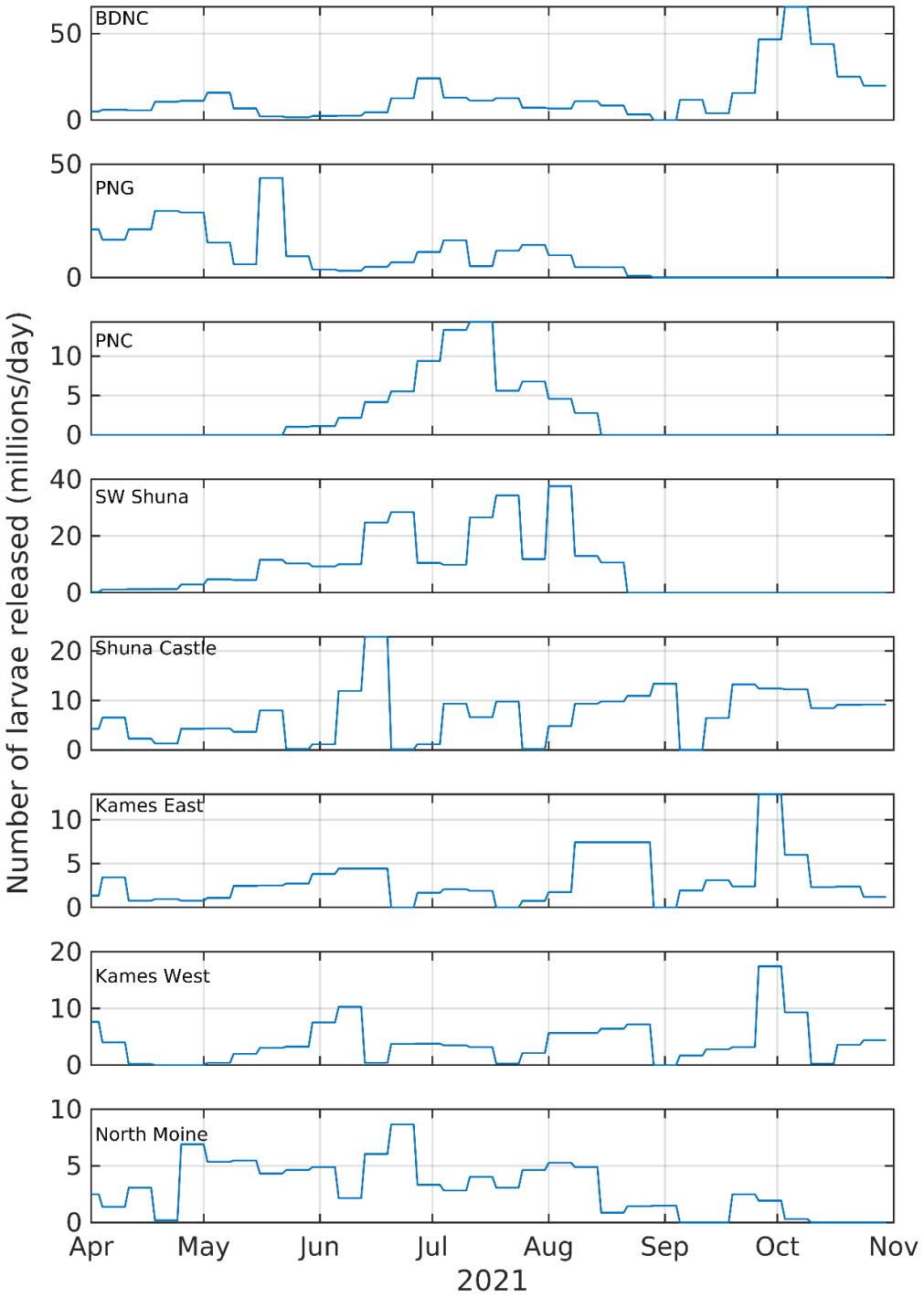

Figure 3.3 Estimated number of larvae released each day from each farm during the field sampling season from 1st April to 30th October 2021.

3.6 Biological field data

The sampling methodology is detailed in Reinardy et al. (2023) Section 2.4 “Field sampling main campaign”. Details of the sea lice captured

and identified are presented in section 3.3 “Sea lice larvae in the wild” in Table 2. Figure 3.4 summarises the measured infective sea lice densities from the field sampling. Essentially monthly surveys were undertaken, with a total of 348 valid samples collected for comparison with the model output. Many of these values were zero (Figure 3.4); see Reinardy et al. (2023) for a discussion of the challenges of sampling planktonic sea lice larvae.

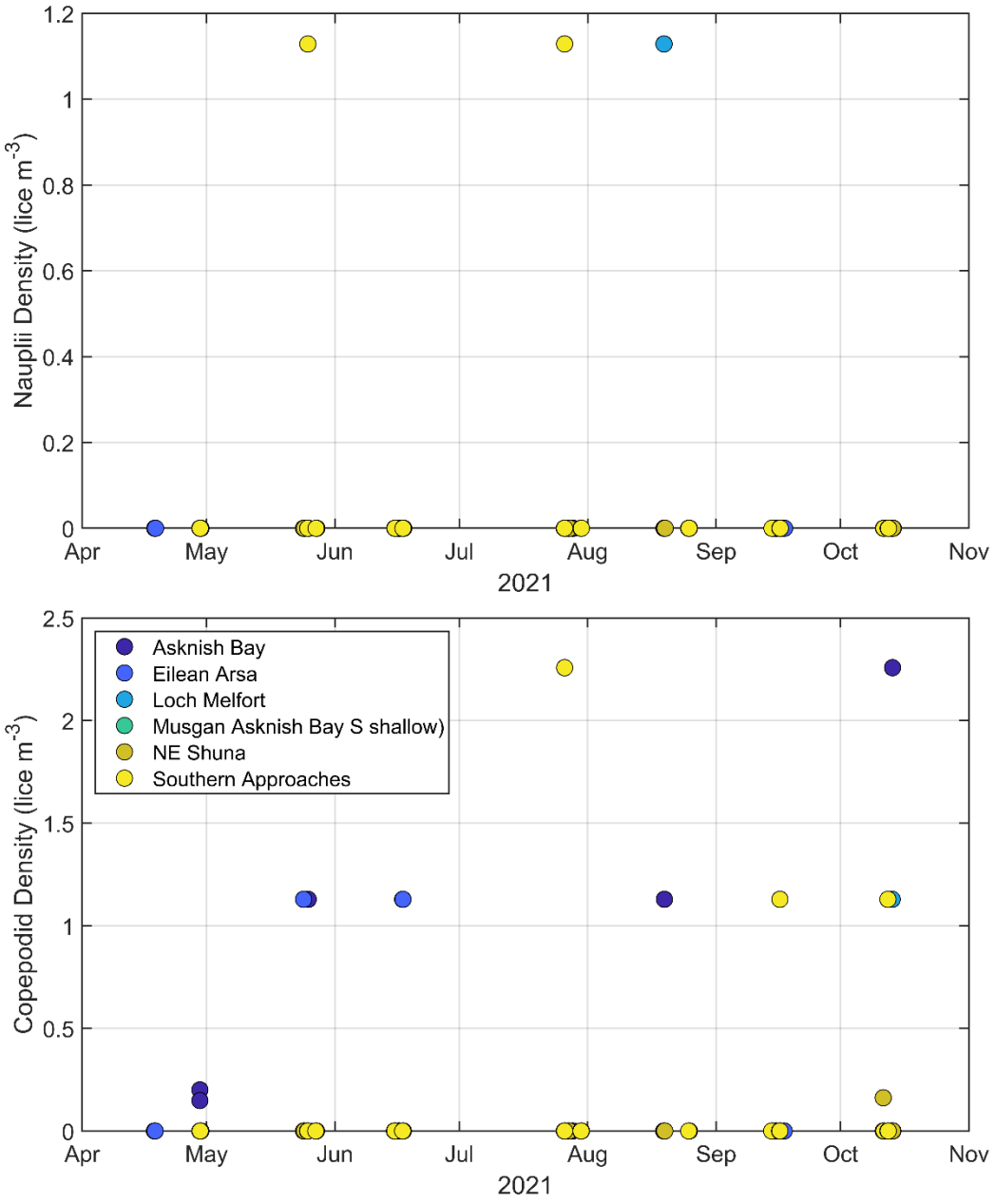

Figure 3.4 Measured nauplii (top) and copepodid (bottom) densities sampled at the six sites during the field sampling campaign in 2021.

3.7 Comparison of field data with particle tracking outputs

Key results from each model are presented in the following sections. Some selected further results are then presented to illustrate general conclusions that can be drawn from the modelling exercise.

3.7.1 UnPTRACK

Time series of modelled copepodid density from the coupled UnPTRACK-WLLSshuna model are shown in Figure 3.5. Lice densities were calculated at the same depth as the observed values using a 2 m depth window (i.e. observed depth ± 1 m). Modelled results were extracted from the time series at the time and depth of the observed data and plotted against the observed data in Figure 3.6.

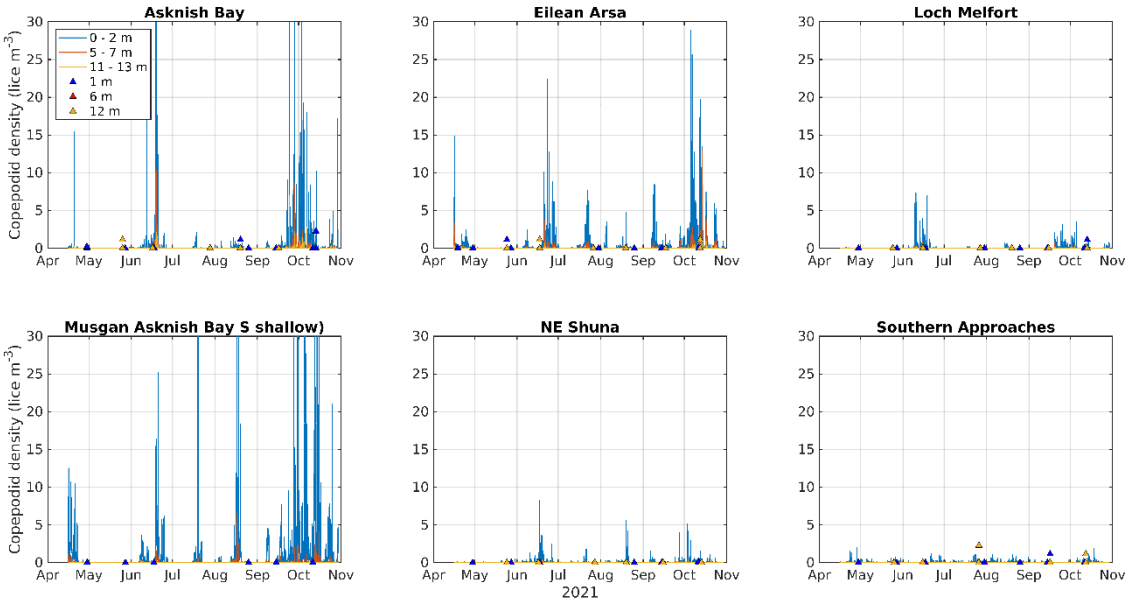

Figure 3.5. Comparison between UnPTRACK modelled and observed copepodid densities sampled at the six sites during the field sampling campaign in 2021. Each plot represents modelled values calculated using a 100 m radial distance centred on the sampling location (—), overlain by the observed values (▲) at the different depths. The UnPTRACK results here used the WLLSshuna hydrodynamic model. Note that the modelled densities were calculated over a depth window of 2 m.

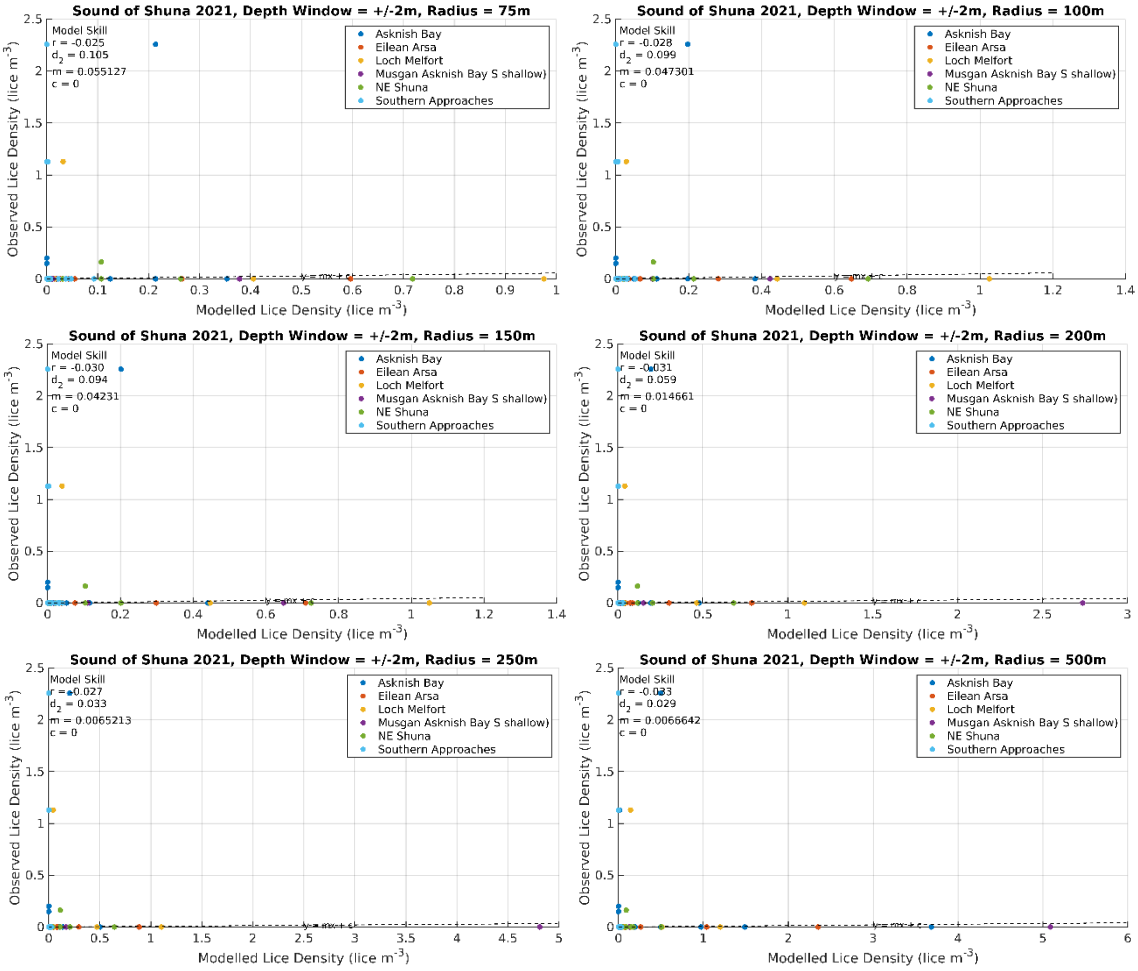

Figure 3.6 Comparison between UnPTRACK modelled and observed copepodid densities sampled at the six sites during the field sampling campaign in 2021. Each plot represents modelled values calculated using a different radial distance centred on the sampling location. The UnPTRACK results here used the WLLSshuna hydrodynamic model. Note that modelled lice densities are given per cubic metre (variable depth particles).

3.7.2 Biotracker

Time series of modelled copepodid density from the coupled Biotracker-WeStCOMS model are shown in Figure 3.7. Lice densities were calculated at the same depth as the observed values using a 2 m depth window (i.e. observed depth ± 1 m). Modelled results were extracted from the time series at the time and depth of the observed data and plotted against the observed data in Figure 3.8.

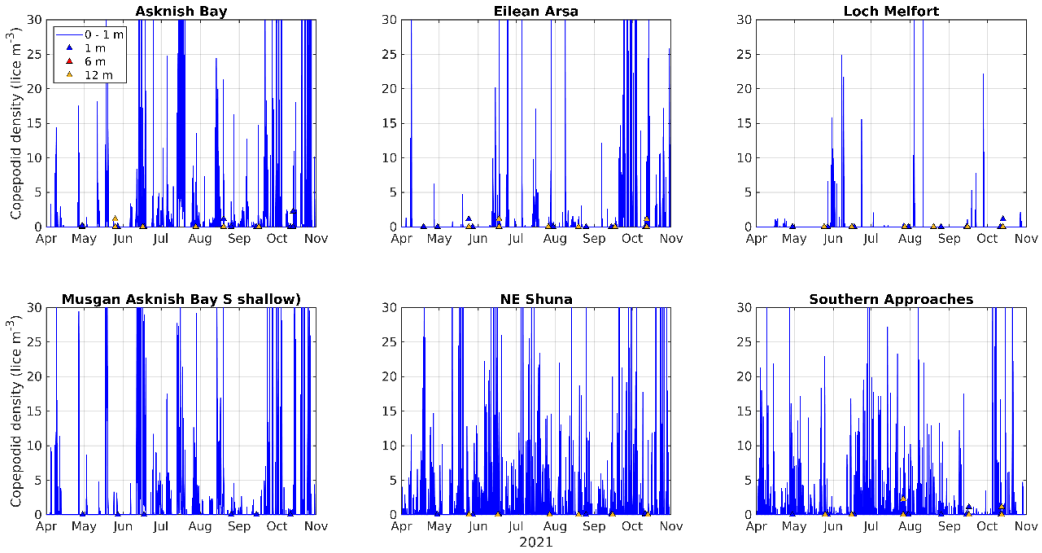

Figure 3.7 Comparison between Biotracker modelled and observed copepodid densities sampled at the six sites during the field sampling campaign in 2021. Each plot represents modelled values calculated using a 100m radial distance centred on the sampling location (—), overlain by the observed values (▲) at the different depths. The Biotracker results here used the WeStCOMS hydrodynamic model. Note that the modelled units of lice m^{-2} were converted to lice m^{-3} by assuming densities were calculated over a depth range of 1 m (fixed depth particles)

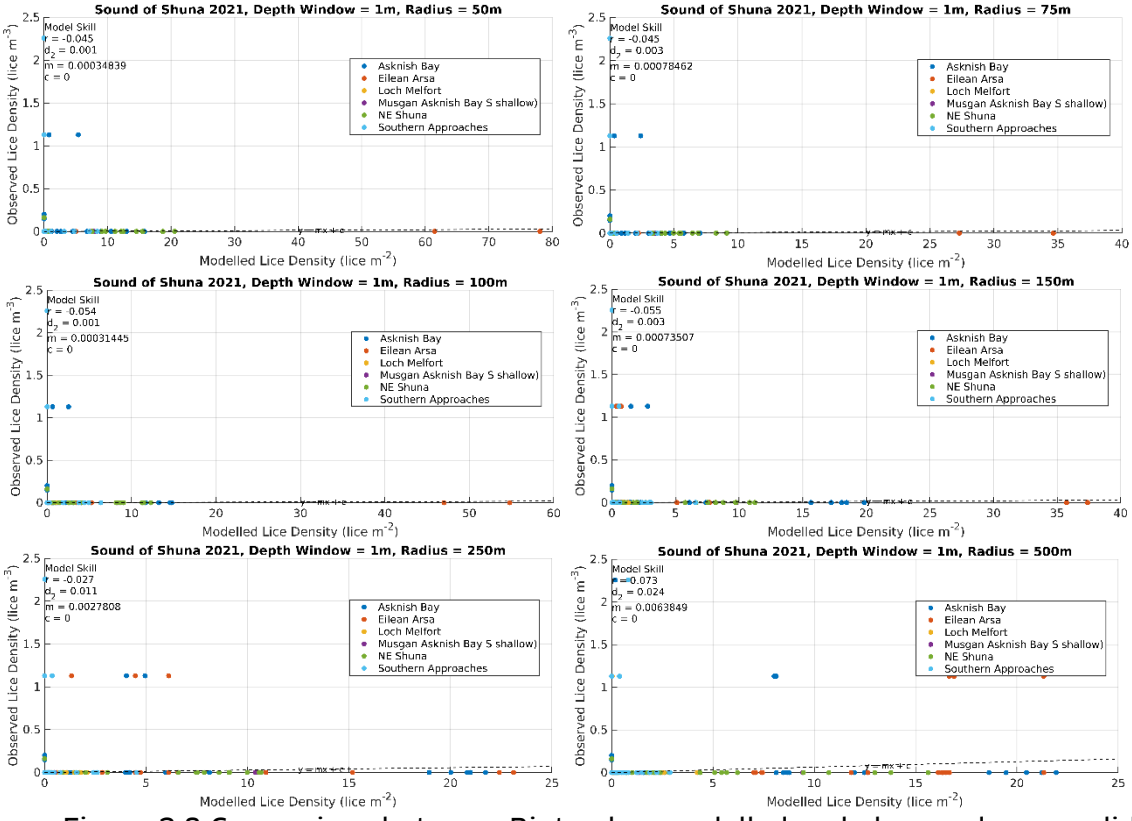

Figure 3.8 Comparison between Biotracker modelled and observed copepodid densities sampled at the six sites during the field sampling campaign in 2021. Each plot represents modelled values calculated using a different radial distance centred on the sampling location. The Biotracker results here used the WeStCOMS hydrodynamic model. Note that modelled lice densities are given per square metre (fixed depth particles).

3.7.3 FISCM

Time series of modelled copepodid density from the coupled FISCM-WLLS2021 model are shown in Figure 3.9. Lice densities were calculated at the same depth as the observed values using a 2 m depth window (i.e. observed depth ± 1 m). Modelled results were extracted from the time series at the time and depth of the observed data and plotted against the observed data in Figure 3.10.

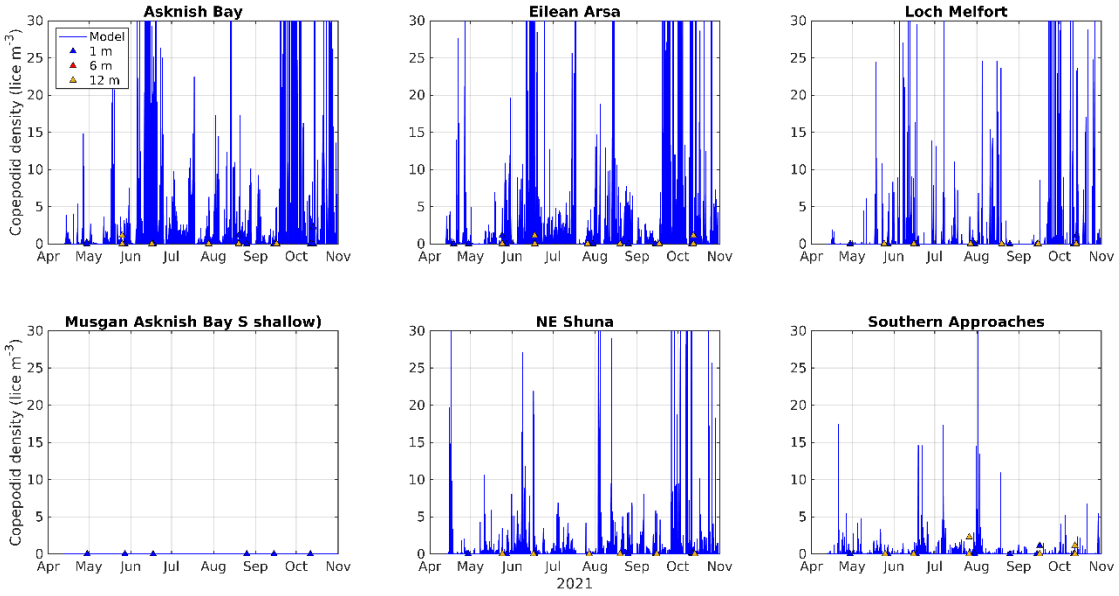

Figure 3.9 Comparison between FISCM modelled and observed copepodid densities sampled at the six sites during the field sampling campaign in 2021. Each plot represents modelled values calculated using a 100m radial distance centred on the sampling location (—), overlain by the observed values (▲) at the different depths. The FISCM results here used the WLLS-2021 hydrodynamic model. Note that the modelled units of lice density are lice m^{-2} (integrated over depth).

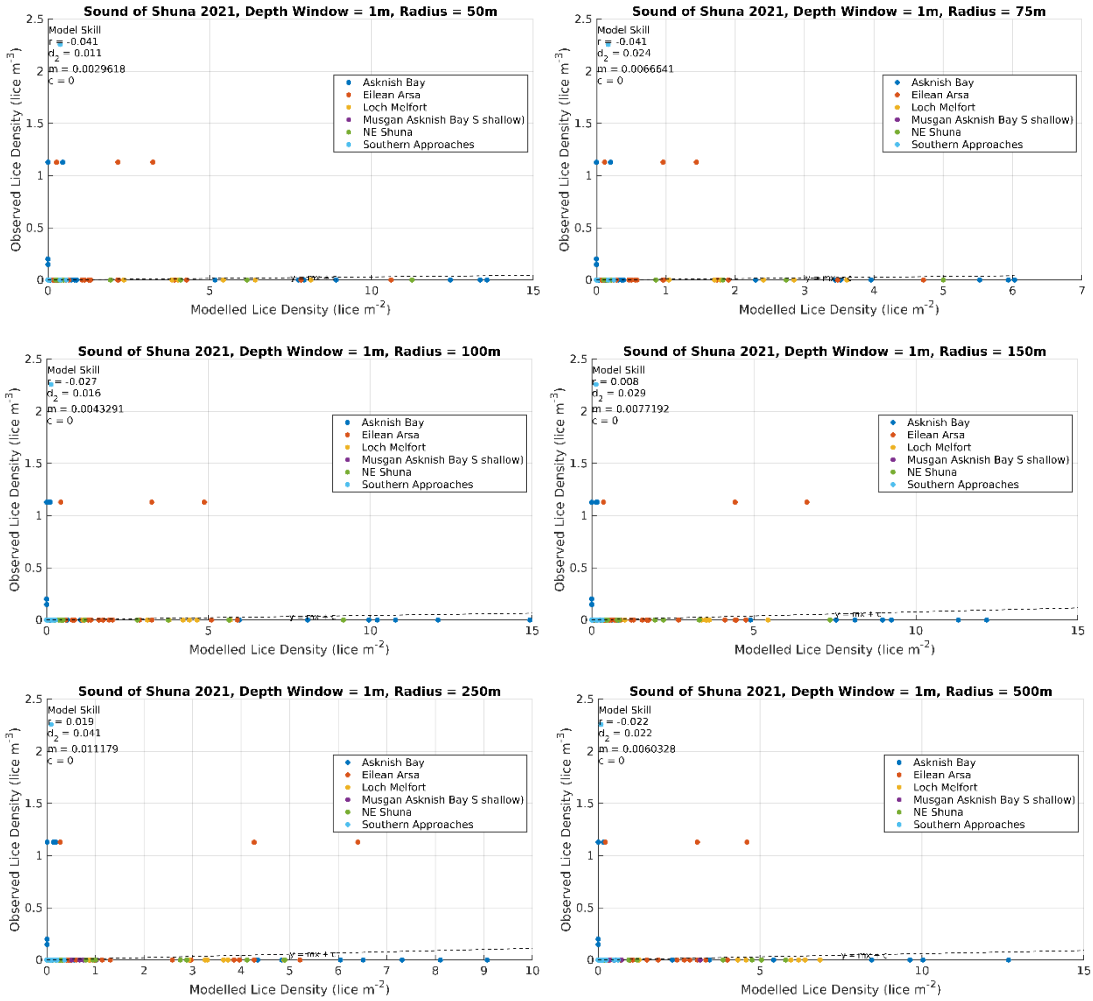

Figure 3.10 Comparison between FISCM modelled and observed copepodid densities sampled at the six sites during the field sampling campaign in 2021. Each plot represents modelled values calculated using a different radial distance centred on the sampling location. The FISCM results here used the WLLS2021 hydrodynamic model. Note that modelled lice densities are given per square metre (particle counts integrated over depth).

3.7.3 Combined Model

The modelled lice densities from the three coupled systems presented in §3.7.1 - §3.7.3 were averaged (arithmetic mean) to provide a "Combined Model" dataset. For this purpose, all modelled densities were calculated by integrated particle numbers over the whole water depth, so that the units are lice m^{-2}. Time series of modelled copepodid density from the Combined model are shown in Figure 3.11. Lice densities were calculated at the same depth as the observed values using a 2 m depth window (i.e. observed depth ± 1 m). Modelled results were extracted from the time series at the

time and depth of the observed data and plotted against the observed data in Figure 3.12.

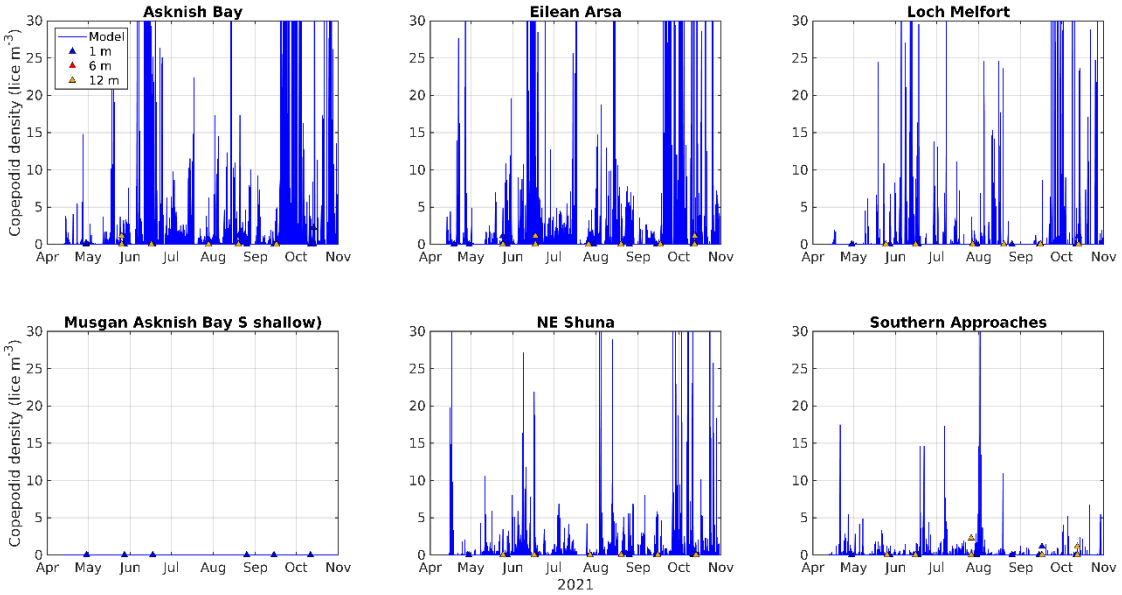

Figure 3.11 Comparison between the combined modelled and observed copepodid densities sampled at the six sites during the field sampling campaign in 2021. Each plot represents modelled values calculated using a 100m radial distance centred on the sampling location (▬), overlain by the observed values (▲) at the different depths. Note that the modelled units of lice density are lice m^{-2} (integrated over depth).

3.8 Modelled Mean Distributions of Infective Lice

The modelled mean distributions of infective lice, averaged over the entire model simulations from 16th April – 30th October 2021, are shown in Figures 3.13 and 3.14. While these are long periods over which to average, and do not therefore represent likely densities that wild fish may encounter, they do illustrate the differences in predicted distributions that different models may produce, even after such long averaging. The simulations from the Biotracker-WeStCOMS and FISCM-WLLS2021 model systems are shown in Figure 3.13. The UnPTRACK PTM was run with three hydrodynamic models for 2021 (Figure 3.14); since the WLLSshuna model does not include a temperature variable and cannot, therefore, simulate a temperature-dependent development, the larval development in all three

runs was set to a fixed development rate (see WLLSshuna in Table 3.2) to ensure biological consistency between the model runs.

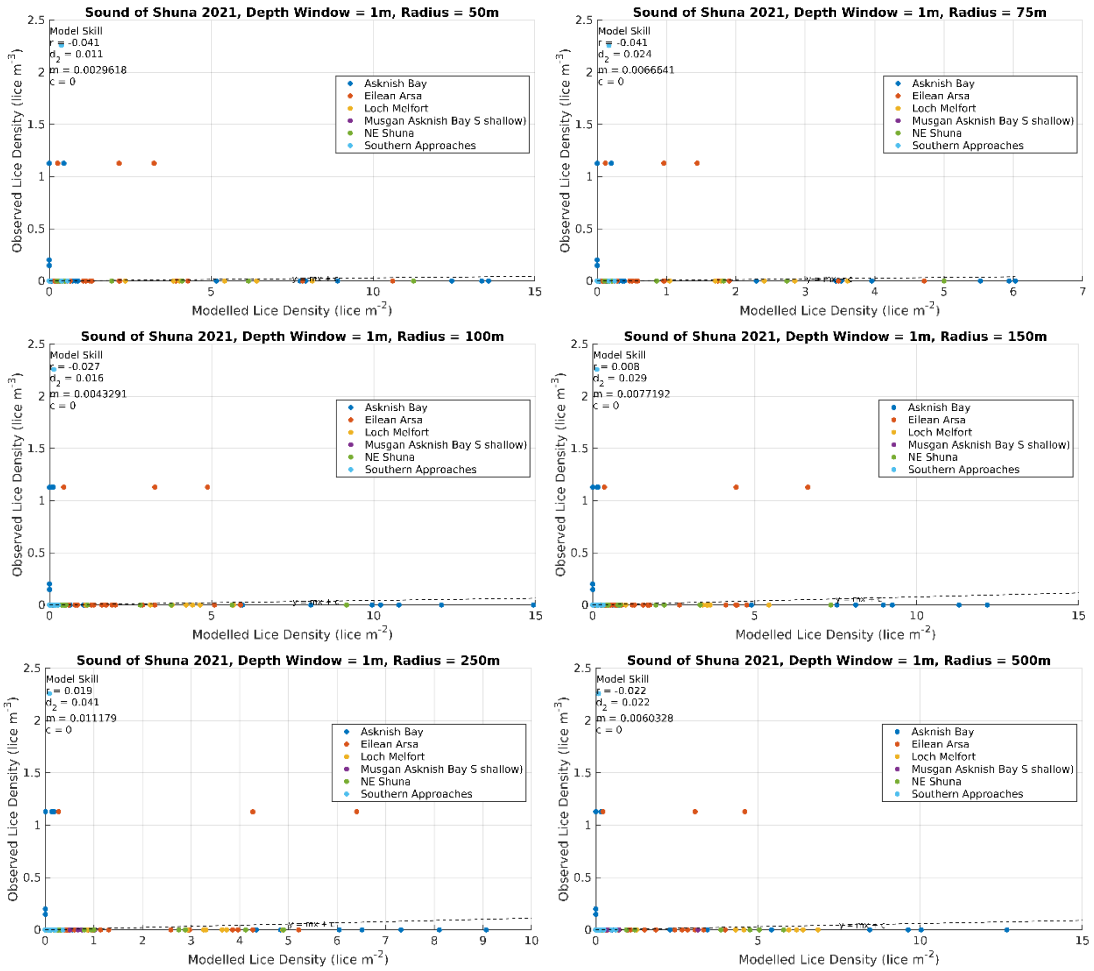

Figure 3.12 Comparison between the combined modelled and observed copepodid densities sampled at the six sites during the field sampling campaign in 2021. Each plot represents modelled values calculated using a different radial distance centred on the sampling location. Note that modelled lice densities are given per square metre (particle counts integrated over depth).

The modelled distributions showed some significant differences, although there were also some commonalities. Modelled infective lice densities were elevated in the waters to the east of Shuna Island in all simulations, with most models showing further accumulation of lice in Asknish Bay and the shoreline around Croabh Haven. Several of the model combinations also predicted elevated lice densities to the west of Shuna Sound at the north end of the Sound of Luing; however, this was not

common to all model results. Some notable differences included densities in Loch Melfort, which were predominantly zero in the runs using the WestCOMS model and higher in the other models; the WestCOMS model used freshwater inputs from an operational meteorological model, whereas the other models used a river flow climatology, which could explain differences towards the heads of the lochs (e.g. Loch Craignish) in the model domains.

Interestingly, given that the biological model was identical in each case, the UnPTRACK simulations also produced some significant differences in the predicted distributions due solely to the different hydrodynamic models (Figure 3.14). This is perhaps not surprising: although absolute differences between the modelled flow fields from the various hydrodynamic models may be relatively small, the integration of small differences over the lifetime of a sea louse (*ca.* 15 days) may result in substantially different transport pathways for an individual, and perhaps radically different predicted infective sea lice distributions.

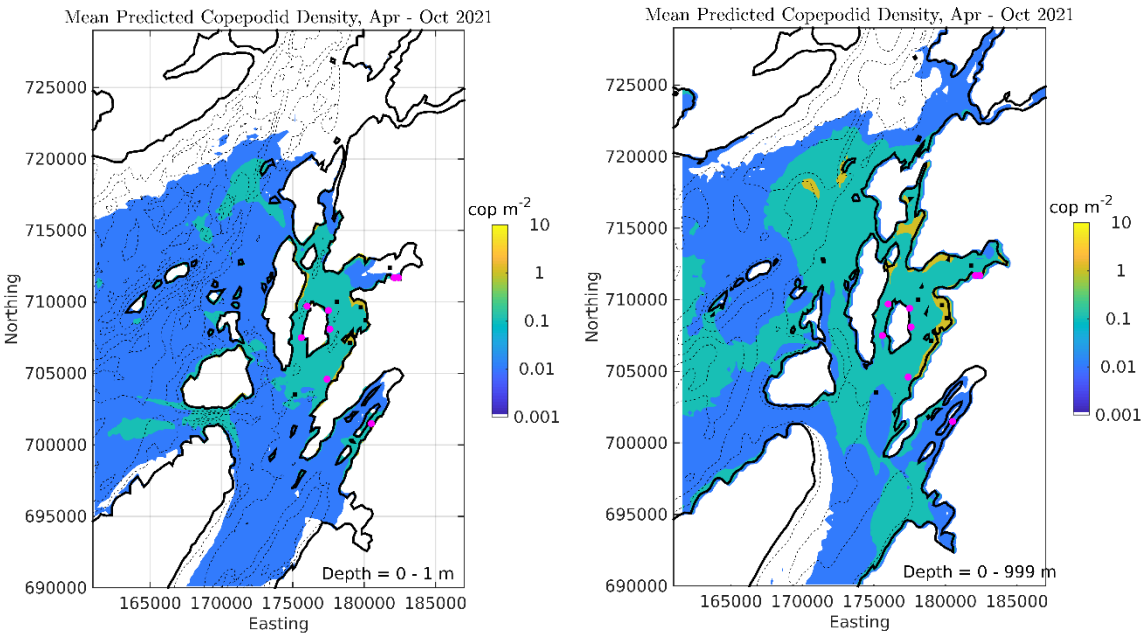

Figure 3.13 Simulation-mean infective lice density distributions for the Biotracker-WeStCOMS (left) and FISCM-WLLS2021 (right) simulations, from 16th April – 30th October 2021.

Combining the model results into an ensemble-mean (5 members) smooths out some of the idiosyncrasies between models and illustrates regions of the domain where the results are more consistent, at both high and low densities (Figure 3.15). Elsewhere, where predictions are more varied, the standard deviation (presented here as the coefficient of variation, CV, defined as the standard deviation divided by the mean) across the ensemble provides a measure of the consistency of the results. Low values of CV represent areas where consistency between models is low (standard deviation is small compared to the mean), whereas high values of CV indicate areas where there is considerable variability between the model predictions. For the present 5-member ensemble of Shuna Sound in 2021, the CV is low (less than 0.5) in the central Shuna Sound , in the waters south of Luing, and in the central outer Firth of Lorne. Values of the CV are high (greater than 1.0) at the heads of Loch Melfort, Loch Craignish and in Loch Crinan, reflecting the different predictions for these areas from the different models (Figures 3.13 and 3.14). Note that values of the CV can be high due to low values of the ensemble-mean; this is likely the cause of the high CV values in the waters adjacent to Mull in the north-west of the plot (Figure 3.15).

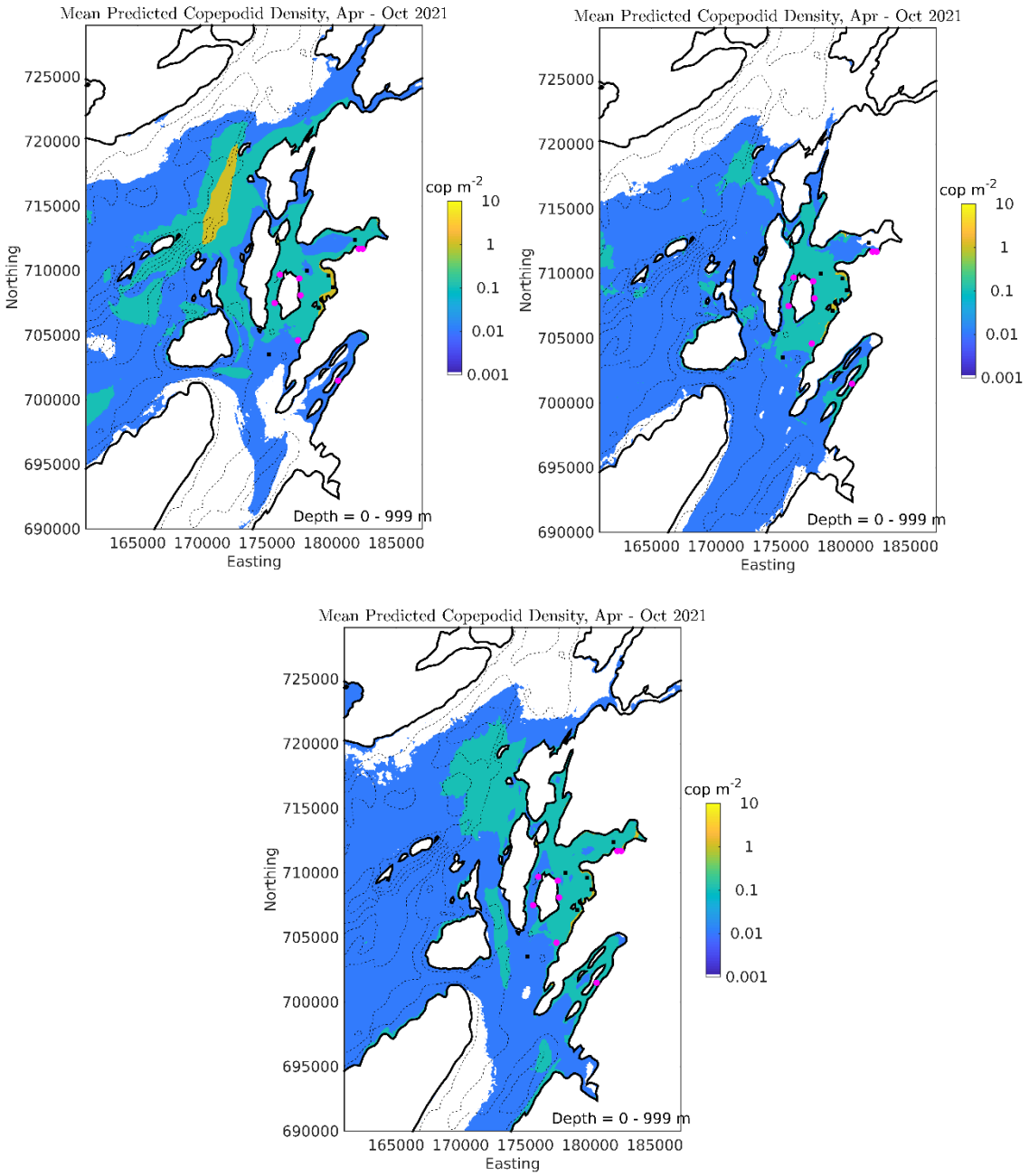

Figure 3.14 Simulation-mean infective lice density distributions from the UnPTRACK model using the WLLSshuna (top left), WeStCOMS (top right) and WLLS2021 (bottom) hydrodynamic models from 16th April – 30th October 2021. For these simulations, UnPTRACK used a fixed larval development rate with both the WeStCOMS and WLLS2021 models to match the WLLSshuna simulation (Table 3.2).

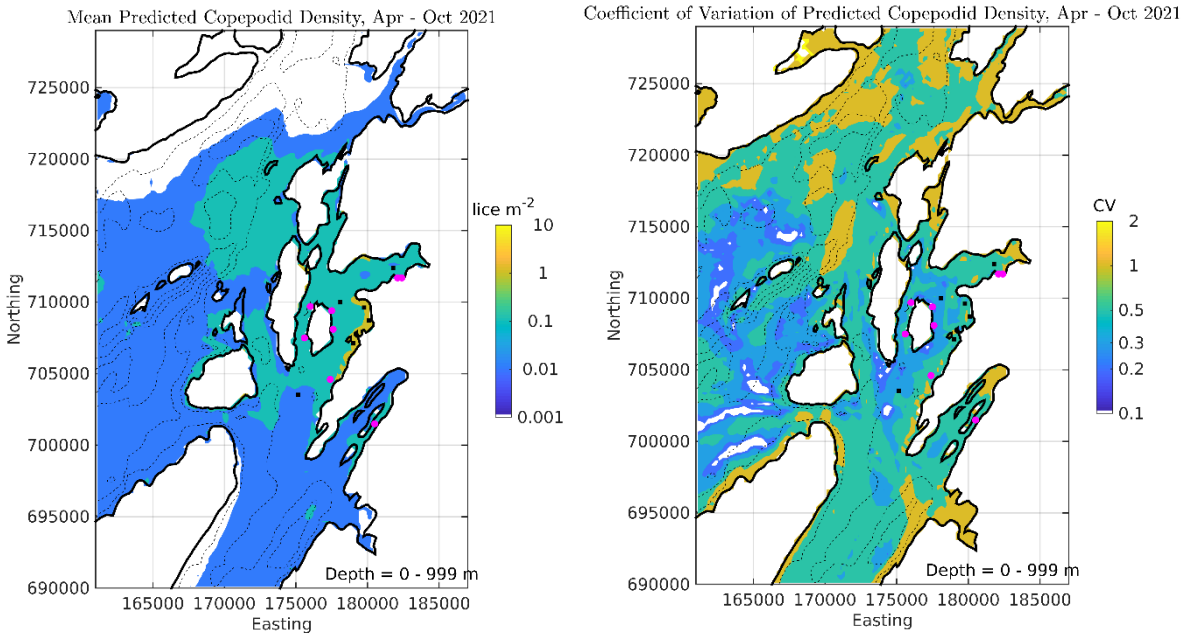

Figure 3.15 Ensemble-mean (left) and coefficient of variation (CV) (right) of infective lice density distributions from the combined (averaged) model dataset from all five simulations shown in Figures Figure 3.13 and 3.14 for 16th April – 30th October 2021.

3.9 Evaluation and Discussion of Bio-Physical Modelling

The comparisons between predicted lice densities from all model combinations, including the additional simulations highlighted in Table 3.2 but not shown in §3.7, and the observed planktonic lice densities were all quantitatively poor. The data were heavily zero-inflated, evident from Figures 3.5 – 3.10 and discussed by Reinardy et al. (2023). In contrast, the modelled lice densities, while zero more than 50% of the time, were also quite frequently non-zero. The temporal variability in modelled lice densities from individual models is evident (Figures 3.5, 3.7 and 3.9) and is also apparent when the model predictions are combined into an arithmetic mean density (Figure 3.11).

No significant linear regression was achieved between the modelled lice densities and the observed planktonic lice data (Figures 3.6, 3.8, 3.10). The calculated Pearson correlation coefficients, r, were typically close to

zero and, again, were not improved by combining the model output (Figure 3.12). Although the results shown above are for the infective copepodid stage only, the results were not better for the nauplius stage.

The poor agreement between model results and planktonic lice data is thought to be due to the larval lice distributions being highly spatially and temporally variable. The temporal variability in copepodid distributions is illustrated in Figure 3.16 for 13th October 2021, as planktonic larvae are moved around by tidal and wind-driven currents. On that date, a infective lice concentration of 2.25 lice m^{-3} was measured at Asknish Bay (Figure 3.4), so lice were present within the bay at that time. The variability is more apparent in animations of the model results, which can be viewed online at: http://marine.gov.scot/information/salmon-parasite-interactions-linnhe-lorn-and-shuna-spills

High spatial and temporal variability in sea lice larvae distributions is not unexpected, given that the larvae are thought to proactively stay at the sea surface (at least during daylight hours) and are therefore subject to complex ocean dynamics arising from the combination of tidal, wind-driven and freshwater-driven dynamics. The presence of fronts in the coastal zone, some of which will be highly transient and some of which may be quasi-permanent, may lead to accumulations of lice larvae during daylight hours (when larvae are staying at the surface) which again may be temporary or more long-lasting. The response of lice distributions to wind forcing is illustrated in Figure 3.17. In May, lice levels inside Shuna Sound were very low, with much of the area having a modelled mean density of less than 0.01 lice m^{-2}. Densities of infective lice exceeded 0.1 lice m^{-2} for less than 10% of the month in the waters east of Shuna Island (as evidenced by the prevalence plot in Figure 3.17). During May, the wind forcing was predominantly northerly (Figure 3.18), and clearly drove a strong export of lice from Shuna Sound before they reached the infective stage. In contrast,

in June, winds were predominantly southerly (Figure 3.18) and mean densities in Shuna Sound were substantially higher, exceeding 1 lice m^{-2} in some areas, with densities exceeding 0.1 lice m^{-2} occurring up to 50% of the month (Figure 3.17). During this period, larval lice were retained by the wind forcing within Shuna Sound , and densities were higher as a results.

The variability in modelled infective densities arises, then, as a result of interactions between tidal and wind-driven currents and baroclinic features such as fronts, and leads to high temporal and spatial variability. Similar findings and conclusions regarding the high spatiotemporal variability of sea lice distributions were reported by Skarðhamar et al. (2019). At the sampling locations in Shuna Sound , infective lice numbers were typically very low, but could increase dramatically for short periods. The box-and-whisker plot (Figure 3.19) illustrates the modelled variability, with mean lice densities being less than 0.5 lice m^{-3} at five of the sites, the exception being Musgan (Table 3.4). These mean values were distorted by the high maximum values; the median modelled infective lice densities were typically zero. For a large proportion of time, generally at least 50%, modelled infective lice densities in the surface 2 m were zero (Table 3.4).

It should be noted that the zero densities may be partly a function of the number of numerical particles used in the simulation. For the UnPTRACK simulations, the particle source rate was 50 particles per source per hour.

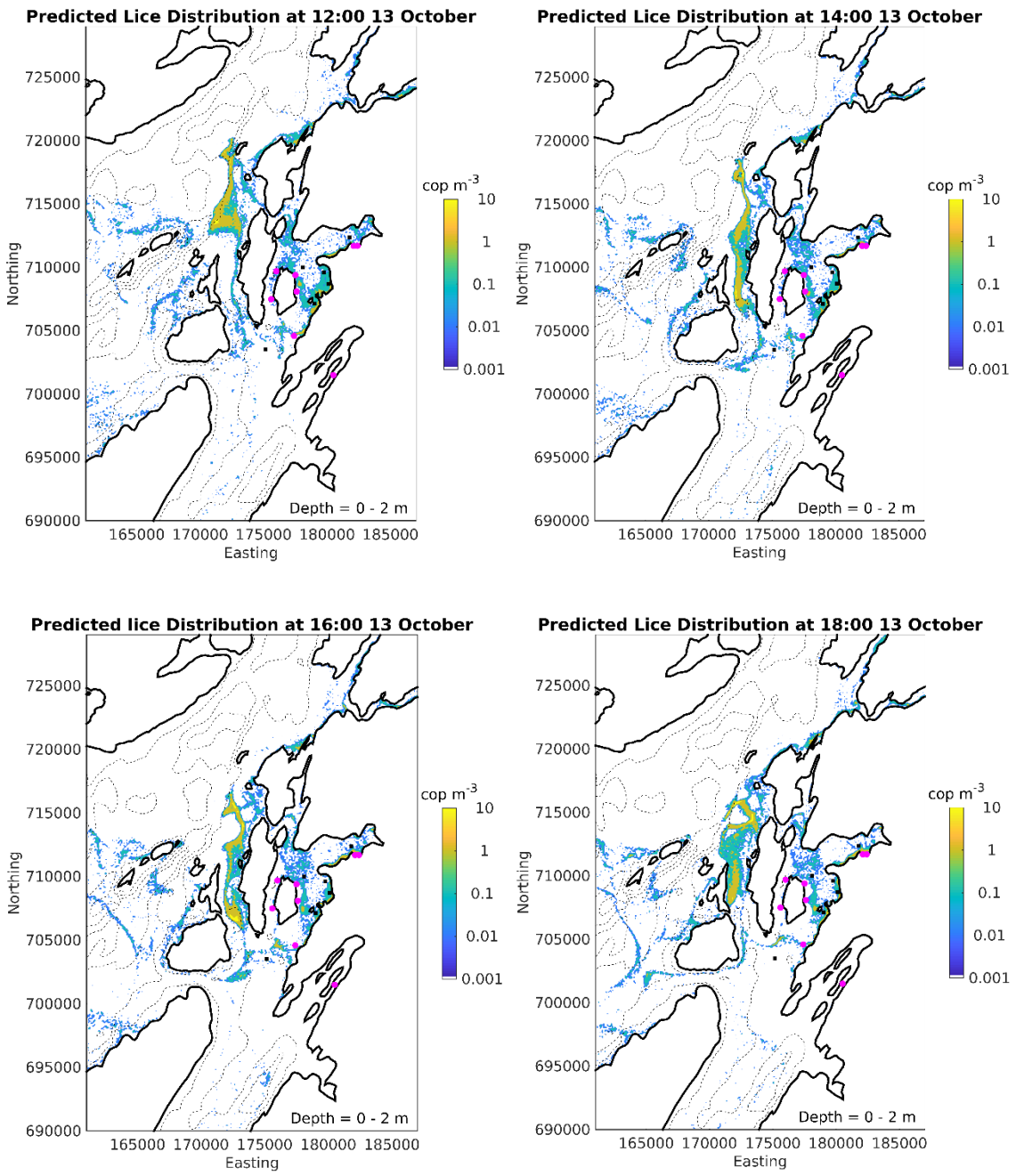

Figure 3.16. Modelled infective lice distributions at two-hourly intervals during the afternoon of 13th October 2021. The plots illustrate the continually changing distribution of lice in Shuna Sound due to advection by the combination of tidal, wind-driven and freshwater-driven currents. The densities were calculated on a 100m x 100m grid.

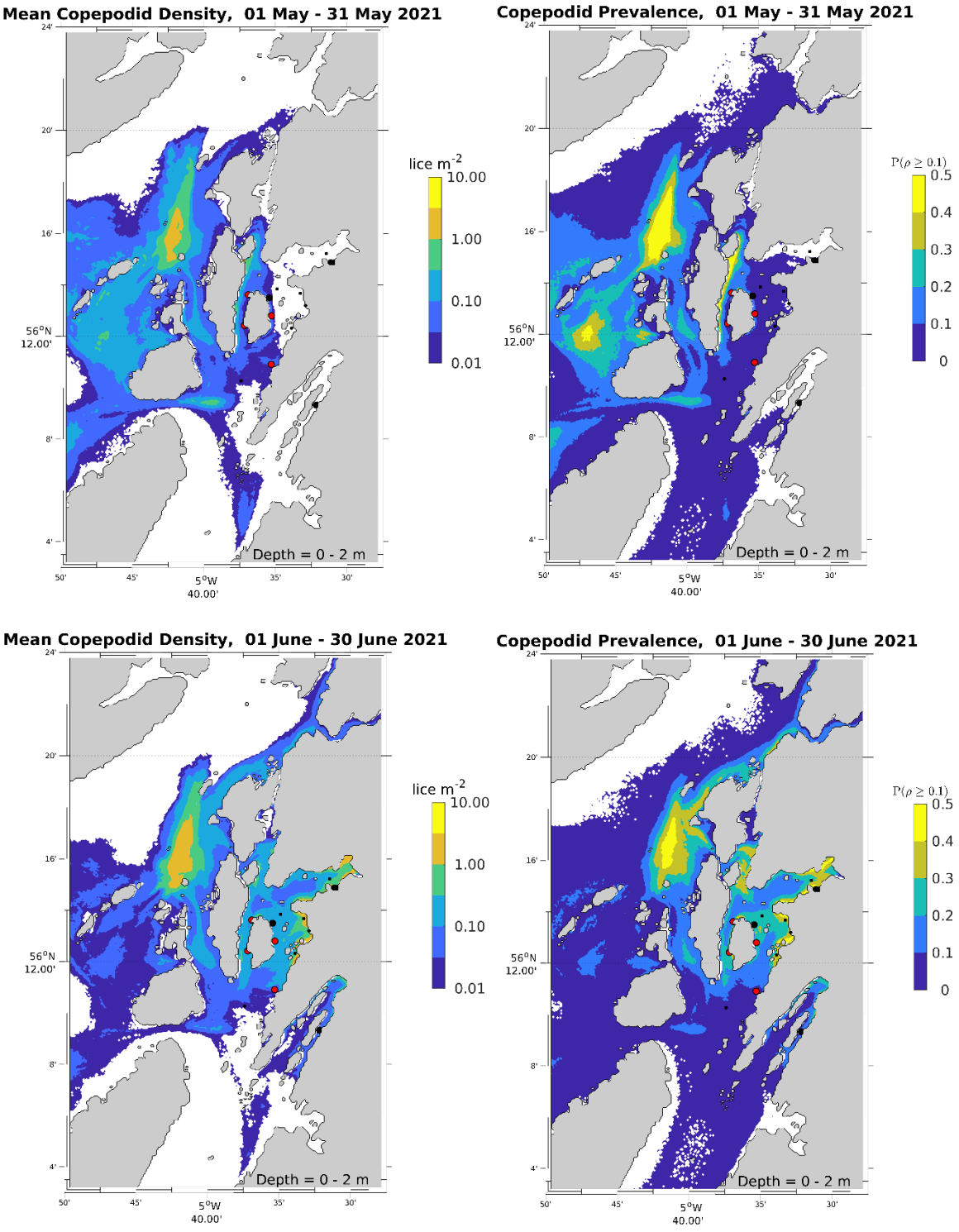

Figure 3.17 Modelled monthly-mean infective lice density distributions (left) and prevalence of densities exceeding 0.1 lice m^{-2} (right) for May 2021 (top) and June 2021 (bottom). The model system was UnPTRACK – WLLSshuna.

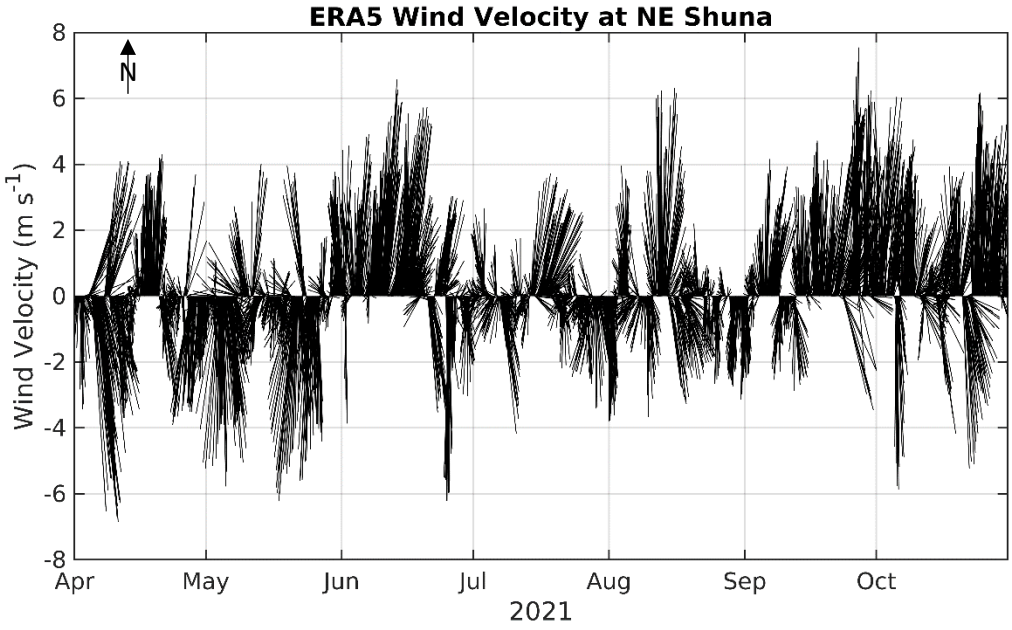

Figure 3.18 Wind vectors at the NE Shuna sampling location from the ECMWF ERA5 reanalysis for April – October 2021.

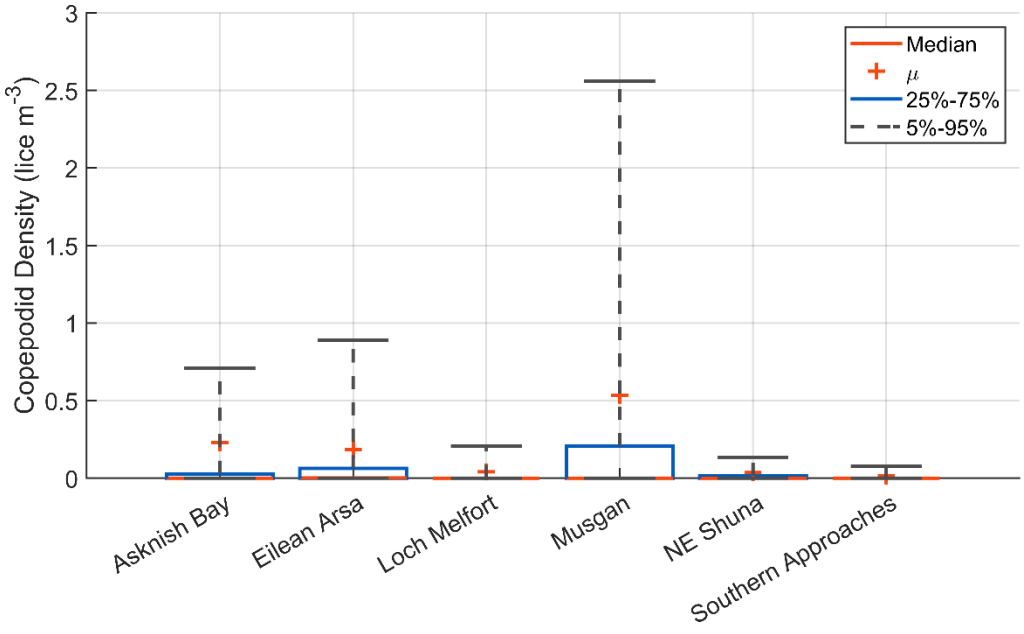

Figure 3.19 Box and whisker plot for modelled infective lice densities (lice m^{-3}) at each site for April – October 2021. The model system was UnPTRACK – WLLSshuna, and the densities were calculated over the surface 2 m of the water column (depth = 0 – 2 m). The plots shows the mean (μ) and median modelled density at each site, with the 25th percentile and 5th percentile ranges also shown.

Table 3.4 Summary statistics of the modelled infective lice densities (lice m^{-3}) at the six sampling stations in Shuna Sound during April – October 2021 using a 100 m radial distance and averaging over the surface 2 m water depth. The model system was UnPTRACK – WLLSshuna. The "No. zeros" row indicates the percentage of time that the modelled infective lice density at each site was zero.

	Asknish Bay	Eilean Arsa	Loch Melfort	Musgan	NE Shuna	Southern Approaches
Mean	0.458	0.367	0.080	1.071	0.070	0.028
Median	0.000	0.003	0.000	0.000	0.000	0.000
St. Dev.	2.647	1.420	0.376	4.439	0.310	0.109
95^{th} percentile	0.710	0.891	0.208	2.558	0.135	0.077
Maximum	67.202	28.889	7.395	108.167	8.329	2.020
No. zeros (%)	58.892	48.678	77.035	52.041	59.949	75.344

The same variability in modelled infective lice densities was evident in the results from the other model systems. For Biotracker-WeStCOMS and FISCM-WLLS2021, calculated densities were depth-integrated (units lice m^{-2}) giving generally higher values than UnPTRACK-WLLSshuna, since all lice particles are counted and densities are not divided by the water depth.

Nevertheless, the variability is similar, with Biotracker-WeStCOMS showing low median and mean values and high maximum values (Figure 3.20); for this model system, modelled infective lice densities at each sample location were zero for at least 60% of the time (Table 3.5). The maximum values were typically in the range 150 – 350 lice m^{-2}, except at Loch Melfort where modelled lice densities were lower in this model combination (Figure 3.20, Table 3.5). The magnitudes of the mean, median and maximum values for the FISCM-WLLS2021 model were similar to those for Biotracker-WeStCOMS (Figure 3.21), but the distribution was different, with higher values at Asknish Bay and Eilean Arsa and relatively low values elsewhere (Table 3.6).

All three modelling systems discussed here predicted predominantly low values of infective lice at the sample locations, interspersed with brief periods of high values. This is typical of buoyant material in the water

column, which may accumulate at fronts and convergences and be advected around. Models that simulate vertical movement of lice larvae through sinking/swimming, vertical advection and diffusion predict greater dispersion as movement away from convergence zones may occur during hours of darkness when lice larvae are not necessarily at the water surface.

The high percentage of time that the models predicted there were zero copepodids at the sample locations may also partly explain why low planktonic lice numbers were sampled in WP3 (and in other studies around the world). Plankton sampling methods usually only sample water for a few minutes (up to 15 minutes in WP3) and sample limited volumes of water. Given the spatial and temporal variability in lice numbers predicted by the models, planktonic sampling at fixed locations needs a lot of luck to capture high numbers of lice. This was perhaps demonstrated by Nelson et al. (2017), who sampled planktonic lice larvae in and around salmon farms in the Bay of Fundy, Canada and collected one sample at a reference station containing 255 copepodids; the other 81 reference samples collected 35 copepodids in total, with a mean larval lice density of 0.08 lice m^{-3}.

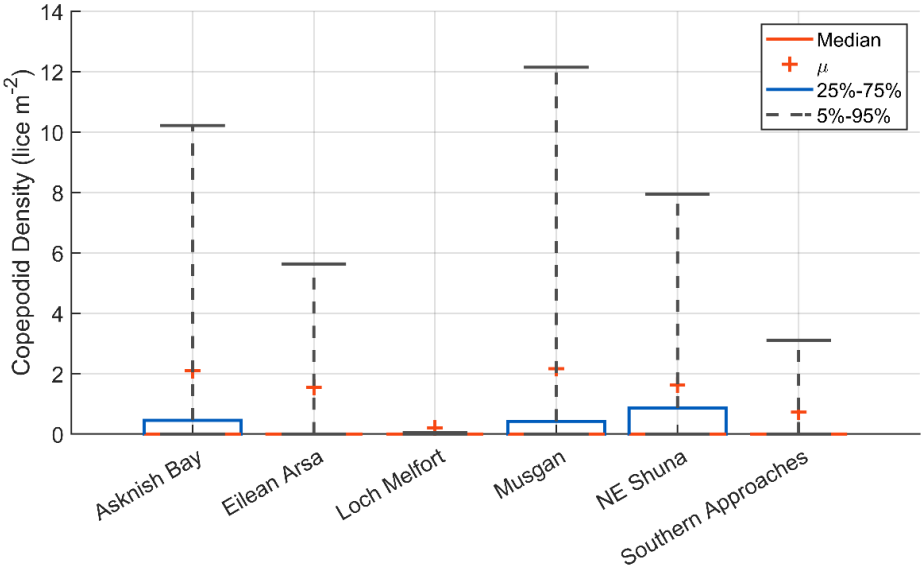

Figure 3.20 Box and whisker plot for modelled infective lice densities (lice m^{-2}) at each site for April – October 2021. The model system was Biotracker – WeStCOMS, and the densities were depth-integrated. The plots shows the mean (μ) and median modelled density at each site, with the 25th percentile and 5th percentile ranges also shown.

Table 3.5 Summary statistics of the modelled infective lice densities (lice m^{-2}) at the six sampling stations in Shuna Sound during April – October 2021 using a 100 m radial distance, and integrating over the full water depth. The model system was Biotracker – WeStCOMS. The "No. zeros" row indicates the percentage of time that the modelled infective lice density at each site was zero.

	Asknish Bay	Eilean Arsa	Loch Melfort	Musgan	NE Shuna	Southern Approaches
Mean	2.102	1.541	0.199	2.163	1.615	0.717
Median	0.000	0.000	0.000	0.000	0.000	0.000
St. Dev.	10.291	9.139	1.598	9.066	5.828	6.121
95th percentile	10.221	5.636	0.044	12.149	7.937	3.108
Maximum	346.754	198.932	46.681	231.985	166.298	349.382
No. zeros (%)	68.245	84.007	94.950	69.276	60.143	78.472

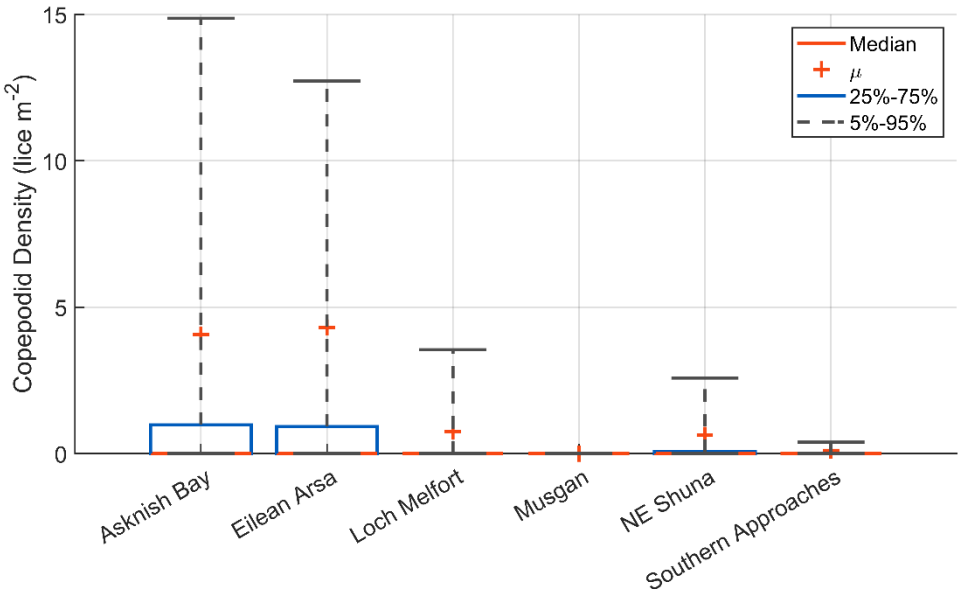

Figure 3.21 Box and whisker plot for modelled infective lice densities (lice m^{-2}) at each site for April – October 2021. The model system was FISCM – WLLS2021, and the densities were depth-integrated. The plots shows the mean (μ) and median modelled density at each site, with the 25th percentile and 5th percentile ranges also shown.

Table 3.6 Summary statistics of the modelled infective lice densities (lice m^{-2}) at the six sampling stations in Shuna Sound during April – October 2021 using a 100 m radial distance, and integrating over the full water depth. The model system was FISCM – WLLS2021. The "No. zeros" row indicates the percentage of time that the modelled infective lice density at each site was zero.

	Asknish Bay	Eilean Arsa	Loch Melfort	Musgan	NE Shuna	Southern Approaches
Mean	4.063	4.306	0.754	0.000	0.637	0.112
Median	0.000	0.000	0.000	0.000	0.000	0.000
St. Dev.	20.107	28.238	3.783	0.000	3.334	0.868
95^{th} percentile	14.814	12.700	3.548	0.000	2.582	0.388
Maximum	436.112	923.321	80.444	0.000	72.715	31.826
No. zeros (%)	51.738	53.727	83.752	100.000	71.189	88.212

Whilst undoubtedly useful and important for attempting to understand the planktonic phase and the environment of larval dispersal, planktonic lice data are difficult to use for model validation. Not only is the sampling likely to miss peaks in larval lice densities, but the high spatial and temporal variability of planktonic lice numbers, and the zero-inflated nature of the data, makes meaningful comparison between model and data challenging. To calibrate and validate a model based on comparison with time series at point locations requires quasi-continuous data. Monthly sampling at a point location, where densities are changing on an hourly basis, is not adequate for model calibration; it would require pinpoint accuracy in time and space from the model, which is, of course, unachievable. Until improved methods of planktonic sampling for larval lice are developed, this field sampling approach does not appear to provide particularly useful data for model calibration and verification purposes.

3.10 Forecasting Sea Lice Dispersal using the SSM Climatology

For management and monitoring purposes, forecasts of sea lice dispersal and distributions in the water column may be desirable. However, operational weather and hydrodynamic forecasting models rarely run reliably more than five days into the future, and predicting the sea lice

distributions at the end of a 15-day life cycle is therefore challenging. One option is to use historical “average” conditions to eliminate unusual dispersal pathways due to abnormal meteorological forcing in a particular year. One such set of “average” conditions is available through Marine Scotland’s 25-year Scottish Shelf Model climatology (De Dominicis, 2018), which provides hourly coastal water circulation, temperature and salinity over one year based on average meteorological forcing from 1990 – 2014. One known shortcoming of the current version (v2.01) of the SSM climatology is that wind stress is persistently from the south-west – there is little variability in the wind forcing to drive dispersal.

We ran the particle tracking model, UnPTRACK, as described above, with the WLLS 25-year climatology to predict lice densities over May – October 2021 (2021 reflects the timing of the sources of lice, not the hydrodynamics which are of course an average). The predicted mean copepodid densities for May – June 2021 are shown in Figure 3.22. The persistent south-west wind in the climatology leads to enhanced densities at the heads of the sea lochs (Melfort and Craignish) and along the eastern side of Asknish Bay and around Craobh Haven. Much of Shuna Sound contained no (or very low levels of) lice. The prevalence of densities exceeding 0.1 lice m^{-2} also reflected the persistent SW wind (Figure 3.22), with very low prevalence through most of the modelled domain and high prevalence where predicted densities were also high. These results appear to be strongly influenced by the methodology used to calculate the climatology, and are probably not a realistic dispersal prediction for these inshore waters, where the persistent SW wind traps and holds particles against the coast.

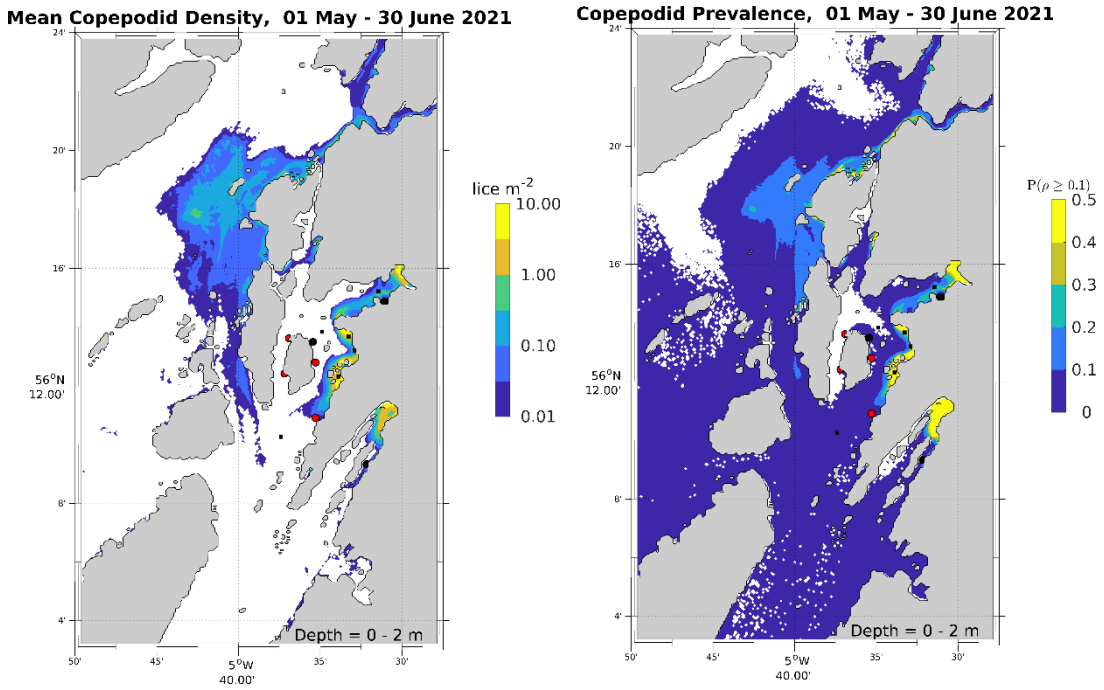

Figure 3.22 Modelled monthly-mean infective lice density distributions (left) and prevalence of densities exceeding 0.1 lice m^{-2} (right) for May – June. The model system was UnPTRACK with the WLLS Climatology.

For completeness, the predicted densities at the 2021 sampling locations were compared with the sample data (Figure 3.23). The comparison between model and data remains poor, perhaps not unexpectedly given the challenges posed by the sampling (as discussed above) and the reservations about the climatology. Having said that, given that reliable information on the actual sea lice distributions in Shuna Sound during 2021 remains elusive, these predicted distributions using the climatology cannot categorically be dismissed as wrong or inaccurate.

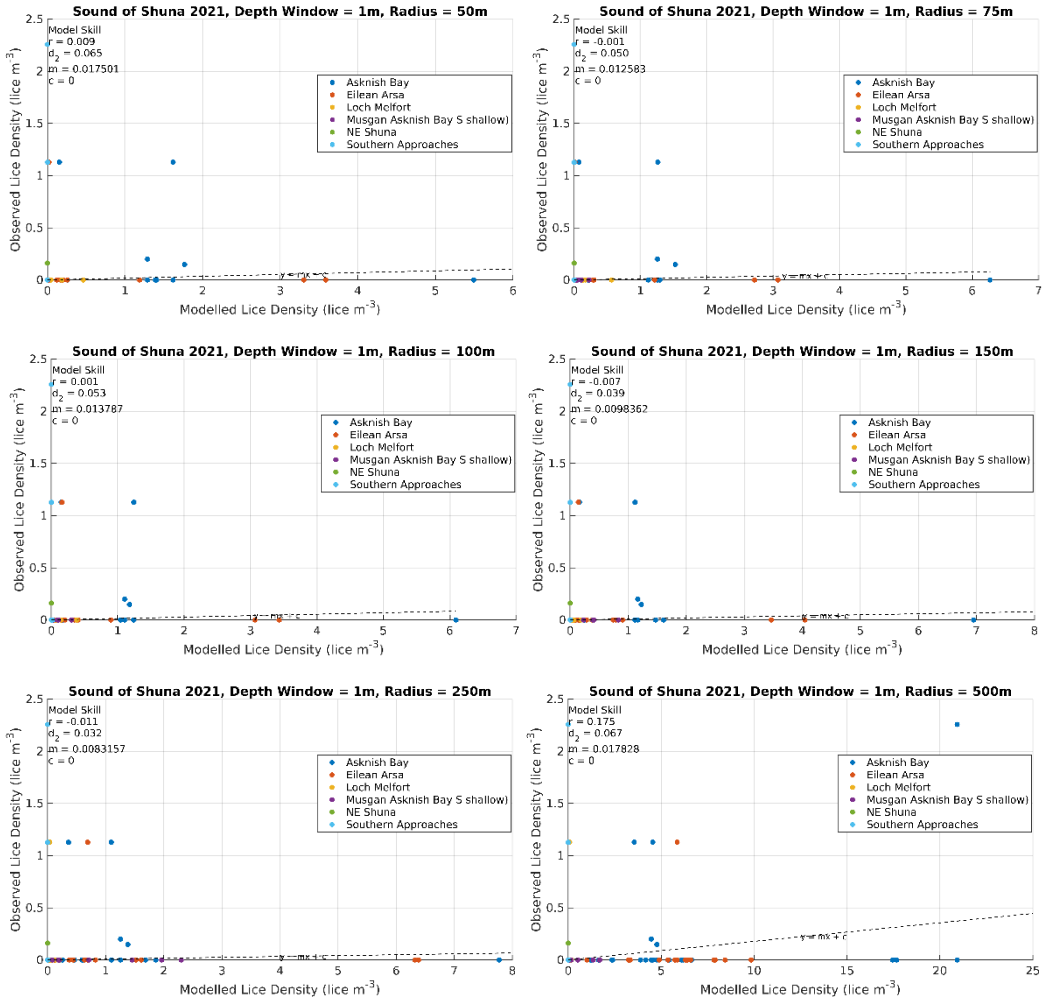

Figure 3.23 Comparison between UnPTRACK modelled and observed copepodid densities sampled at the six sites during the field sampling campaign in 2021. Each plot represents modelled values calculated using a different radial distance centred on the sampling location. The UnPTRACK results here used the WLLS Climatology hydrodynamic output. Note that modelled lice densities are given per cubic metre (variable depth particles).

4. Lessons Learned from Bio-Physical Modelling

Plankton sampling does not appear to provide a robust dataset for model calibration given the apparent very high temporal and spatial variability of sea lice distributions, which demands (an unachievable level of) pinpoint accuracy from models to deliver a positive relationship between observed and modelled sea lice larval density. Whilst the plankton data are useful and important for characterising the planktonic environment and estimating background sea lice densities, plankton

sampling cannot, given resource constraints, provide data of sufficient spatial and temporal coverage to allow a robust calibration. A comparison could be made with Harmful Algal Bloom modelling and management, which has benefitted hugely from the synoptic distributions of marine algae provided by satellite imagery on a regular basis. Field sampling of planktonic sea lice requires comparable innovations in methodology (Bui et al., 2021) before adequate *in situ* data for model calibration can become available.

Given these difficulties, the lack of agreement between model and data does not mean the models are wrong; broadly they may still be correct. Indeed, the reasonable (though limited) calibration of the hydrodynamic models in this workpackage, and the known ability of the biological models from test cases to accurately simulate advection and diffusion, suggests that the modelled movement of particles (and therefore lice) should be broadly correct. Nevertheless, the model combinations produce sometimes starkly different predictions of lice distributions (Figures 3.13 – 3.14). This is a result of integrating the slightly different velocity fields between the models over the (approximately) 15-day lifetime of the larval lice: lagrangian modelling integrates small differences in modelled velocity into large differences in individual larval transport pathways and potentially radically different predicted infective sea lice distributions. This poses a challenge for sea lice regulation and management: the use of different hydrodynamic models will almost certainly result in different predicted distributions of lice, and given limitations in the ability to verify the predicted distributions against field data, it may be challenging to rationalise conflicting predictions and establish reliable assessment of the risks posed by sea lice to wild fish. It is important to recognise that neither modelling nor observations alone can provide the full truth, whereas viewing them as complementary sources of

information and utilising them together may provide a fuller picture of the real environment (Skogen et al., 2021; Johnsen et al., 2021).

In the absence of planktonic field data with sufficient temporal and spatial coverage, full calibration and testing of the individual component models becomes of utmost importance. In particular, here we have found that the modelled distributions of larval lice are very sensitive to the flow and scalar fields from the hydrodynamic model. A comprehensive calibration of the underlying hydrodynamic model could include assessment of the velocity fields against (preferably) multiple current profile datasets, comparison of modelled temperature and salinity profiles against CTD data, and ideally simulation of lagrangian data from dye or drifter release studies. Unfortunately, within this workpackage, data were not available for such a full calibration; however, an example of a full calibration is given in WP4.

Particle tracking models also need to demonstrate accuracy in their fundamental capabilities. Standard tests exist for demonstrating accuracy in advection (Brickman et al., 2009) and diffusion (e.g. North et al. 2006). Standard tests do not presently exist for demonstrating accuracy in simulating biological behaviour, such as vertical migration, but could be developed. Satisfactory calibration in this manner can provide, in the absence of appropriate field data, a large degree of confidence that the models are capable of simulating sea lice dispersal accurately and that predicted results should be broadly realistic.

The presentation of results from sea lice dispersal models is the subject of some debate. Clearly, presenting snapshots of distributions at an instant in time may illustrate the potential peak values in lice numbers that may sporadically occur but, given the transient nature of such peaks and the unreliability of model forecasts on such short temporal scales (compare

the differences between model snapshots in Appendix 2), such snapshots are not particularly helpful or relevant to sea lice management. Instead, mean distributions averaged over a relevant time scale are more informative of the risk posed by sea lice to wild fish. That poses the challenge of defining suitable timescales: an example may be the migration time required for a wild fish to swim through the coastal zone to the open sea, which requires knowledge of salmonid migration routes and swimming speeds. Such questions are presently the subject of active discussion in Scotland. However, such time scales are likely to be of the order of days, or even weeks, so longer-term averages offer both a better indication of risk to wild fish and reduce the discrepancies between models, although, as we have seen, discrepancies still remain.

When multiple models of sea lice dispersal are available, building an ensemble of results from the collective output may provide a more robust estimate of risk. The use of ensemble models is explored more thoroughly in WP4; here, we took the average of the modelled mean densities from five model runs (not including the simulations that used the WLLS climatology, Table 3.2). The results highlighted the elevated modelled concentrations around Asknish Bay and the coastline around Craobh Haven (Figure 3.15). The high values to the west of Shuna Sound predicted in one model run have been moderated by the averaging. Similarly, the zero values at the head of Loch Melfort and Loch Craignish predicted by the simulations using WestCOMS have increased to moderate levels (~0.1 lice m^{-2}). While the modelled ensemble cannot be quantitatively tested, due to the challenges with the planktonic sea lice data discussed above, the ensemble approach removes some of the idiosyncratic predictions associated with individual model predictions. Variability across the ensemble was represented here by the coefficient of variation across the

five ensemble members (Figure 3.15), and provided a visualisation of areas where model results were consistent and areas where they differed.

5. Conclusions and Next Steps

5.1 Hydrodynamic modelling for sea lice particle tracking

Outcomes from sea lice dispersal models depend fundamentally on the underlying hydrodynamic model. Sea lice larvae are transported around the coastal zone for approximately 15 days. Over these time scales, lagrangian modelling can integrate small differences in modelled velocity into large differences in individual larval transport pathways and potentially radically different predicted infective sea lice distributions. The use of different hydrodynamic models, even with identical sea lice dispersal models, will almost certainly result in different predicted distributions of lice.

Hydrodynamic modelling of Scottish coastal waters is extremely challenging, with complex coastlines, large tides, strong winds and intermittent heavy rainfall and river flow all contributing to a dynamic and constantly changing coastal ocean environment. The challenge of predicting realistic flow fields, water temperature and salinity in this environment should not be underestimated.

5.2 Sea lice dispersal (particle tracking) models

Particle tracking modelling is a standard modelling methodology that has developed over several decades to simulate the advection and dispersal of pelagic biota, chemical contaminants and particulate wastes in the marine environment. The models are relatively simple, and provided that they are carefully coded, should reliably advect and diffuse particles in

the flow fields of the ambient environment. There is little reason to think that the modelled transport of sea lice larvae by these PT models does not accurately reflect that (also modelled) environment. However, as noted above, simulation of that hydrodynamic environment is more challenging and the outputs more open to question.

In this work-package, the unsuitablility of the planktonic sea lice data for model calibration and evaluation made it difficult to assess the models and the model parameterisation. The models illustrated the high temporal and spatial variability of the sea lice distributions in the water column explaining, at least in part, the challenge of sampling for sea lice by traditional plankton sampling methods. Similar findings and conclusions regarding the high spatiotemporal variability of sea lice distributions were reported by Skarðhamar et al. (2019). Planktonic sampling at fixed locations needs a lot of luck to capture high numbers of lice. This was perhaps demonstrated by Nelson et al. (2017), who sampled planktonic lice larvae in and around salmon farms in the Bay of Fundy, Canada and collected one sample at a reference station containing 255 copepodids; the other 81 reference samples collected 35 copepodids in total, with a mean larval lice density of 0.08 lice m^{-3}. Numerous other planktonic sampling studies have found generally low numbers of sea lice in the water column, with occasional hot-spots where numbers are higher (see Bui et al., 2021 and references therein). This is characteristic of buoyant material in the ocean, such as plastic, which accumulates at convergence zones and is advected around the coastal zone by tidal and wind-driven currents. The modelled lice distributions in this workpackage suggest that, for much of the time (more than 50% in all cases) lice abundances at the sampling locations and elsewhere were zero (or, at least, very low).

The challenge lies in establishing what infection risk, if any, these transient and moving peaks in sea lice larval abundance pose to wild fish and how best to quantify that risk. Using time-averaged plots of mean density (e.g. Figure 3.17) allows identification of areas which are particularly prone to higher sea lice numbers. Defining the period of that time-averaging remains a matter of debate, but may be best related in some way to migration times of wild fish through an area. These time-averaged plots do not illustrate the patchy distributions of sea lice in the environment, so videos showing hourly locations of sea lice have also been produced (see http://marine.gov.scot/information/salmon-parasite-interactions-linnhe-lorn-and-shuna-spills).

5.3 Using an ensemble model approach to quantify model uncertainty

Combining the results from a number of model runs, whether using different models or the same model with different parameter sets, into an ensemble-mean smooths out some of the idiosyncrasies of particular model runs and illustrates regions of the domain where the results are more consistent, at both high and low densities (Figure 3.15). The coefficient of variation (i.e. the ensemble standard deviation divided by the ensemble mean) provides a measure of the consistency of the results between ensemble members. Thus areas where some models predict high lice densities and other models predict low lice densities have a high coefficient of variation.

The ensemble methodology allows some interpretation of the uncertainty of model predictions to be made. Based on the results here, this seems to be particularly pertinent for the hydrodynamic model outputs, which, while absolute differences between modelled flow fields may be

quite small, may lead to substantial differences between predicted sea lice distributions. The challenges involved in incorporating ensemble methods into a management and regulatory regime are recognised. Nevertheless, where multiple predictions of sea lice distributions using different hydrodynamic models are made, some effort to refine and ascertain the robustness of the results will be necessary.

6. References

Adams TP (2019) BioTracker - biological particle tracking in unstructured and structured hydrodynamic grids. Scottish Association for Marine Science, Oban, UK; BioTracker

Adams TP, Aleynik D, Black KD (2016) Temporal variability in sea lice population connectivity and implications for regional management protocols. 8:585–596.

Adams TP, Aleynik D, Burrows MT (2014) Larval dispersal of intertidal organisms and the influence of coastline geography. Ecography 37:698–710

Adams, T., K. Black, C. MacIntyre, I. MacIntyre and R. Dean, (2012). Connectivity modelling and network analysis of sea lice infection in Loch Fyne, west coast of Scotland. Aquaculture Environment Interactions, 3, 51–63.

Adams T, Marshall S, Brown S, Black K (2021) Validating a biophysical parasite model with fish farm pen and plankton trawl data. Aquac Environ Interact 13:425–437.

Aleynik D, Adams TP, Davidson K (2022) Optimising the connectivity of salmon farms: role of exposure to wind, tides and isolation. In: Global Blue Economy: Analysis, Developments, and Challenges. p 488Adams et al. 2012

Aleynik D, Dale AC, Porter M, Davidson K (2016) A high resolution hydrodynamic model system suitable for novel harmful algal bloom

modelling in areas of complex coastline and topography. Harmful Algae 53:102–117

Amundrud, T. L., & Murray, A. G. (2009). Modelling sea lice dispersion under varying environmental forcing in a Scottish sea loch. Journal of fish diseases, 32(1), 27-44.

Brickman et al., 2009 Brickman, D., Ådlandsvik, B., Thygesen, U., Parada, C., Rose, K., Hermann, A. and Edwards, K., (2009). Particle tracking. Manual of Recommended Practices for Modelling Physical-biological Interactions in Fish Early-life History, 295, p.14e31.

Brooker, A. J., Skern-Mauritzen, R., & Bron, J. E. (2018). Production, mortality, and infectivity of planktonic larval sea lice, Lepeophtheirus salmonis (Krøyer, 1837): current knowledge and implications for epidemiological modelling. ICES Journal of Marine Science, 75(4), 1214-1234.

Bui, S., Dalvin, S., Vågseth, T., Oppedal, F., Fossøy, F., Brandsegg, H., Jacobsen, Á., á Norði, G., Fordyce, M.J., Michelsen, H.K., Finstad, B. and Skern-Mauritzen, R., (2021). Finding the needle in the haystack: Comparison of methods for salmon louse enumeration in plankton samples. Aquaculture Research, 52: 3591-3604. https://doi.org/10.1111/are.15202

Cantrell DL, Filgueira R, Revie CW, Rees EE, Vanderstichel R, Guo M, Foreman MGG, Wan D, Grant J (2019) The relevance of larval biology on spatiotemporal patterns of pathogen connectivity among open-marine salmon farms. Can J Fish Aquat Sci. 77: 505-519 cjfas-2019-0040. https://doi.org/10.1139/cjfas-2019-0040

Chen, C., H. Liu, and R.C. Beardsley, (2003). An unstructured, finite-volume, three-dimensional, primitive equation ocean model: Application to coastal ocean and estuaries. J. Atmos. Ocean. Tech., 20, 159 – 186.

Corrochano-Fraile A, Adams TP, Aleynik D, Bekaert M, Carboni S (2022) Predictive biophysical models of bivalve larvae dispersal in Scotland. Front Mar Sci 0:1710.

Costelloe M, Costelloe J, O'Donohoe G, Coghlan NJ, Oonk M, Van Der Heijden (2009) Planktonic Distribution of Sea Lice Larvae, Lepeophtheirus Salmonis, in Killary Harbour, West Coast of Ireland. Journal of the Marine Biological Association of the UK 78, 853-874

Dabrowski, T., Lyons, K., Nolan, G., Berry, A., Cusack, C., & Silke, J. (2016). Harmful algal bloom forecast system for SW Ireland. Part I: Description and validation of an operational forecasting model. *Harmful algae*, *53*, 64-76.

Davidson K, Whyte C, Aleynik D, Dale A, Gontarek S, Kurekin AA, McNeill S, Miller PI, Porter M, Saxon R, Swan S (2021) HAB reports: Online Early Warning of Harmful Algal and Biotoxin Risk for the Scottish Shellfish and Finfish Aquaculture Industries. Front Mar Sci 8:350.

De Dominicis, M., O'Hara Murray, R., Wolf, J., Gallego, A. (2018). The Scottish Shelf Model 1990 – 2014 climatology version 2.01. doi: 10.7489/12037-1

Gillibrand, P.A. (2022); UnPTRACK: A multi-purpose particle tracking model for unstructured grids. Mowi Scotland Ltd, 33 pp. https://github.com/gillibrandpa/unptrack.git

Gillibrand, P.A.; Lane, E.M.; Walters, R.A. and Gorman, R.M., (2011). Forecasting extreme sea surface height and coastal inundation from tides, surge and wave setup. Austr. J. Civil Eng., 9, 99-112.

Gillibrand, P.A., B. Siemering, P.I. Miller and K. Davidson, (2016a). Individual-Based Modelling of the Development and Transport of a Karenia mikimotoi Bloom on the North-West European Continental Shelf. Harmful Algae, DOI: 10.1016/j.hal.2015.11.011

Gillibrand, P.A., Walters, R.A., and McIlvenny, J. (2016b) Numerical simulations of the effects of a tidal turbine array on near-bed velocity and local bed shear stress. Energies, 2016, vol 9, no. 10, pp. 852. DOI: 10.3390/en9100852

Gillibrand, P.A. and K.J. Willis, (2007). Dispersal of Sea Lice Larvae from Salmon Farms: A Model Study of the Influence of Environmental Conditions and Larval Behaviour. Aquatic Biology, 1, 73-75.

Graham, J. A., O'Dea, E., Holt, J., Polton, J., Hewitt, H. T., Furner, R., Guihou, K., Brereton, A., Arnold, A., Wakelin, S., Castillo Sanchez, J. M., and Mayorga Adame, C. G.:(2018) AMM15: a new high-resolution NEMO configuration for operational simulation of the European north-west shelf, Geosci. Model Dev., 11, 681–696, https://doi.org/10.5194/gmd-11-681-2018.

Hunter J.R., Craig, P.D., Phillips, H.E., (1993). On the use of random walk models with spatially variable diffusivity. J Comput. Phys., 106:366–376

Jackson, F.L., I.A. Malcolm, D.M. Hannah; (2016) A novel approach for designing large-scale river temperature monitoring networks. Hydrology Research 1 June 2016; 47 (3): 569–590. doi: https://doi.org/10.2166/nh.2015.106

Ji, R., Ashjian, C.J., Campbell, R.G., Chen, C., Gao, G., Davis, C.S., Cowles, G.W., and Beardsley, R.C. (2011) Life history and biogeography of calanus copepods in the Arctic Ocean: An individual-based modeling study. Progress In Oceanography 96(1): 40–56.

Johnsen IA, Asplin LC, Sandvik AD, Serra-Llinares RM, (2016) Salmon lice dispersion in a northern Norwegian fjord system and the impact of vertical movements. Aquacult Environ Interact 8: 99-116. https://doi.org/10.3354/aei00162

Johnsen I.A., Harvey A., Sævik P.N., Sandvik AD, Ugedal, O., Ådlandsvik, B., Wennevik, V., Glover, KI.A., Karlsen, O., (2021). Reply to Jansen and Gjerde's (2021) critique of the salmon louse infection model reported in Johnsen et al. (2021). ICES J Mar Sci 78: 3852-3857.

Lane, E.M.; Gillibrand, P.A.; Arnold, J.R. and Walters, R.A., (2011). Tsunami inundation modeling with RiCOM. Austr. J. Civil Eng., 9, 83-98.

Liu, C., Cowles, G. W., Churchill, J. H., and Stokesbury, K.D.E., (2015) Connectivity of the bay scallop (Argopecten irradians) in Buzzards Bay, Massachusetts, U.S.A. Fisheries Oceanography, 24, 364– 382.

McIlvenny, J. , Tamsett, D., Gillibrand, P.A. and Goddijn-Murphy, L., (2016). Sediment Dynamics in a Tidally Energetic Channel: The Inner Sound, Northern Scotland. Journal of Marine Science and Engineering, 4, 31; doi:10.3390/jmse4020031

Murray, A.G., Shephard, S., Asplin, L., Adams, T.P., Ådlandsvik, B., Gallego, A.G., Hartnett, M., Johnsen, I.A., Jones, S.R.M, Moriarty, M., Nash, S., Pert, C.C., Rabe, B., Gargan, P.G., (2022). A standardised generic framework of sea lice model components for application in coupled hydrodynamic-particle models. In: Treasurer, J., Bricknell, I. and Bron, J. (Eds.), Sea Lice Biology and Control, 5M Books Ltd, pp.167 – 187.

Nelson, E. J., Robinson, S. M. C., Feindel, N., Sterling, A., Byrne, A., & Pee Ang, K. (2017). Horizontal and vertical distribution of sea lice larvae (Lepeophtheirus salmonis) in and around salmon farms in the Bay of Fundy, Canada. Journal of Fish Diseases, 41(6), 885– 899.

North EW, Hood RR, Chao SY, Sanford LP (2006) Using a random displacement model to simulate turbulent particle motion in a baroclinic frontal zone: A new implementation scheme and model performance tests. J Mar Syst 60: 365–380

Plew, D. R.; Stevens, C. L. (2013) Numerical modelling of the effect of turbines on currents in a tidal channel–Tory Channel, New Zealand. Renew. Energy 2013, 57, 269-282.

Reinardy, H. Last, K., Brunner L., Twigg, G., McLeod, E., Ofori, A., Stollberg, I., Reed S., (2023) Final report on sampling and analyses of sea lice larvae in Shuna Sound. SPILLS Project Report, February 2023.

Samsing F., Oppedal F., Dalvin S., Johnsen I., Vågseth T., and Dempster T. (2016) Salmon lice (Lepeophtheirus salmonis) development times, body size, and reproductive outputs follow universal models of temperature

dependence Can. J. Fish. Aquat. Sci. 73: 1841–1851 dx.doi.org/10.1139/cjfas-2016-0050

Sandvik AD, Johnsen IA, Myksvoll MS, Sævik PN, Skogen MD (2020) Prediction of the salmon lice infestation pressure in a Norwegian fjord. ICES J Sea Res 77: 746-756. DOI: 10.1093/icesjms/fsz256

Skarðhamar, J., Nilsen Fagerli, M., Reigstad, M., Sandvik, A. D., & Bjørn, P. A., (2019). Sampling planktonic salmon lice in Norwegian fjords. Aquaculture Environment Interactions, 11, 701– 715.

Skogen, M., Ji, R., Akimova, A., Daewel, U., Hansen, C., Hjøllo, S., van Leeuwen, S. M., Maar, M., Macias. D., Mousing, E.A., Almroth-Rosell, E., Sailley, S.F., Spence, M.A., Troost, T.A., van de Wolfshaar, K., (2021). Disclosing the truth: are models better than observations? Marine Ecology Progress Series, https://doi.org/10.3354/meps13574.

Stien A, Bjørn P.A., Heuch P.A. Elston D.A. (2005) Population dynamics of Salmon lice Lepeophtheirus salmonis on Atlantic salmon and sea trout. Marine Ecological Progress Series 290, 263 – 275.

van Sebille, E., Griffies, S.M., Abernathey, R., Adams, T.P. et al., (2018). Lagrangian ocean analysis: Fundamentals and practices. Ocean Modelling, 121, 49 – 75. DOI: https://doi.org/10.1016/j.ocemod.2017.11.008

Vieno, M., Heal, M. R., Williams, M. L., Carnell, E. J., Nemitz, E., Stedman, J. R., and Reis, S.(2016) The sensitivities of emissions reductions for the mitigation of UK PM2.5, Atmos. Chem. Phys., 16, 265-276, 10.5194/acp-16-265-2016.

Vieno, M., Heal, M. R., Hallsworth, S., Famulari, D., Doherty, R. M., Dore, A. J., Tang, Y. S., Braban, C. F., Leaver, D., Sutton, M. A., and Reis, S. (2014) The role of long-range transport and domestic emissions in determining atmospheric secondary inorganic particle concentrations across the UK, Atmos. Chem. Phys., 14, 8435-8447, 10.5194/acp-14-8435-2014.

Visser, A.W., (1997). Using random walk models to simulate the vertical distribution of particles in a turbulent water column. Mar. Ecol. Prog. Ser., 158, 275-281.

Walters, R. A. (2005a) Coastal ocean models: two useful finite element methods. Cont. Shelf Res., 25(7), 775-793.

Walters, R. A. (2005b) A semi-implicit finite element model for non-hydrostatic (dispersive) surface waves. Int. J. Num. Meth. Fluids, 49(7), 721-737.

Walters, R.A. (2016) A coastal ocean model with subgrid approximation. Ocean Mod. 102, 45-54.

Walters, R.A.; Casulli, V. (1998) A robust, finite element model for hydrostatic surface water flows. Comm. Num. Methods Eng. 14, 931–940.

Walters, R.A.; Gillibrand, P.A.; Bell, R.; Lane, E.M. (2010) A Study of Tides and Currents in Cook Strait, New Zealand. Ocean Dyn. 60, 1559-1580.

Walters, R. A.; Tarbotton, M. R.; Hiles, C. E. (2013) Estimation of tidal power potential. Renew. Energy, 51, 255-262.

Willis, K.J, P.A. Gillibrand, C.J. Cromey and K.D. Black, (2005). Sea lice treatments on salmon farms have no adverse effect on zooplankton communities: A case study. Marine Pollution Bulletin, 50, 806 – 816.

Willmott, C. J.; Ackleson, S. G.; Davis, R. E.; Feddema, J. J.; Klink, K. M.; Legates, D. R. O'Donnell, J.; Rowe, C. M. (1985). Statistics for evaluation and comparison of models, J. Geophys. Res., 90, 8995– 9005.

Wolf, J., Yates, N., Brereton, A., Buckland, H., De Dominicis, M., Gallego, A., et al., (2016). The Scottish shelf model. part 1: shelf-wide domain. Scottish Mar. Fresh. Sci. 7:151.

7. Appendix 1. Hydrodynamic Model Calibration

7.1 WLLSshuna

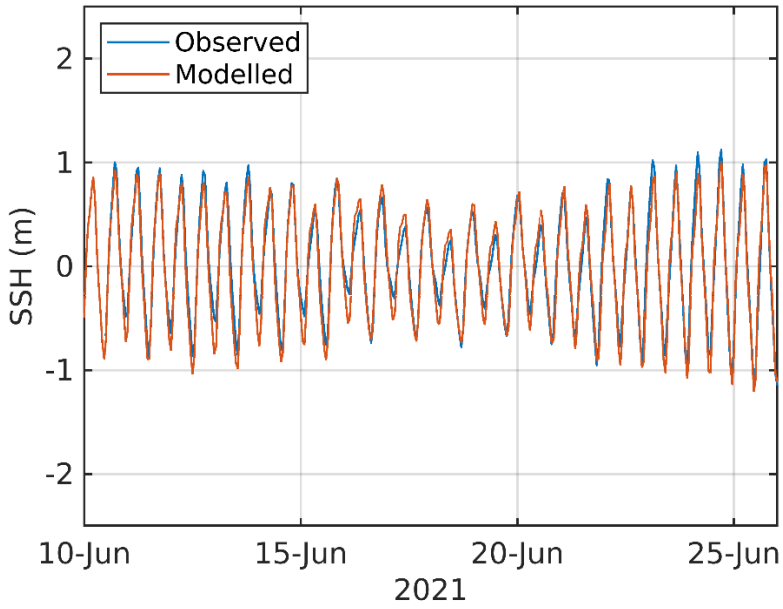

Figure 7.1. Comparison of 15 days of the observed (top) and modelled (bottom) sea surface height at the PNG site in Shuna Sound from June 2021.

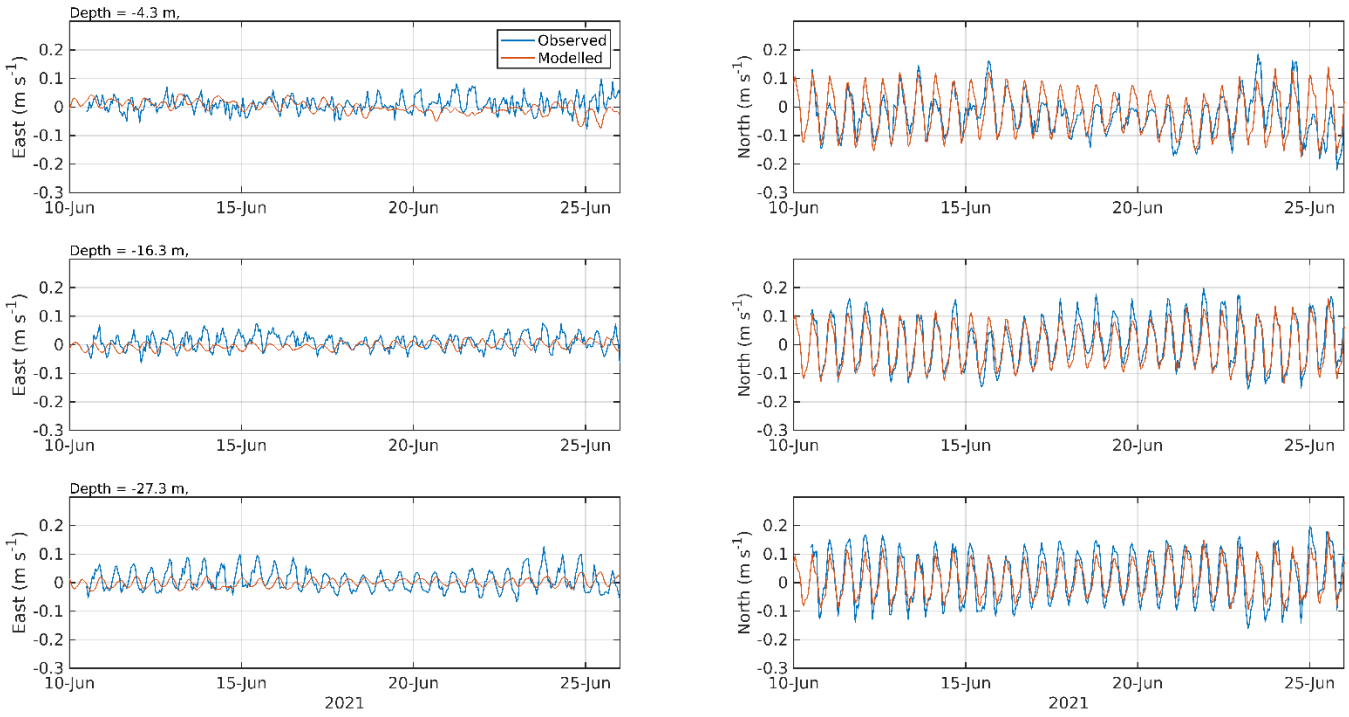

Figure 7.2. Comparison of 15 days of the observed and modelled East (left) and North (right) components of velocity at three depths, near-surface (top), mid-depth (middle) and near-bed (bottom) from the PNG site in Shuna Sound during June 2021.

Table 7.1 WLLSshuna model performance statistics for East and North velocity at the PNG site in Shuna Sound at the three depths for the full simulation from 10th June – 11th August 2021. The model skill, d_2, is the Index of Agreement from Willmott et al. (1985), where $0 \leq d_2 \leq 1$ with higher values indicating a better model fit with data.

		East	North
Sub-surface cell	Model skill, d_2	0.36	0.88
	Mean Absolute Error (MAE) (m/s)	0.03	0.03
	Root-Mean-Square Error (RMSE) (m/s)	0.04	0.04
Mid-depth cell	Model skill, d_2	0.34	0.95
	Mean Absolute Error (MAE) (m/s)	0.02	0.03
	Root-Mean-Square Error (RMSE) (m/s)	0.03	0.04
Near-bed cell	Model skill, d_2	0.44	0.94
	Mean Absolute Error (MAE) (m/s)	0.03	0.03
	Root-Mean-Square Error (RMSE) (m/s)	0.03	0.03

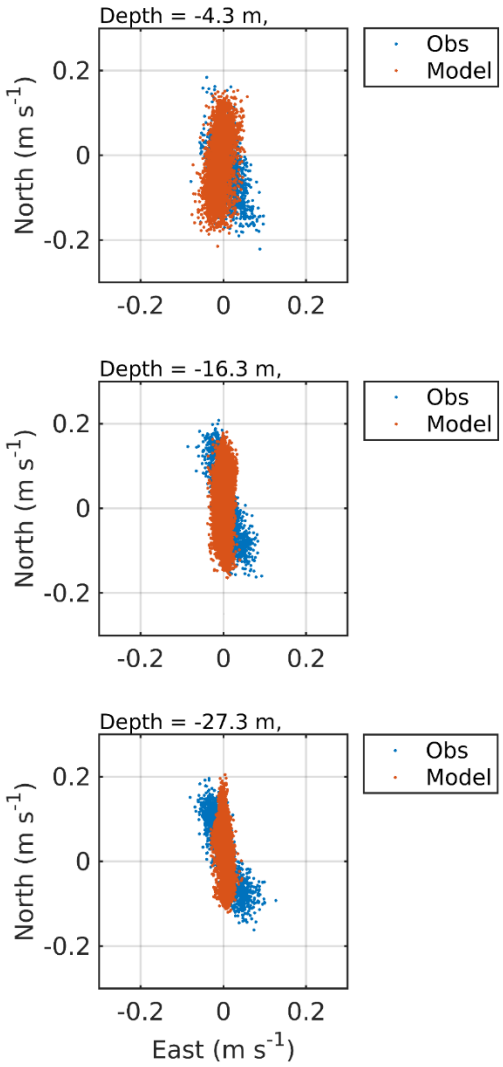

Figure 7.3. Scatter plots of the observed and modelled velocity at three depths, near-surface (top), mid-depth (middle) and near-bed (bottom) from the PNG site in Shuna Sound during June - August 2021.

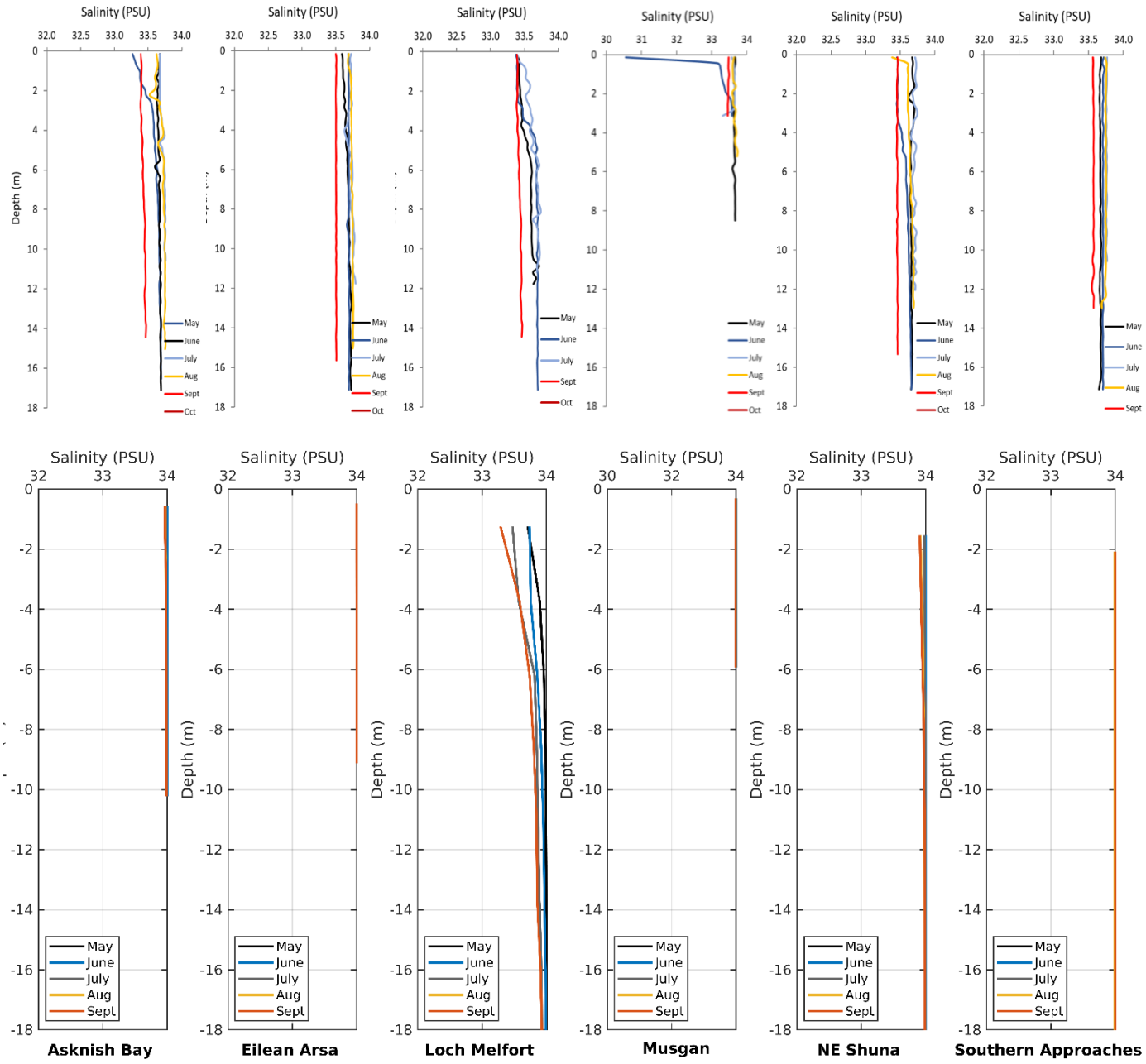

Figure 7.4. Comparison of the observed (top, Reinardy et al., 2023) and modelled (bottom) monthly profiles of salinity at the six planktonic sea lice sampling locations from the WLLSshuna model.

7.2 WeStCOMS

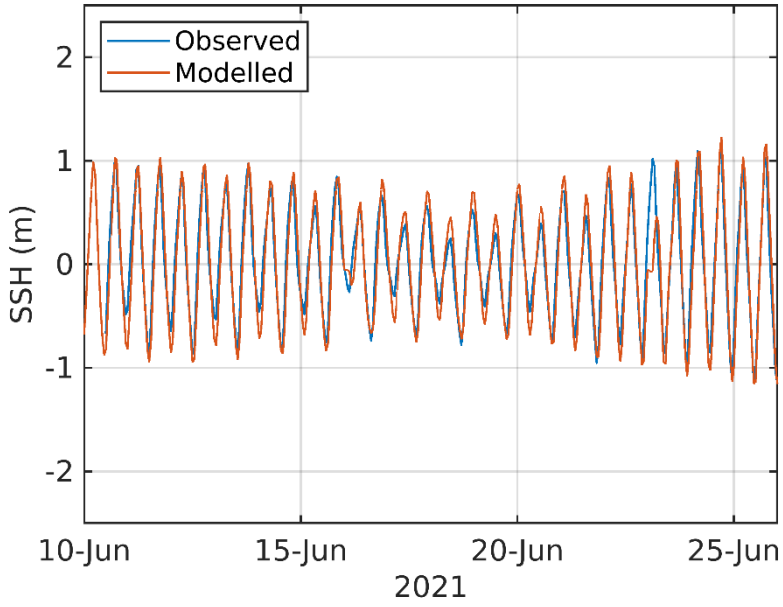

Figure 7.5. Comparison of 15 days of the observed (top) and modelled (bottom) sea surface height at the PNG site in Shuna Sound from June 2021.

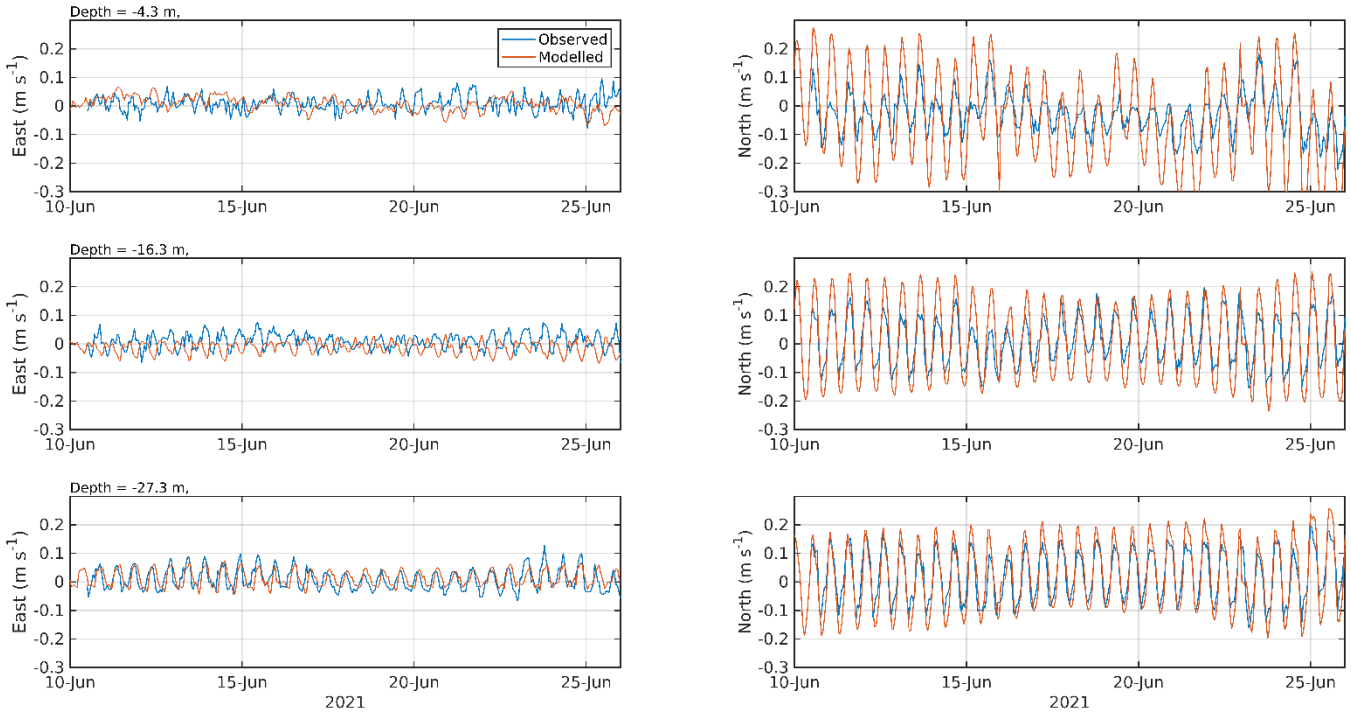

Figure 7.6. Comparison of 15 days of the observed and modelled East (left) and North (right) components of velocity at three depths, near-surface (top), mid-depth (middle) and near-bed (bottom) from the PNG site in Shuna Sound during June 2021.

Table 7.2 WeStCOMS model performance statistics for East and North velocity at the PNG site in Shuna Sound at the three depths for the full simulation from 10th June – 11th August 2021. The model skill, d_2, is the Index of Agreement from Willmott et al. (1985), where $0 \leq d_2 \leq 1$ with higher values indicating a better model fit with data.

		East	North
Sub-surface cell	Model skill, d_2	0.34	0.69
	Mean Absolute Error (MAE) (m/s)	0.03	0.09
	Root-Mean-Square Error (RMSE) (m/s)	0.04	0.11
Mid-depth cell	Model skill, d_2	0.17	0.92
	Mean Absolute Error (MAE) (m/s)	0.04	0.05
	Root-Mean-Square Error (RMSE) (m/s)	0.04	0.06
Near-bed cell	Model skill, d_2	0.79	0.94
	Mean Absolute Error (MAE) (m/s)	0.02	0.04
	Root-Mean-Square Error (RMSE) (m/s)	0.03	0.05

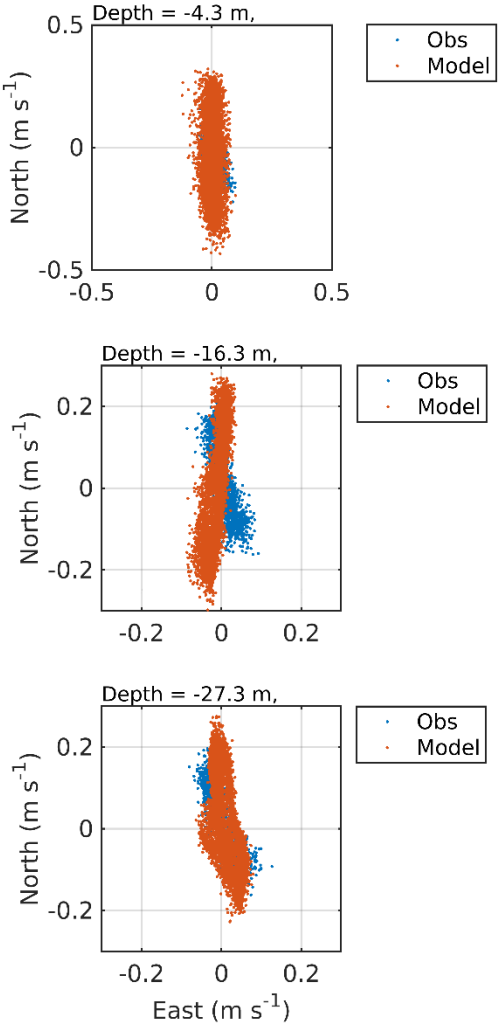

Figure 7.7. Scatter plots of the observed and modelled velocity at three depths, near-surface (top), mid-depth (middle) and near-bed (bottom) from the PNG site in Shuna Sound during June - August 2021.

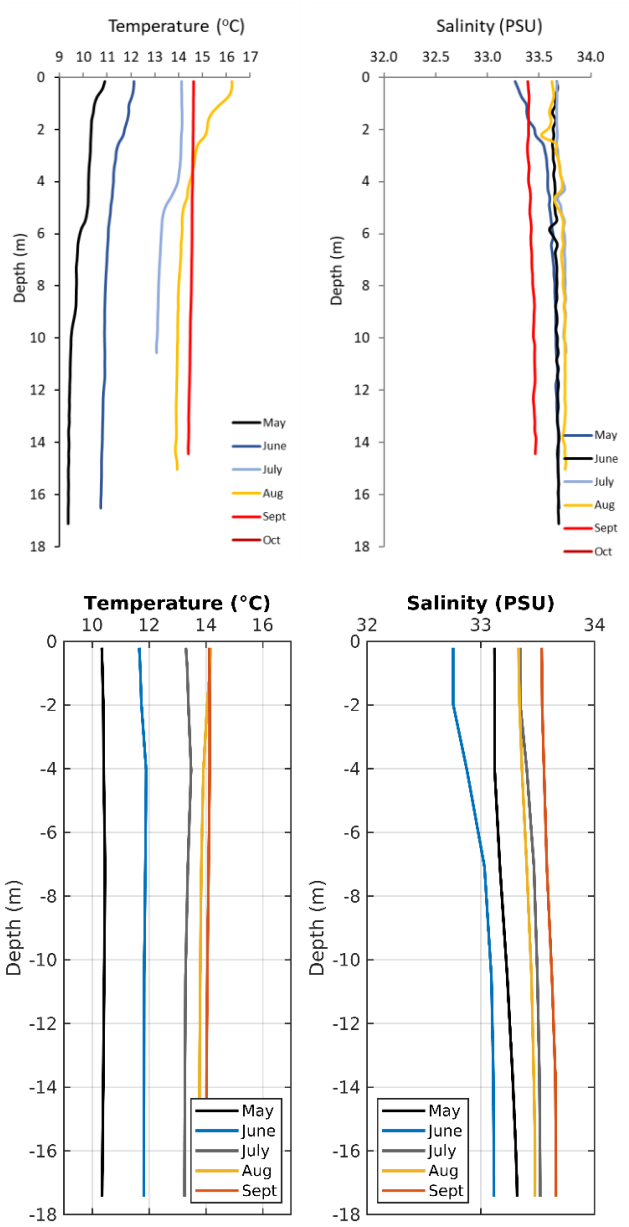

Figure 7.8. Comparison of the observed (top, Reinardy et al., 2023) and modelled (bottom) monthly profiles of temperature and salinity at Asknish Bay from the WeStCOMS model.

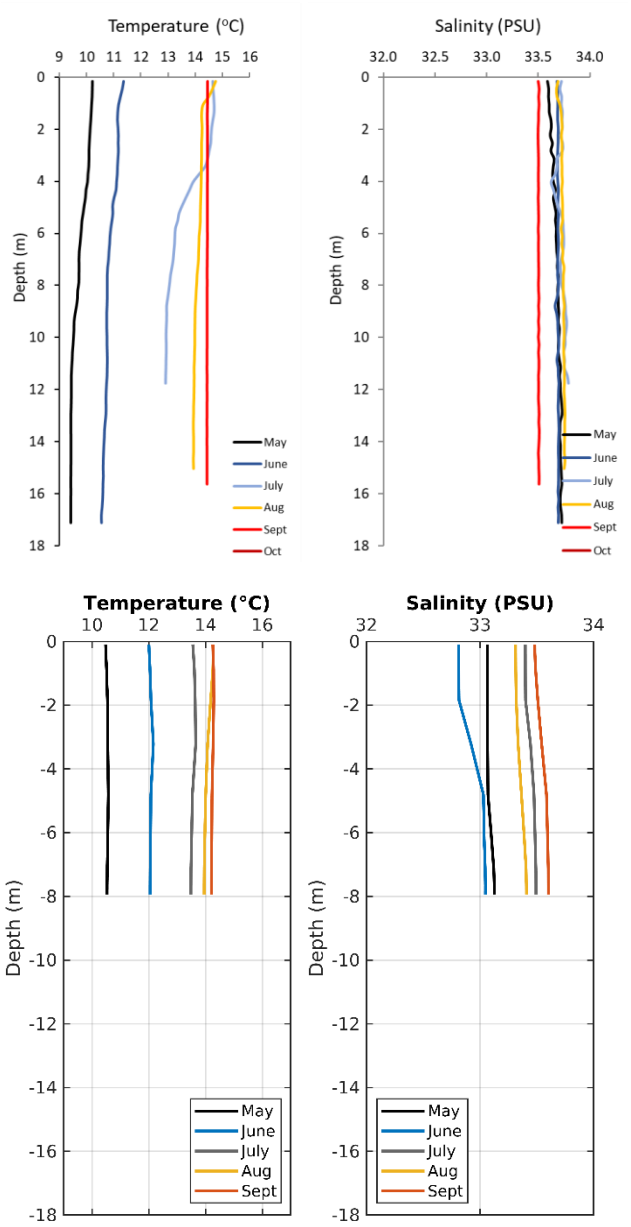

Figure 7.9. Comparison of the observed (top, Reinardy et al., 2023) and modelled (bottom) monthly profiles of temperature and salinity at Eilean Arsa from the WeStCOMS model.

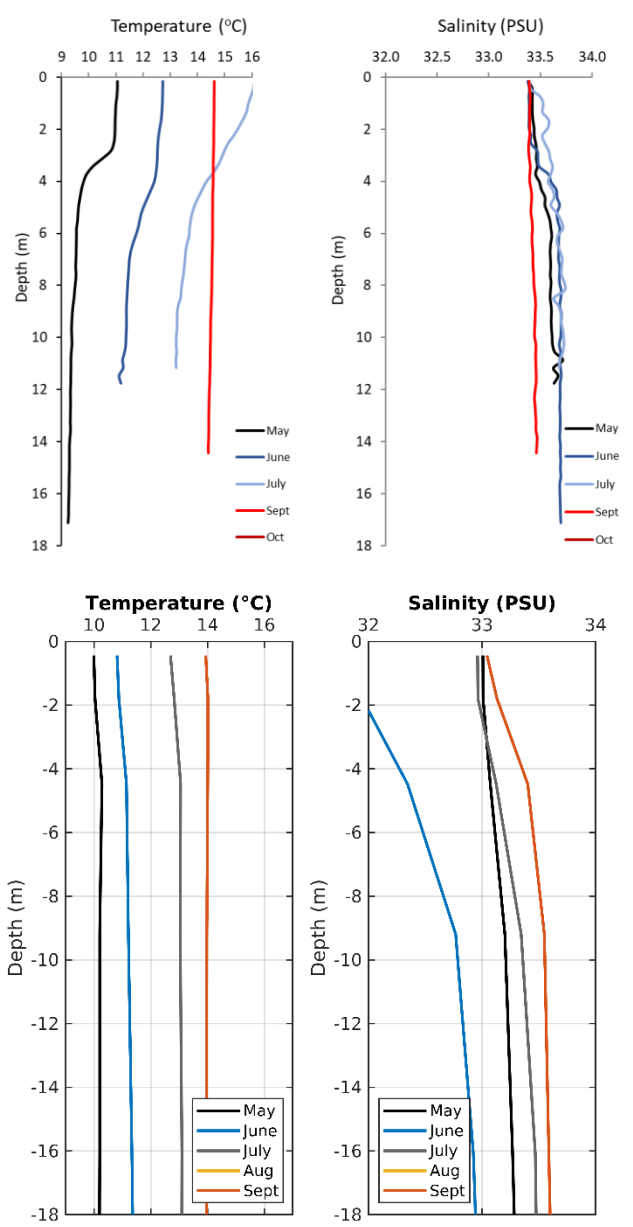

Figure 7.10. Comparison of the observed (top, Reinardy et al., 2023) and modelled (bottom) monthly profiles of temperature and salinity at Loch Melfort from the WeStCOMS model.

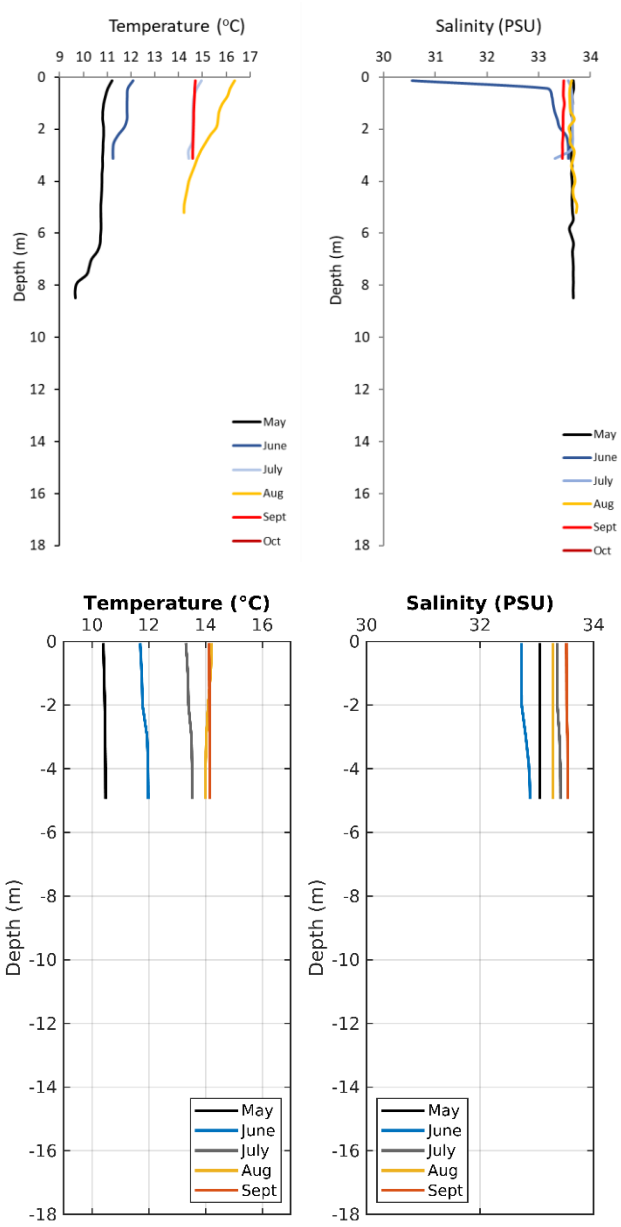

Figure 7.11. Comparison of the observed (top, Reinardy et al., 2023) and modelled (bottom) monthly profiles of temperature and salinity at Musgan from the WeStCOMS model.

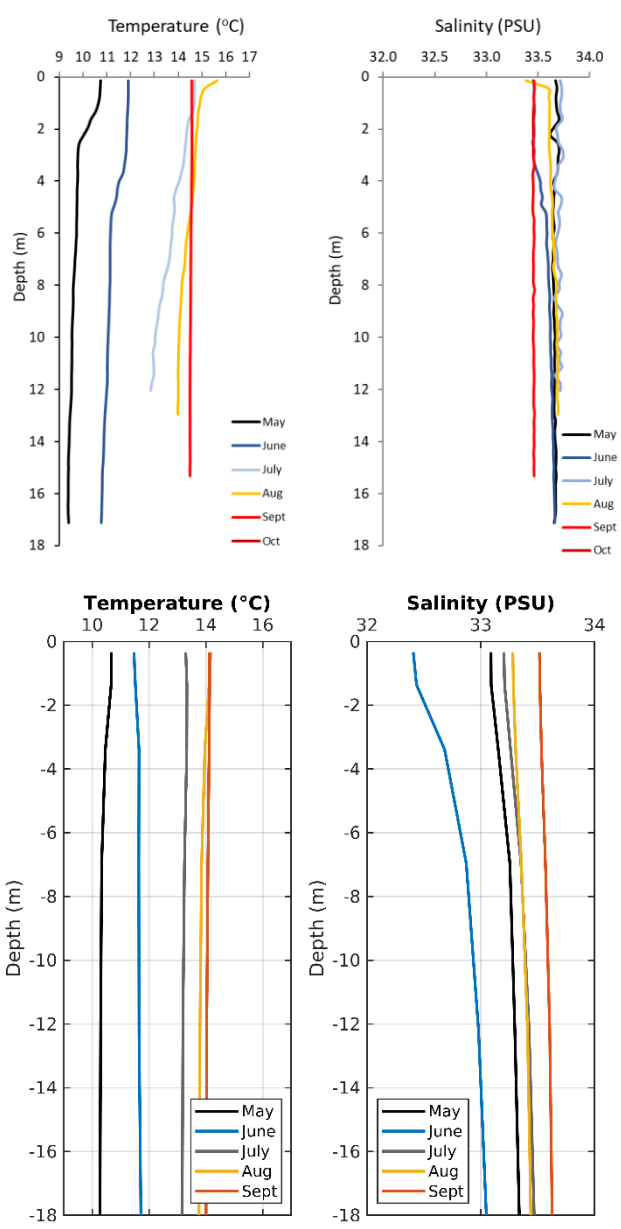

Figure 7.12. Comparison of the observed (top, Reinardy et al., 2023) and modelled (bottom) monthly profiles of temperature and salinity at NE Shuna from the WeStCOMS model.

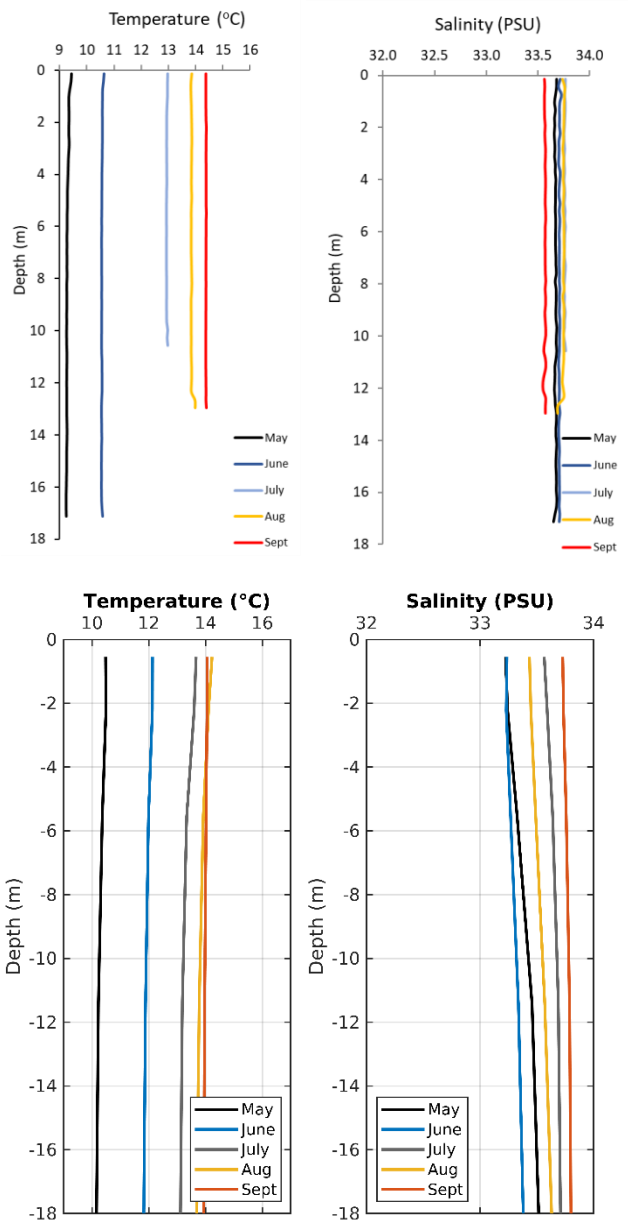

Figure 7.13. Comparison of the observed (top, Reinardy et al., 2023) and modelled (bottom) monthly profiles of temperature and salinity at Southern Approaches from the WeStCOMS model.

7.3 WLLS 2021

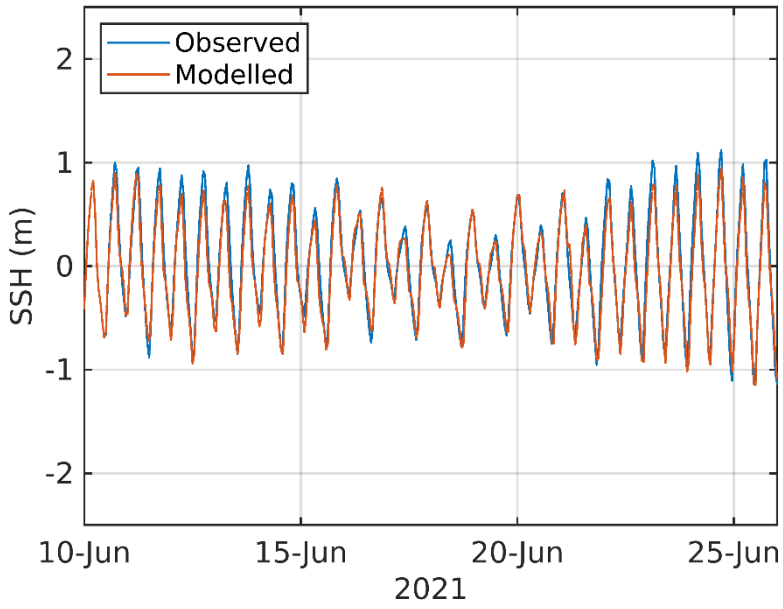

Figure 7.14. Comparison of 15 days of the observed (top) and modelled (bottom) sea surface height at the PNG site in Shuna Sound from June 2021.

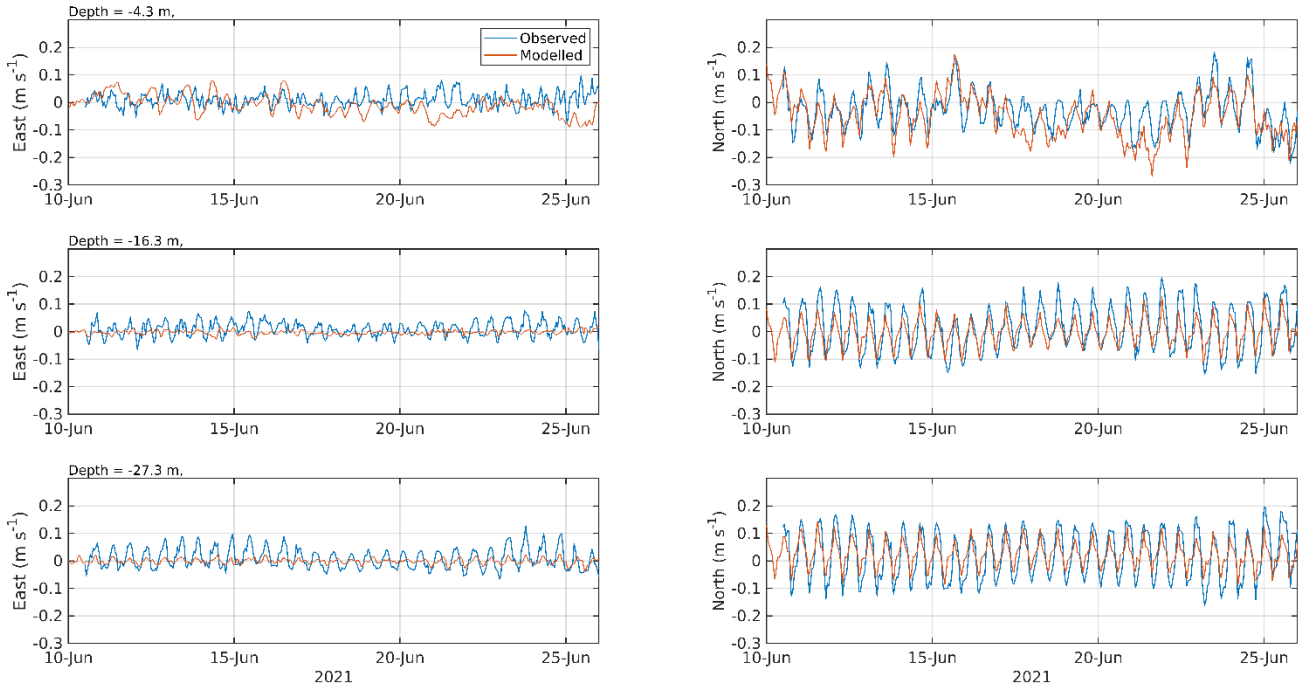

Figure 7.15. Comparison of 15 days of the observed and modelled East (left) and North (right) components of velocity at three depths, near-surface (top), mid-depth (middle) and near-bed (bottom) from the PNG site in Shuna Sound during June 2021.

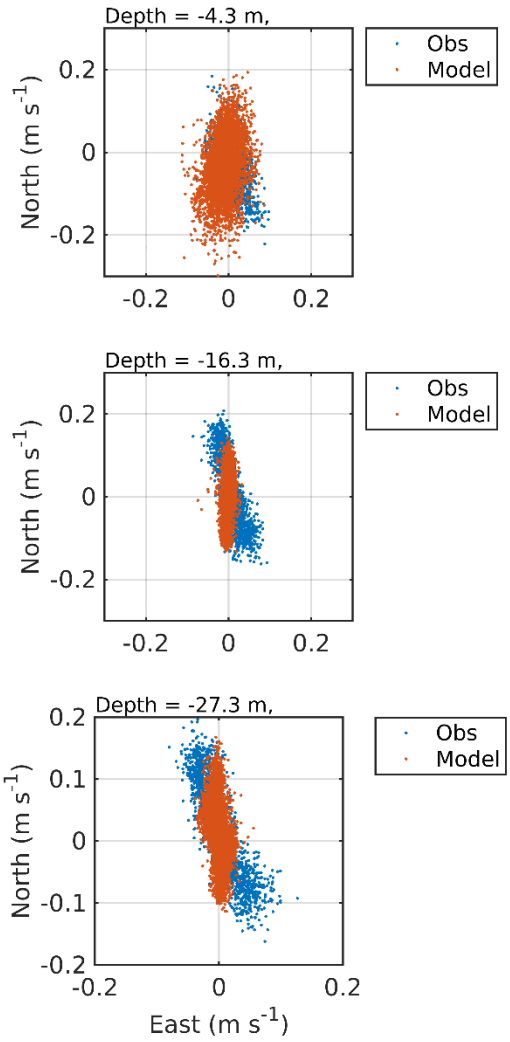

Figure 7.16. Scatter plots of the observed and modelled velocity at three depths, near-surface (top), mid-depth (middle) and near-bed (bottom) from the PNG site in Shuna Sound during June - August 2021.

Table 7.3 WLLS-2021 model performance statistics for East and North velocity at the PNG site in Shuna Sound at the three depths for the full simulation from 10th June – 11th August 2021. The model skill, d_2, is the Index of Agreement from Willmott et al. (1985), where $0 \leq d_2 \leq 1$ with higher values indicating a better model fit with data.

		East	North
Sub-surface cell	Model skill, d_2	0.41	0.75
	Mean Absolute Error (MAE) (m/s)	0.03	0.04
	Root-Mean-Square Error (RMSE) (m/s)	0.04	0.06
Mid-depth cell	Model skill, d_2	0.32	0.78
	Mean Absolute Error (MAE) (m/s)	0.02	0.05
	Root-Mean-Square Error (RMSE) (m/s)	0.03	0.06
Near-bed cell	Model skill, d_2	0.58	0.79
	Mean Absolute Error (MAE) (m/s)	0.02	0.05
	Root-Mean-Square Error (RMSE) (m/s)	0.03	0.05

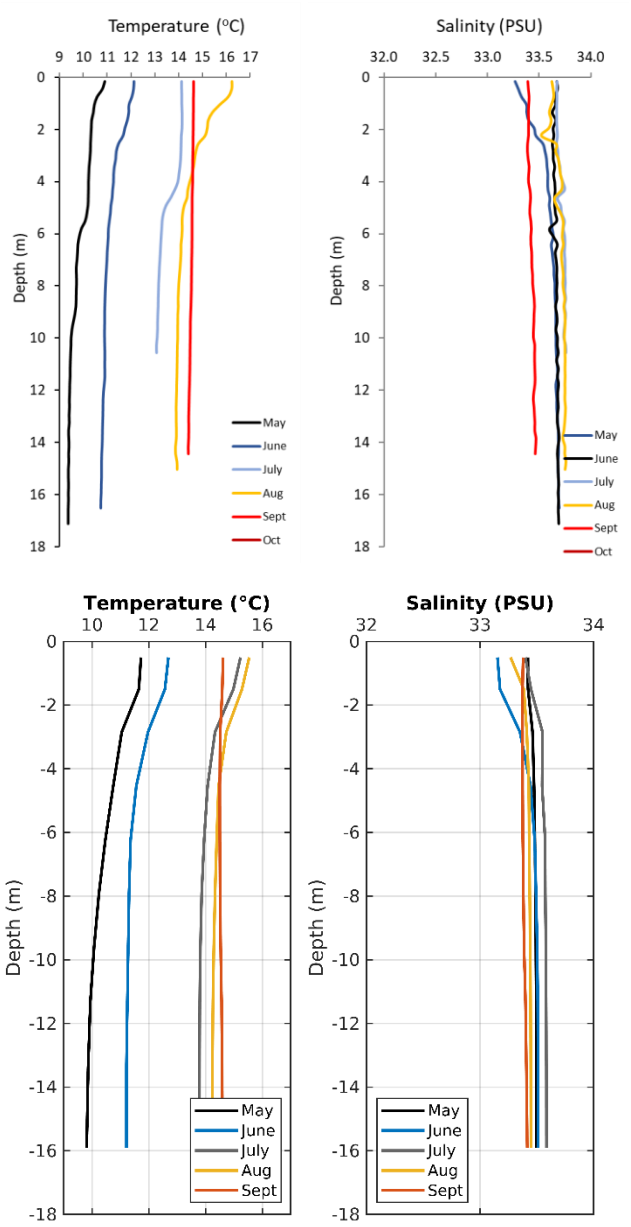

Figure 7.17. Comparison of the observed (top, Reinardy et al., 2023) and modelled (bottom) monthly profiles of temperature and salinity at Asknish Bay from the WLLS-2021 model.

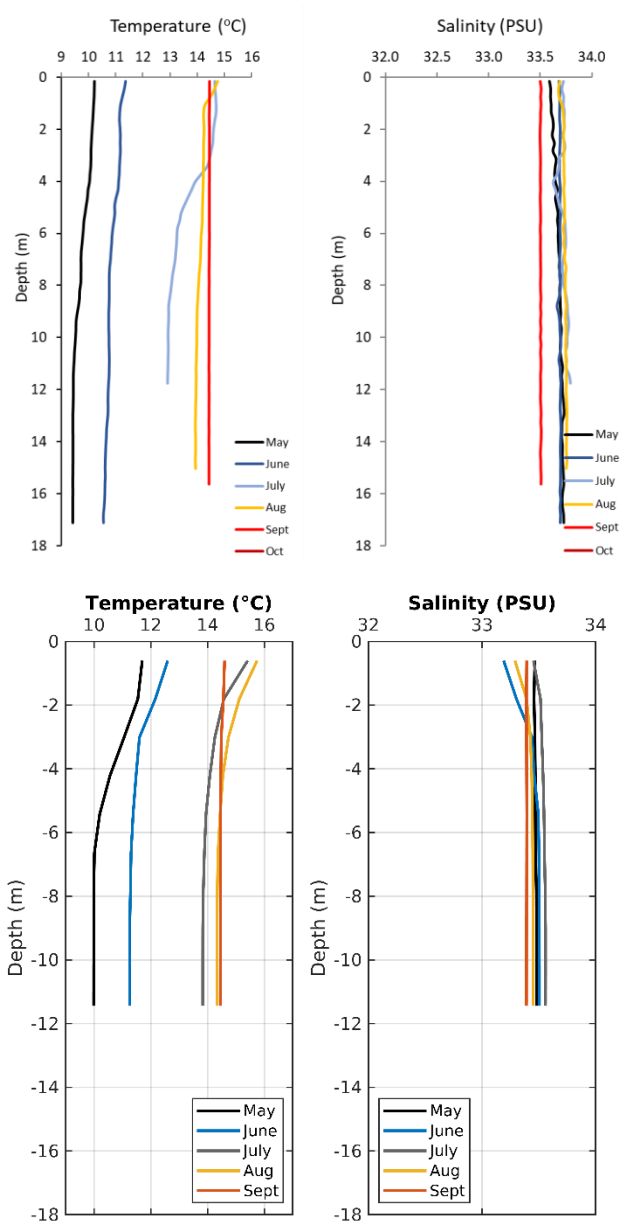

Figure 7.18. Comparison of the observed (top, Reinardy et al., 2023) and modelled (bottom) monthly profiles of temperature and salinity at Eilean Arsa from the WLLS-2021 model.

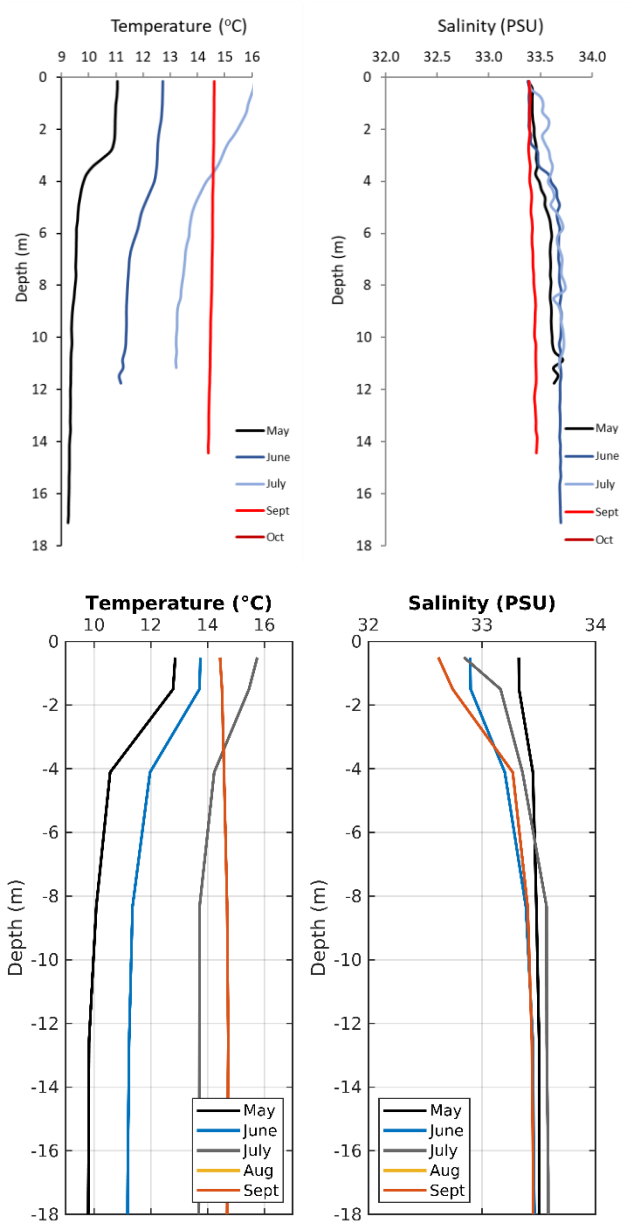

Figure 7.19. Comparison of the observed (top, Reinardy et al., 2023) and modelled (bottom) monthly profiles of temperature and salinity at Loch Melfort from the WLLS-2021 model.

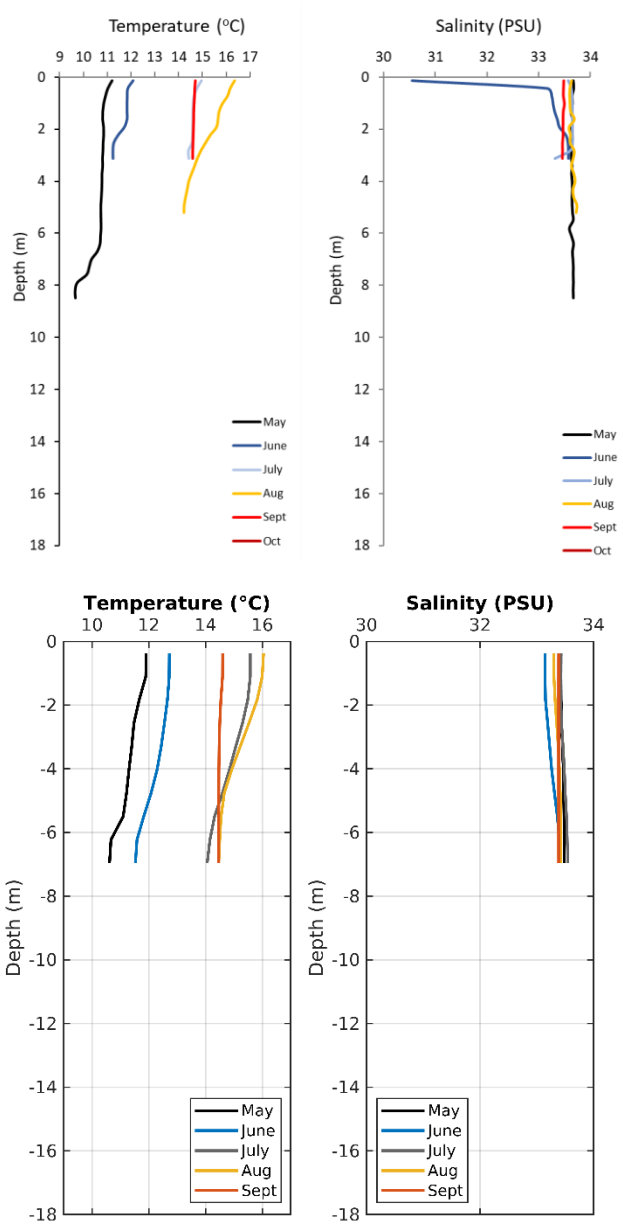

Figure 7.20. Comparison of the observed (top, Reinardy et al., 2023) and modelled (bottom) monthly profiles of temperature and salinity at Musgan from the WLLS-2021 model.

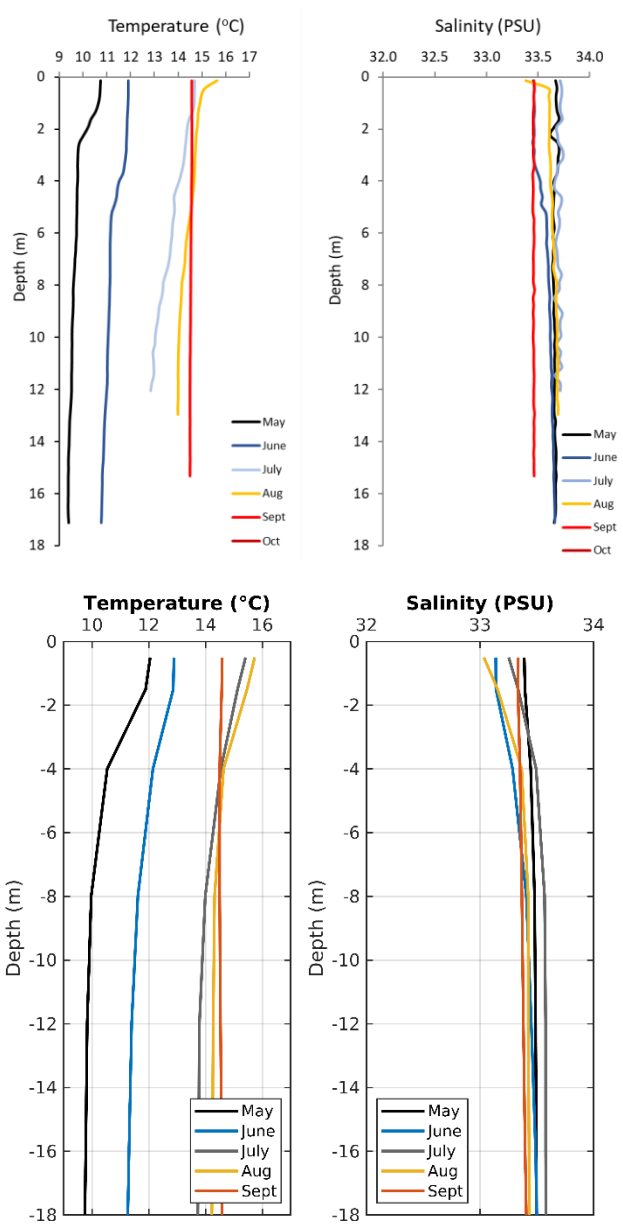

Figure 7.21. Comparison of the observed (top, Reinardy et al., 2023) and modelled (bottom) monthly profiles of temperature and salinity at NE Shuna from the WLLS-2021 model.

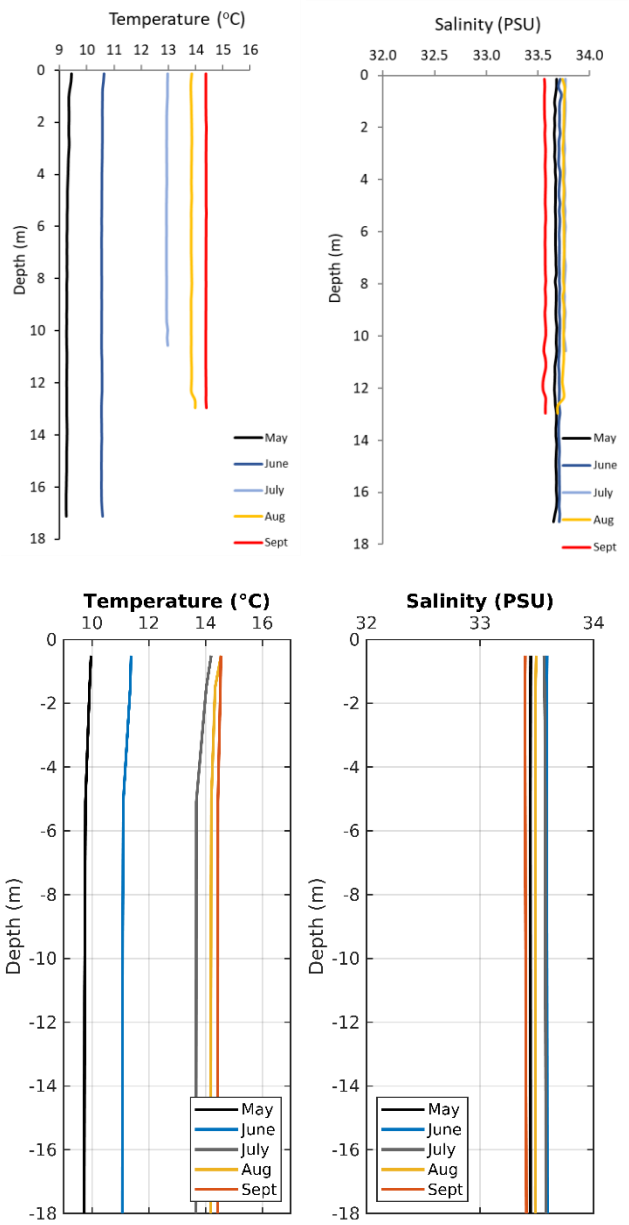

Figure 7.22. Comparison of the observed (top, Reinardy et al., 2023) and modelled (bottom) monthly profiles of temperature and salinity at Southern Approaches from the WLLS-2021 model.

7.4 WLLS Climatology

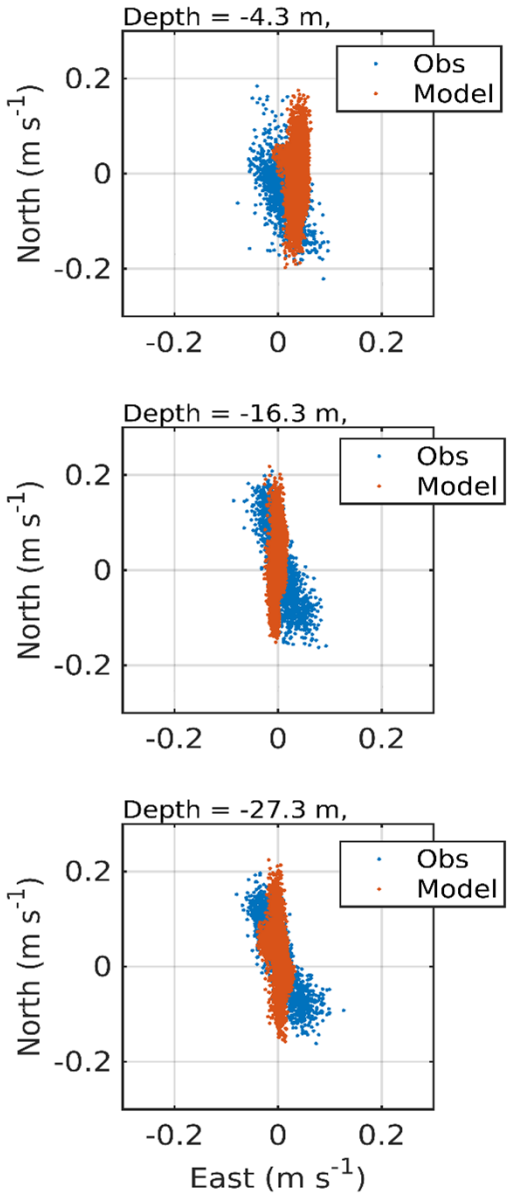

Figure 7.23. Scatter plots of the observed and modelled velocity at three depths, near-surface (top), mid-depth (middle) and near-bed (bottom) from the PNG site in Shuna Sound during June - August 2021.

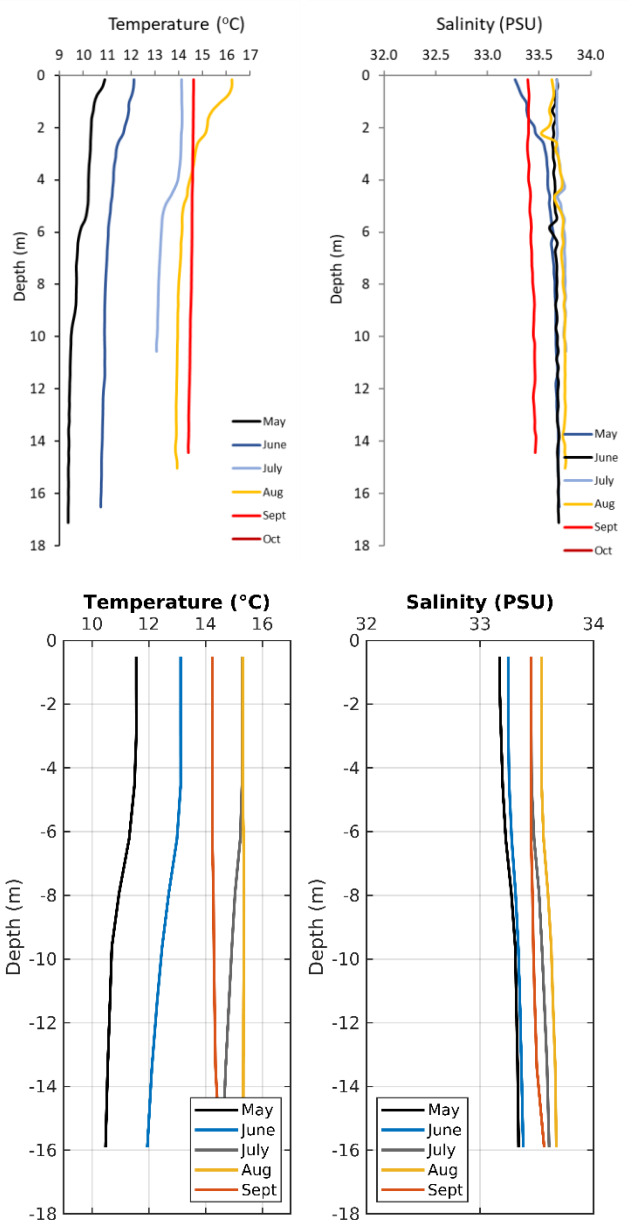

Figure 7.24. Comparison of the observed (top, Reinardy et al., 2023) and modelled (bottom) monthly profiles of temperature and salinity at Asknish Bay from the WLLS Climatology model.

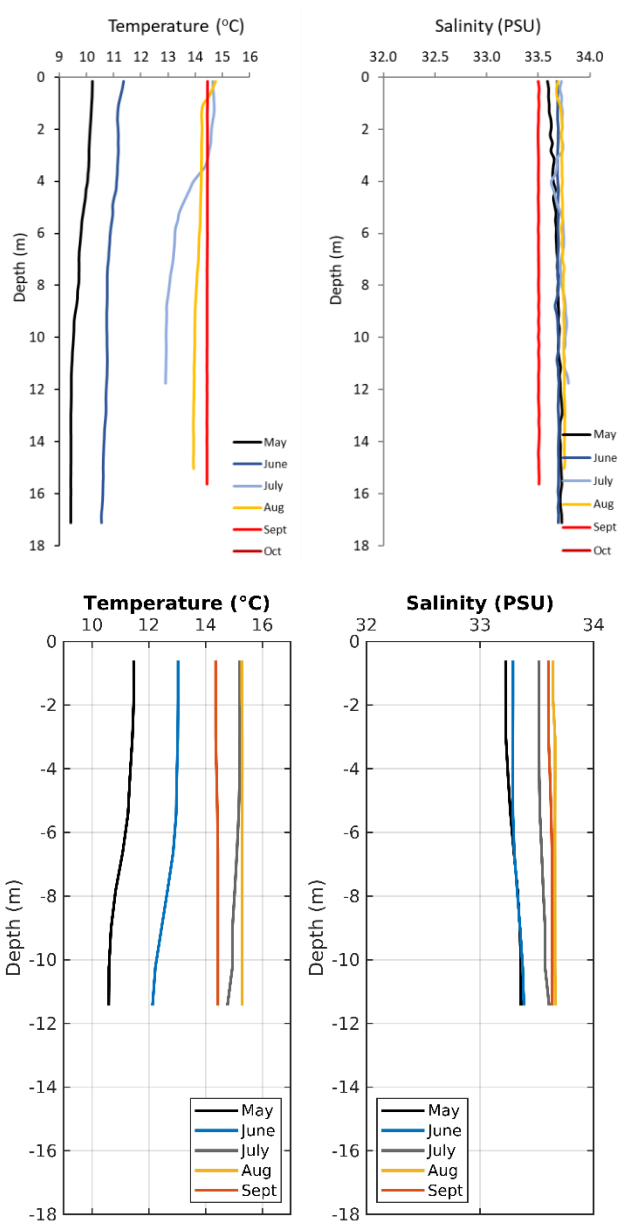

Figure 7.25. Comparison of the observed (top, Reinardy et al., 2023) and modelled (bottom) monthly profiles of temperature and salinity at Eilean Arsa from the WLLS Climatology model.

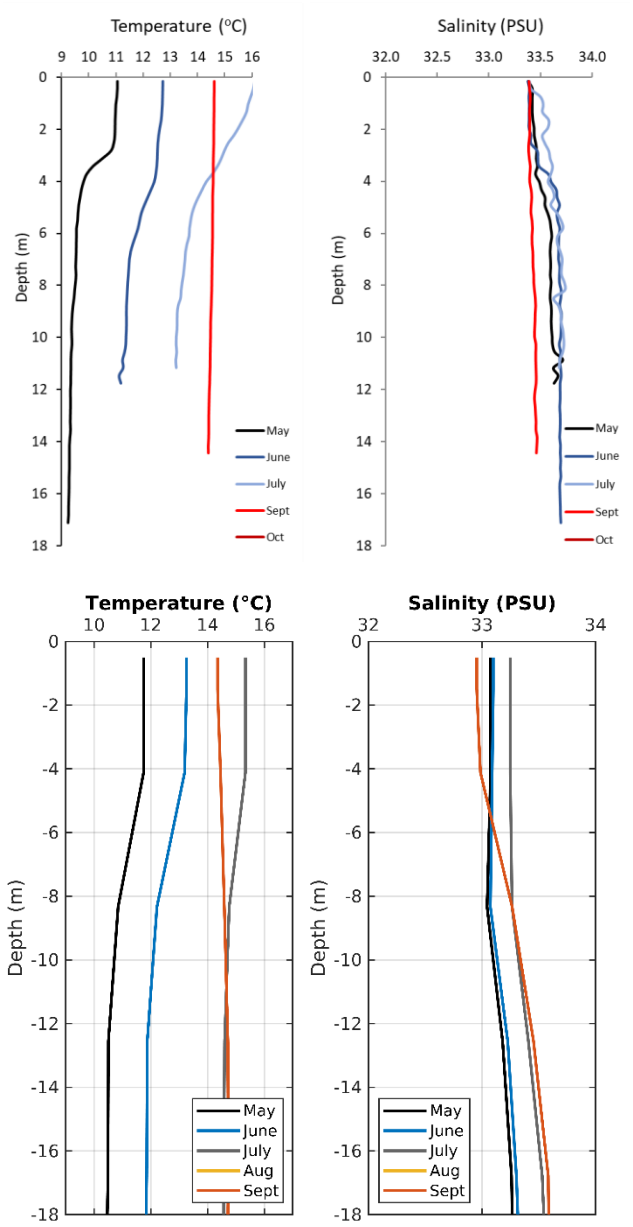

Figure 7.26. Comparison of the observed (top, Reinardy et al., 2023) and modelled (bottom) monthly profiles of temperature and salinity at Loch Melfort from the WLLS Climatology model.

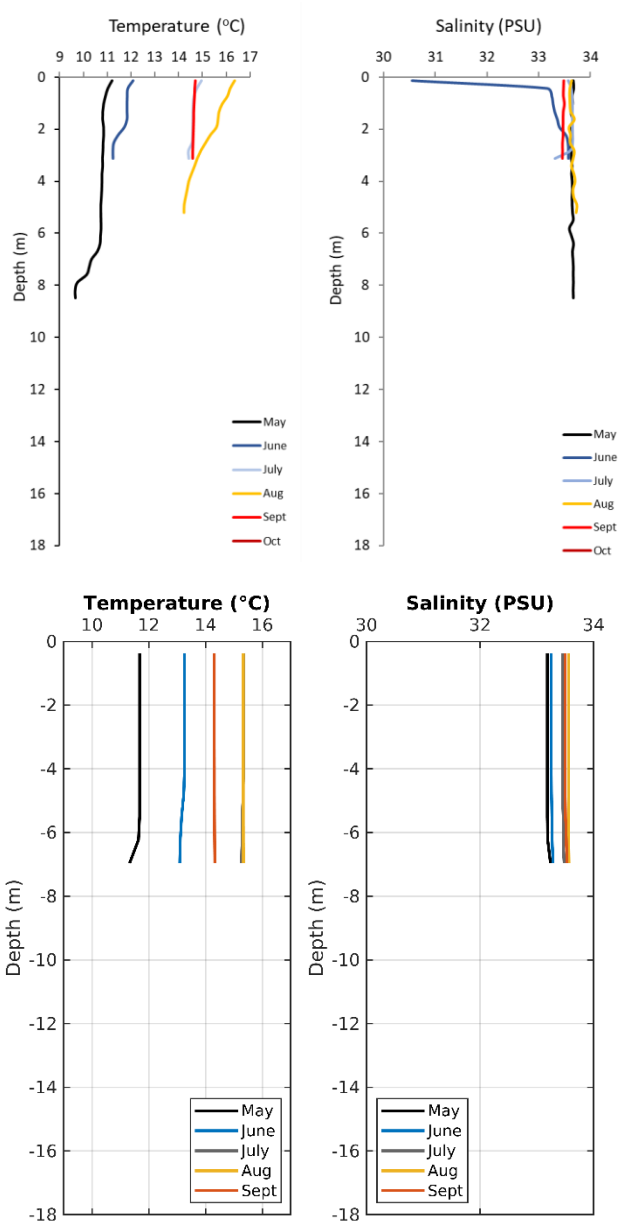

Figure 7.27. Comparison of the observed (top, Reinardy et al., 2023) and modelled (bottom) monthly profiles of temperature and salinity at Musgan from the WLLS Climatology model.

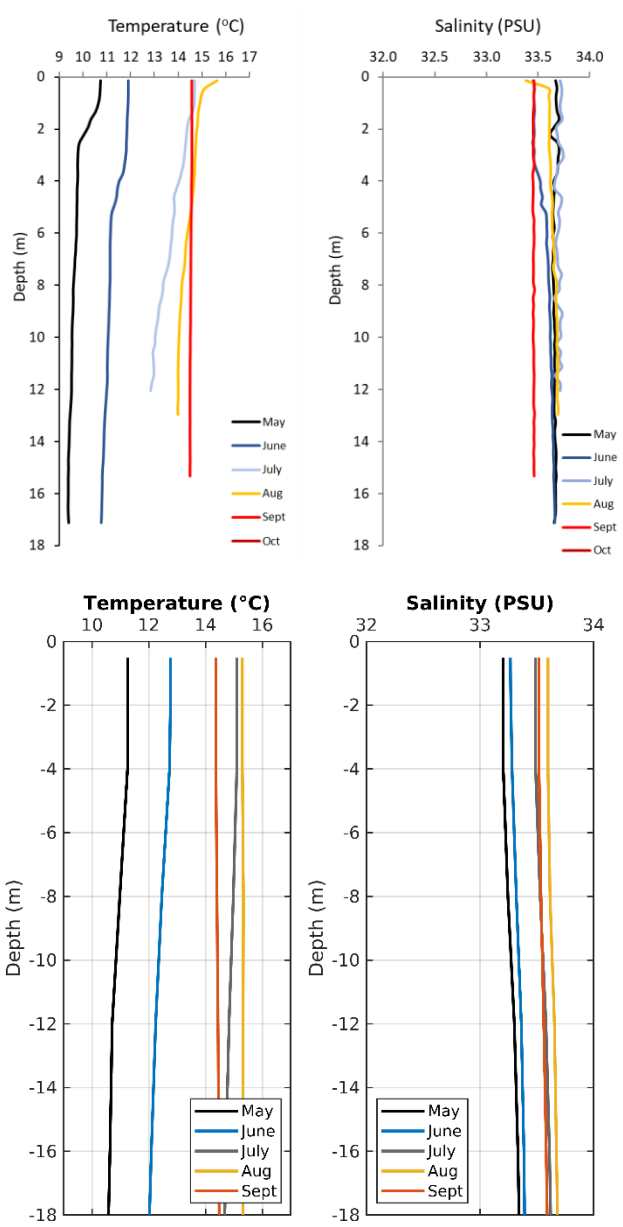

Figure 7.28. Comparison of the observed (top, Reinardy et al., 2023) and modelled (bottom) monthly profiles of temperature and salinity at NE Shuna from the WLLS Climatology model.

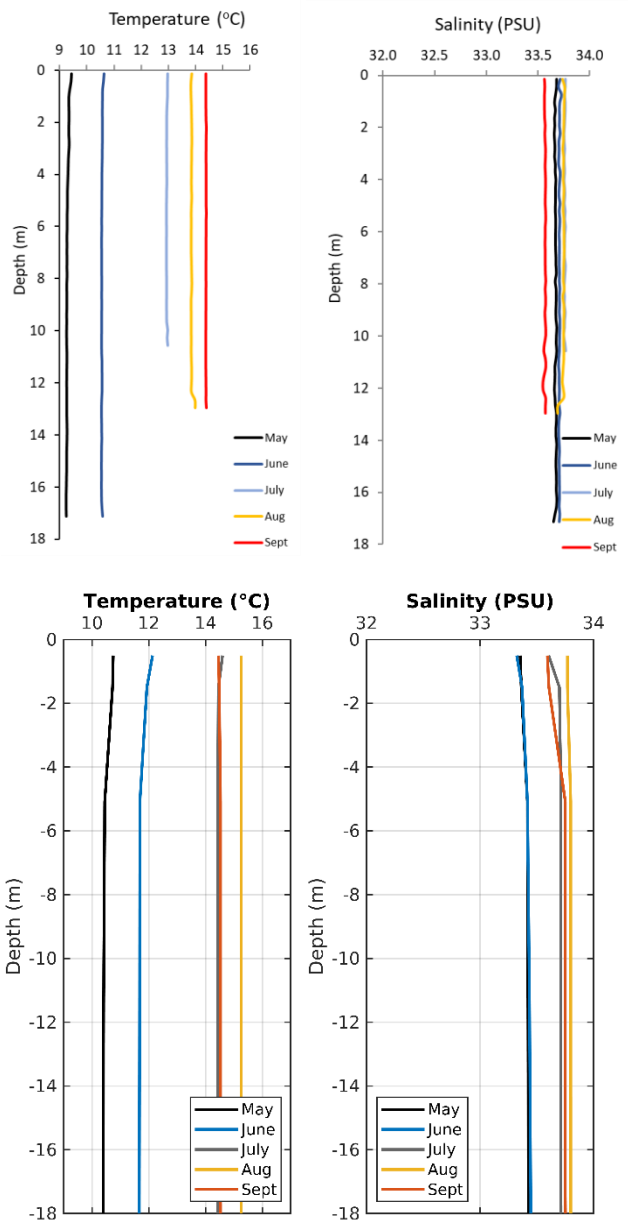

Figure 7.29. Comparison of the observed (top, Reinardy et al., 2023) and modelled (bottom) monthly profiles of temperature and salinity at Southern Approaches from the WLLS Climatology model.

8. Appendix 2. Additional sea lice dispersal model validation figures

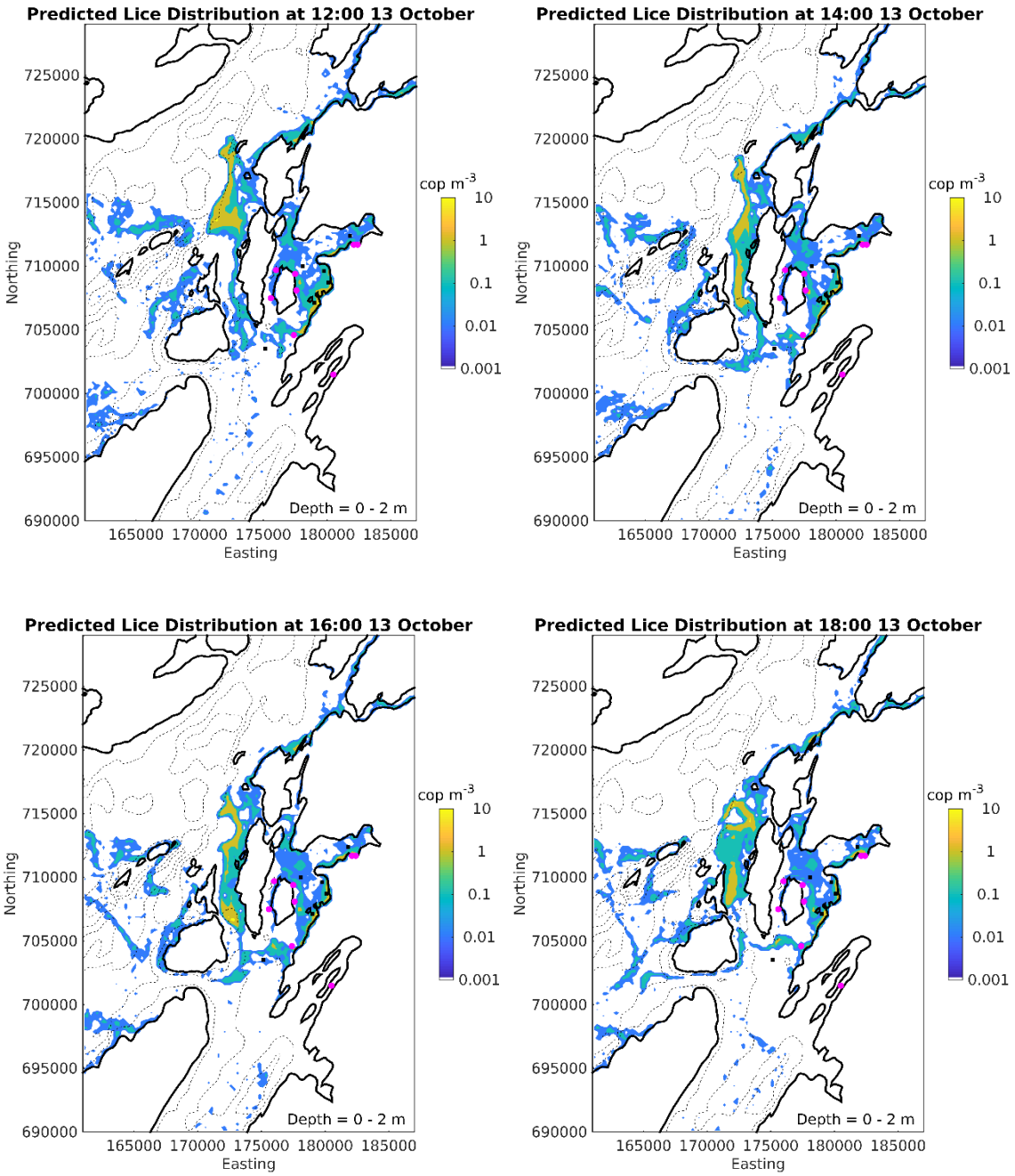

Figure 8.1. Modelled infective lice distributions (lice m^{-3}) at two-hourly intervals during the afternoon of 13th October 2021 using the UnPTRACK-WLLSshuna modelling system. The plots illustrate the continually changing distribution of lice in Shuna Sound due to advection by the combination of tidal, wind-driven and freshwater-driven currents. The densities were calculated over the surface 2m on a 250m x 250m grid.

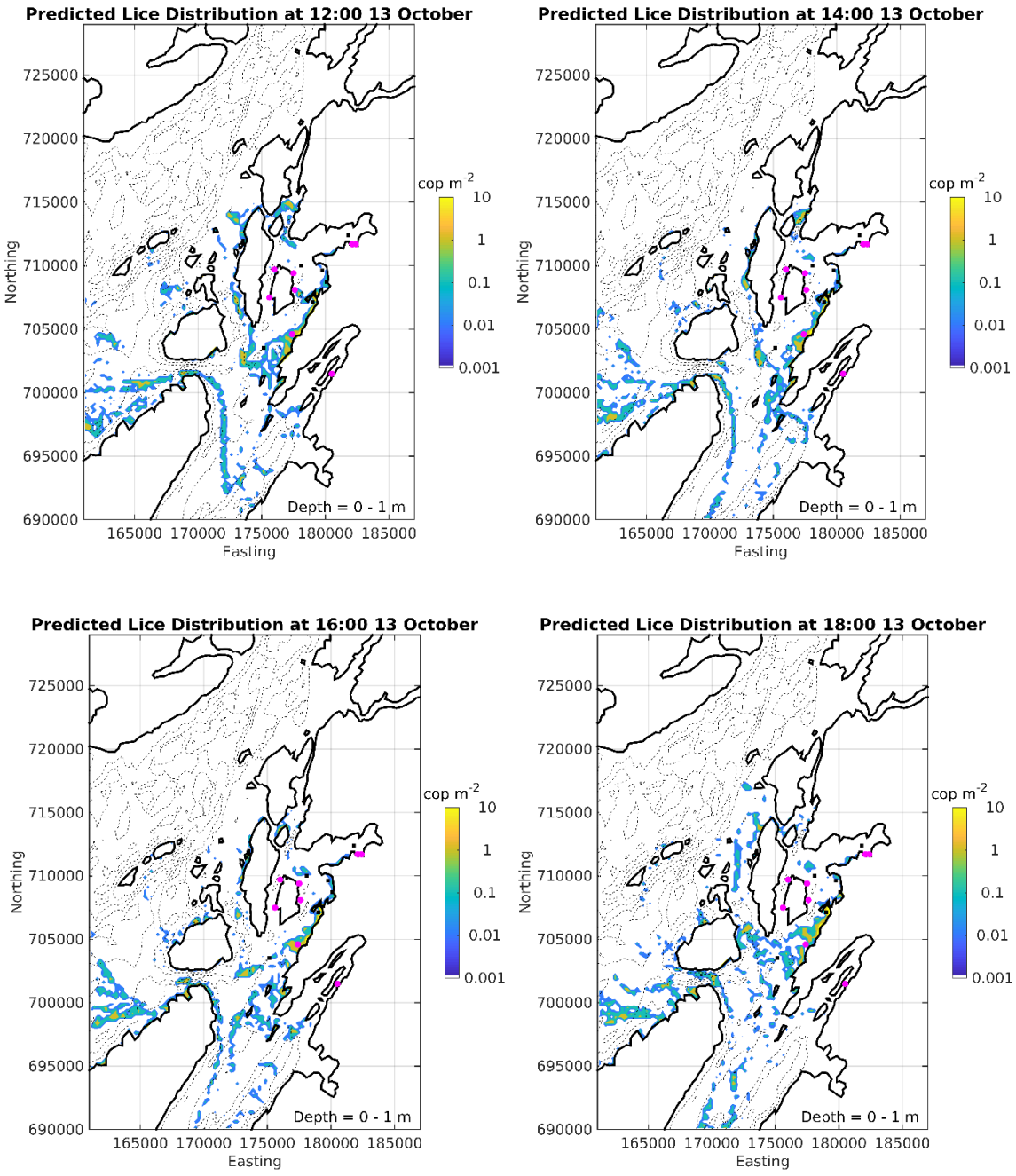

Figure 8.2. Modelled infective lice distributions (lice m^{-2}) at two-hourly intervals during the afternoon of 13th October 2021 using the Biotracker-WestCOMS modelling system. The plots illustrate the continually changing distribution of lice in Shuna Sound due to advection by the combination of tidal, wind-driven and freshwater-driven currents. The densities were depth-integrated and calculated on a 250m x 250m grid.

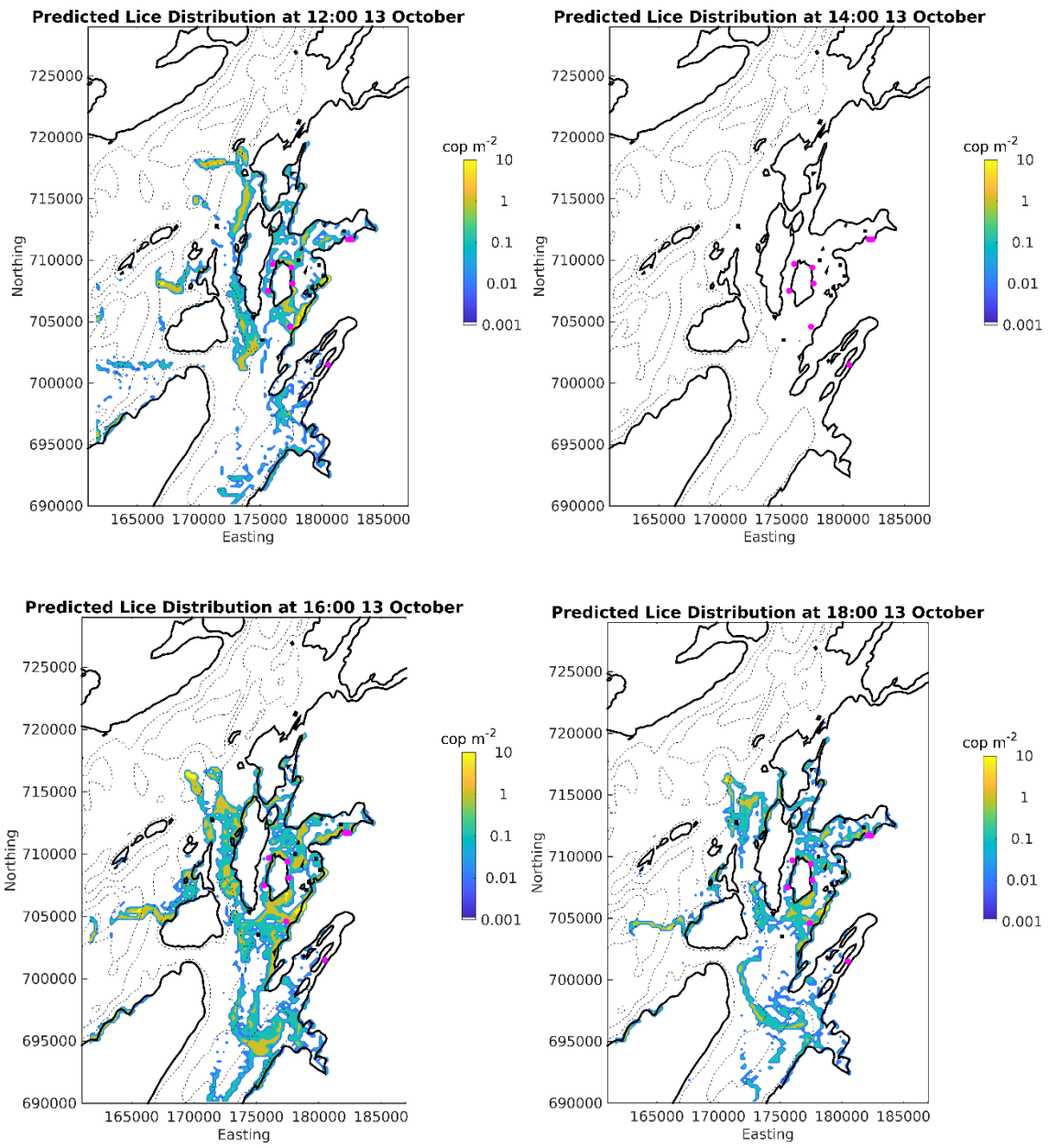

Figure 8.3. Modelled infective lice distributions (lice m^{-2}) at two-hourly intervals during the afternoon of 13th October 2021 using the FISCM-WLLS2021 modelling system. The plots illustrate the continually changing distribution of lice in Shuna Sound due to advection by the combination of tidal, wind-driven and freshwater-driven currents. The densities were depth-integrated and calculated on a 250m x 250m grid.

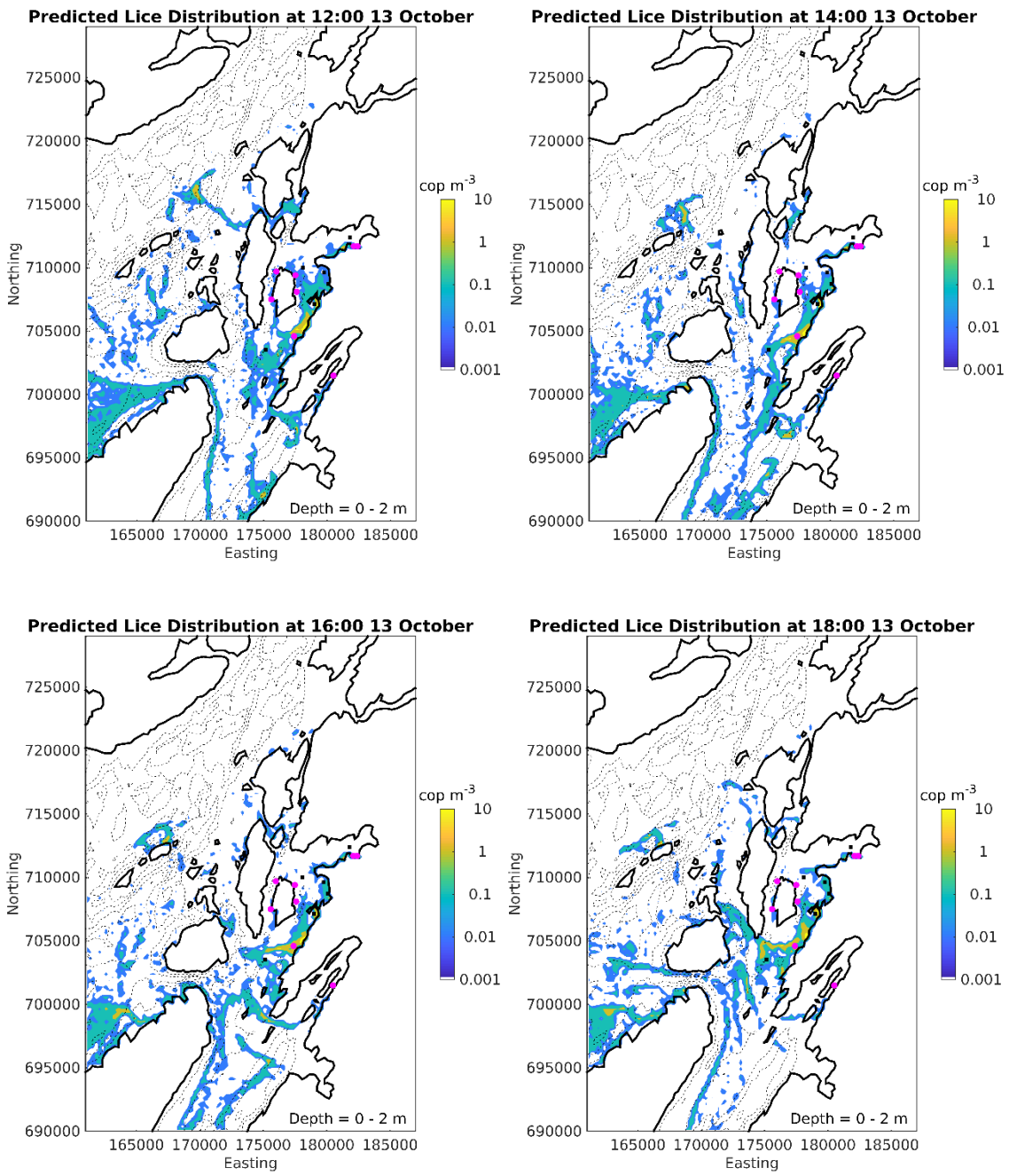

Figure 8.4. Modelled infective lice distributions (lice m^{-3}) at two-hourly intervals during the afternoon of 13th October 2021 using the UnPTRACK-WestCOMS modelling system. The plots illustrate the continually changing distribution of lice in Shuna Sound due to advection by the combination of tidal, wind-driven and freshwater-driven currents. The densities were calculated over the surface 2 m on a 250m x 250m grid.

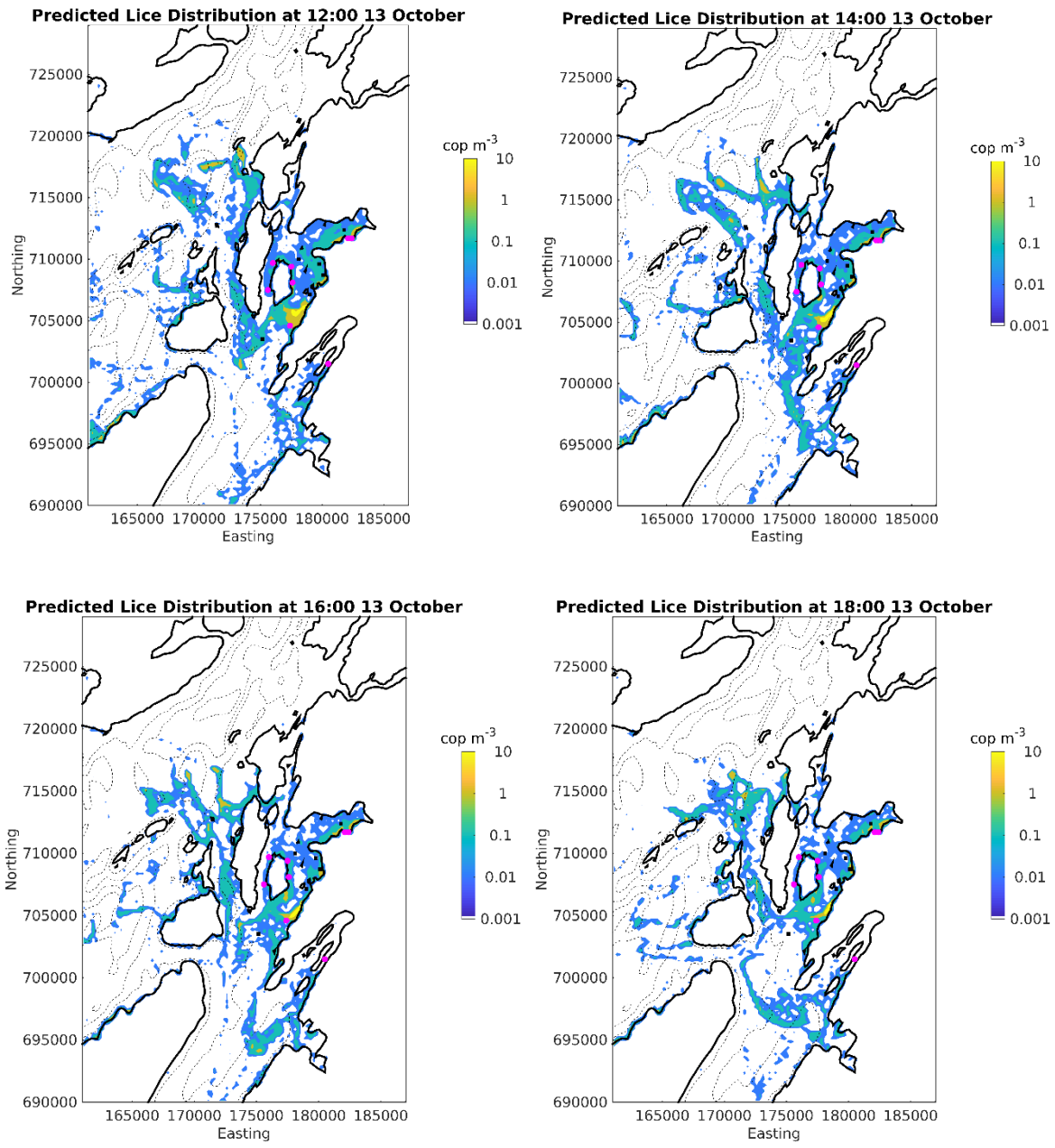

Figure 8.5. Modelled infective lice distributions (lice m^{-3}) at two-hourly intervals during the afternoon of 13th October 2021 using the UnPTRACK-WLLS2021 modelling system. The plots illustrate the continually changing distribution of lice in Shuna Sound due to advection by the combination of tidal, wind-driven and freshwater-driven currents. The densities were calculated over the surface 2 m on a 250m x 250m grid.

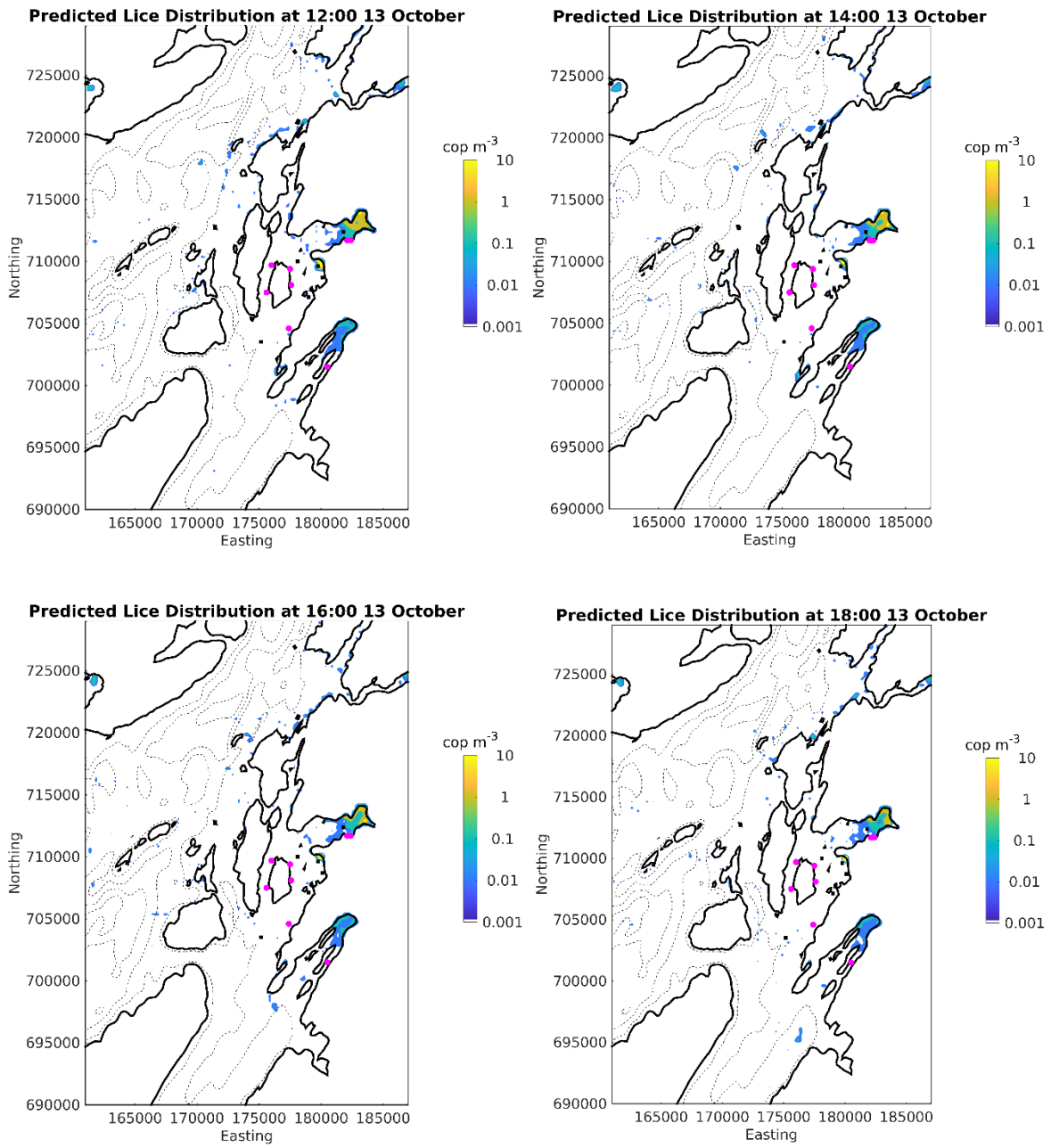

Figure 8.6. Modelled infective lice distributions (lice m^{-3}) at two-hourly intervals during the afternoon of 13th October 2021 using the UnPTRACK-WLLS Climatology modelling system. The plots illustrate the distributions of lice in Shuna Sound in response to advection by the combination of tidal, wind-driven and freshwater-driven currents. The densities were calculated over the surface 2 m on a 250m x 250m grid.